Investigating the molecular pathway through which L-Lactate interacts with synaptic NMDAR to modulate neuronal plasticity

Dissertation by

Engy K Ibrahim

In Partial Fulfillment of the Requirements

For the Degree of

Doctor of Philosophy

King Abdullah University of Science and Technology

Thuwal, Kingdom of Saudi Arabia

December, 2016

EXAMINATION COMMITTEE PAGE

The dissertation/thesis of Engy K Ibrahim is approved by the examination committee.

Committee Chairperson: Dean Prof.Pierre J Magistretti
Committee Members: Dean Prof.Pierre J Magistretti, Dr. Jean Yves Chatton, Prof. Jasmeen Merzaban, Prof. Manuel Aranda

ABSTRACT

Investigating the molecular pathway through which L-Lactate interacts with synaptic NMDAR to modulate neuronal plasticity

Engy K Ibrahim

In the brain, glycogen, the storage form of glucose, is exclusively localized in astrocytes (Magistretti and Allaman, 2015). Glycogenolysis leads to the production of L-lactate, which is shuttled to neurons for ATP production. Interestingly, L-lactate was recently shown to be not only a source of energy, but also a signaling molecule to neurons. This was demonstrated through the inhibition of L-lactate production or transport in an inhibitory avoidance paradigm, where the rodents developed amnesia. This inhibition of memory consolidation was rescued by L-lactate and not by equicaloric glucose emphasizing that L-lactate acts as a signaling molecule as well (Suzuki et al., 2011). A recent study in our laboratory suggests that the action of L-lactate takes place through a cascade of molecular events via the modulation of N-methyl-D-aspartate receptor (NMDAR) activity (Yang et al., 2014). Since NADH produced similar results to those seen with L-lactate, it was hypothesized that the action of the latter is based on altering the redox state of the cell, in particular in view of the fact that redox-sensitive sites are present on the NMDAR. However, the precise molecular mechanism underlying the apparent change in the NMDAR activity is not fully elucidated. The objective of this study is to explore those mechanisms.

ACKNOWLEDGEMENTS

I would like to sincerely thank Prof. Magistretti for giving me the opportunity to do research in his lab. I was so honored when he accepted me as his first lab member in KAUST. The journey of discovery and innovation under his supervision was full of fruitful knowledge and excitement. I also would like to extend my gratitude to Dr. Hubert Fiumelli, my mentor, who helped me on each and every step on the way. He taught me a lot of valuable lessons both on the technical and analytical sides and for that I am very grateful. I also would like to deeply thank Evelyne Ruchti who taught me a lot on the technical level, she was always happily and willingly providing help and support in a very positive manner. My thankfulness also goes to all lab colleagues who work together as a great team. I would also like to thank all my fellow PhD students; Pakiza, Manar, Hanan and Michael for all the moral support. I was also honored to train the master student Ohood. On another note, I would like to thank my family. My father who is the reason I am where I am today, he taught me that the more education you get, the higher you value is. My mother had always been my source of moral support along the way and that was priceless, she brought me up to be the person I am today. My husband who supported me tremendously during the time of my thesis writing and never failed to encourage and push me forward, I owe him a lot for that. My son who provided me with super innocent smiles and hugs and is my main motivation in life.

TABLE OF CONTENTS

LIST OF ABBREVIATIONS

AD	alzheimer's disease
ALS	amyotrophic lateral sclerosis
AMPAR	α-amino-3-hydroxy-5-methyl-4-isoxazolepropionic acid
ANLS	astrocyte neuron lactate shuttle
Arc	activity regulated cytoskeleton-associated protein
ATD	amino terminal domain
ATP	adenosine triphosphate
AXD	alexander disease
BDNF	brain derived neurotrophic factor
BSA	bovine serum albumin
CHO	Chinese hamster ovary
CNS	central nervous system
CTD	intra-cellular carboxyl domain
D-AP5	D-(-)-2-Amino-5-phosphonopentanoic acid
DMSO	dimethyl sulfoxide
dNTP	deoxynucleotides
DTNB	5,5'-dithio-bis-(2- nitrobenzoic acid)
DTT	dithiothrietol
F_0	average fluorescence of the baseline
GFP	green fluorescence protein
HBSS	Hanks' Balanced Salt Solution
HE	hepatic encephalopathy
HEK	human embryonic kidney
HEPES	4-(2-hydroxyethyl)-1-piperazineethanesulfonic acid
HI-FBS	heat inactivated fetal bovine serum
I lac	a specific inward current triggered by L-Lactate
LB	Lysogeny broth
LBD	ligand binding domain
LDH	lactate dehydrogenase
LTP	long term potentiation
MCT	monocarboxylate transporter
NA	noradrenaline
NAD+	nicotinamide adenine dinucleotide
NADH	reduced form of NAD+
NMDAR	*N*-methyl-D-aspartate receptor
PAGE	polyacrylamide gel electrophoresis
PBS	phosphate buffered saline
PCR	polymerase chain reaction
PFA	paraformaldehyde
PI	protease inhibitor
PVDF	polyvinylidene fluoride
ROI	region of interest
ROS	reactive oxygen species

RT	room temperature
SEM	standard error of the mean
SOC	super optimal broth catabolite repression
TMD	trans-membrane domain
VIP	vasoactive intestinal peptide
WT	wild type
zif-268	zinc finger protein 225

LIST OF ILLUSTRATIONS

LIST OF TABLES

Chapter 1

Literature review

1.1 General description of brain energy metabolism

In the adult brain, glucose is the main energy substrate and it is fully oxidized giving a respiratory quotient near to 1. Based on oxygen consumption measurements, glucose utilization is significantly higher than calculated. This could possibly be due to glycolysis; however, the lactate production is minor. Another two explanations for glucose processing are the pentose phosphate pathway and glycogen synthesis, other possible fates may be structural rather than energetic. High structural demands are correlated to neuronal plasticity due to expansions of the lipid bilayer of membranes at synaptic sites and new protein synthesis (Magistretti, 2008).

Brain energy metabolism is strongly coupled to synaptic activity and hence subject to spatially and temporally defined regulatory mechanisms (Kadekaro et al, 1987). Astrocytes are involved in the transit of energy substrates from the circulation to supply neurons (Andriezen, 1893). Indeed, astrocytes have specialized structures forming at their extremities called end-feet to surround cerebral blood vessels (Kacem *et al*, 1998). The presence of specific glucose transporters (GLUT1) at the surface of these structures (Morgello *et al*, 1995; Yu and Ding, 1998) strengthens the idea that it represents an uptake site for glucose, which moves from the circulation to enter the brain parenchyma. In parallel, astrocytes have other processes that ensheath synapses for the

communications between neurons and astrocytes. Such features provide the anatomical basis to implicate astrocytes in a coupling mechanism between synaptic activity and glucose utilization (Pellerin and Magistretti, 1994) and confirms the role of astrocytes in coupling synaptic activity with the local regulation of blood flow (Gordon *et al*, 2008). However, the mechanisms for neurovascular coupling is somehow complex and redundant (Kocharyan *et al*, 2008). Indeed, neuronal activity stimulates the release of vasoactive substances by astrocytes, such as prostanoids, enabling the dynamic coupling of cerebral blood flow with the local energy demand (Gordon et al, 2007; Iadecola et al, 2007).

Astrocytes provide glucose derived Lactate to active neurons through coupling via gap junctions to support the energetic demand of these neurons (Rouach *et al*, 2008). Astrocytes and neurons have different metabolic profiles where glycolytic and glycogen pathways are dominant in astrocytes and lactate utilization is dominant in neurons (Itoh *et al*, 2003; Bouzier-Sore *et al*, 2006). Even if neurons do have glycolytic activity, it is more prominent in Astrocytes (Bittner *et al*, 2010). It was also shown that neurons are not capable of up regulating glycolysis upon need (Herrero-Mendez et al, 2009). This enhancement of glycolytic activity (at the expense of oxidative metabolism) is due to the low expression of an essential component of the malate–aspartate shuttle in astroglial mitochondria (Ramos *et al*, 2003; Xu *et al*, 2007). It is worth mentioning, that Astrocytes enhance their glucose uptake when exposed to glutamate, a case not seen in neurons (Pellerin and Magistretti, 1994; Takahashi *et al*, 1995Keller *et al*, 1996 Bittner *et al*,

2010). This was also shown using a fluorescent deoxyglucose analog in cerebellar slices (Barros *et al*, 2009).

Glycogen is almost exclusively localized in astrocytes (Magistretti, 2008). Moreover, accumulation of glycogen in neurons, results in progressive myoclonus epilepsy, also known as Lafora disease. In neurons, glucose metabolism is done through the oxidative branch of the pentose phosphate pathway, where reducing agents are produced and play a protective antioxidant role. Given the previous information, we can conclude that neurons cannot afford to process glucose through the glycogen cycle (Magistretti and Allaman, 2007).

Both glucose and lactate can be exported to neurons as a source of fuel (Dringen et al., 1993). Glycogenolysis also results in the release of lactate from astrocytes (Dringen et al., 1993), Using the glutamate-stimulated glycolysis and/or glycogenolysis stimulated by neuromodulators such as noradrenaline and vasoactive intestinal peptide (VIP), it was shown that lactate can be transported between astrocytes and neurons (Magistretti et al., 1999; Pellerin and Magistretti, 1994; Magistretti, 2006; Magistretti and Morrison, 1988). Lactate is transported via monocarboxylate transporters (MCTs), which are proton-linked membrane carriers that transport monocarboxylates like lactate, pyruvate and ketone bodies across the cell membrane. MCT4 is expressed mainly by astrocytes, while MCT2 mainly by neurons and MCT1 by in astrocytes, endothelial cells of micro vessels ependymocytes and oligodendrocytes (Pierre and Pellerin, 2005; Rinholm et al., 2011).

In an attempt to show the correlation between learning and Lactate release, it was shown that learning results in glycogenolysis-dependent lactate release in the hippocampus critical for memory formation. Moreover, lactate was shown to increase in the human brain upon sensory and cognitive stimuli (Urrila et al., 2004). In addition, when glycogen phosphorylation was inhibited in mice, it induced amnesia, which was not reversed after a foot shock reminder, suggesting that impaired glycogen metabolism at the time of training persistently impairs memory consolidation or storage.

Astrocytes are key players in brain homeostasis, via the numerous cooperative metabolic processes they share with neurons, such as the supply of energy metabolites and neurotransmitter recycling functions. Furthermore, any damage in astrocytic function is increasingly being recognized as an important contributor to neuronal dysfunction **(**Allaman et al, 2011).

1.2 ANLS (Astrocyte Neuron Lactate Shuttle), L-Lactate and its role as a signaling molecule.

The main energy reserve in astrocytes is glycogen and is used as a lactate source to sustain glutamatergic neurotransmission and synaptic plasticity. Lactate is also emerging as a neuroprotective agent and a key signal to regulate blood flow. The ANLS (Astrocyte Neuron Lactate Shuttle) model now serves to better understand the coupling between neuronal activity and energy demands as it relates to neuronal plasticity, neurodegeneration and functional brain imaging (Pellerin, Mgistretti, 2012).

ANLS suggests: 1) Glutamate, a neurotransmitter released at over 80% of synapses, is a neuronal signal able to trigger glucose uptake into astrocytes. 2) This effect of glutamate is due to the activation of glutamate transporters and the associated Na+ co-transport that activates the Na/K+ ATPase, an energy consuming process 3) The fate of glucose uptake is lactate, which indicates activation of aerobic glycolysis. The ANLS hypothesis is summarized in Fig 1. It was also shown that lactate is produced in the extracellular medium immediately surrounding neurons and that this lactate derived from astrocytes could meet the energetic demands of active neurons (Pellerin and Magistretti, 1994). Moreover, the concentration of glutamate in the extracellular milieu was shown to be tightly correlated to the Na/K+ ATPase and the ATP consumption levels in astrocytes (Magistretti and Chatton, 2005).

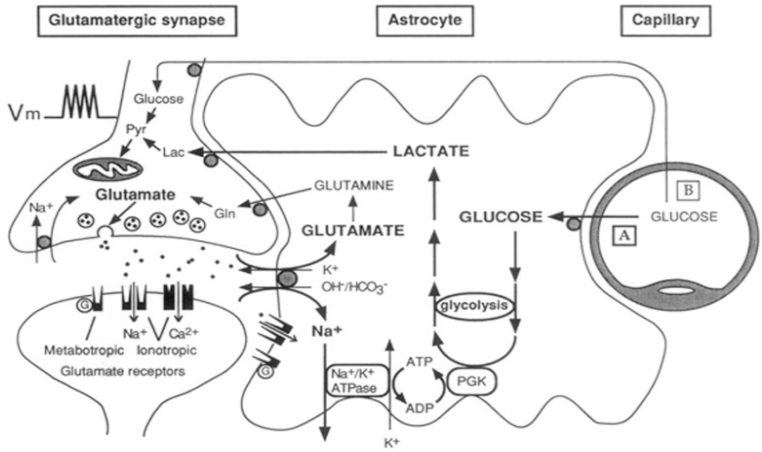

Figure 1 summary of the ANLS hypothesis. Pellerin and Magistretti, Proc Natl Acad Sci USA ,1994

Interestingly, lactate (and more specifically lactic acid) was considered as a toxic waste for brain cells that they must get rid of, despite the fact that it is an important energy

source (Dienel and Hertz, 2001). However, evidences accumulated over more than 50 years have shown that lactate is one of the rare alternative oxidative substrate for neurons (McIlwain, 1953; Pellerin, 2003). Moreover, in physiological conditions both substrates (glucose and lactate) are present, however lactate is largely preferred as an oxidative energy substrate by neurons (Itoh *et al*, 2003; Bouzier-Sore *et al*, 2003, 2006; Ivanov *et al*, 2011), although glucose utilization also occurs in neurons (reviewed in Mangia *et al*, 2009). Prominent lactate utilization by the brain and more specifically by neurons has also been confirmed *in vivo* (Smith *et al*, 2003; Serres *et al*, 2004).

In summary, lactate can be produced by astrocytes in response to two types of neuronal signals: aerobic glycolysis stimulated by glutamate and glycogenolysis triggered by VIP (vasoactive intestinal peptide), NA (noradrenalin), or adenosine (Magistretti and Morrison, 1988; Magistretti *et al*, 1986)

Since lactate is suggested to play an important role in cellular and organelle redox balance (Brooks, 2009), we may also hypothesize that lactate also mediates coordinated astrocyte-neuron cell-cell and intracellular responses important for cell signaling (Gordon et al., 2008) and regulation of gene expression in addition to representing an energy source. It is worth noting, that lactate is shown to be a potent neuroprotective agent in several experiments (Magistretti et al, 2006; Belanger et al 2009). An example being that lactate can rescue neuronal activity during glucose deficiency when infused through the astrocytic network (Rouach et al, 2008).

1.3 Diseases related to learning and memory and why it is important to learn about the underlying mechanisms.

ANLS had been proposed to be essential for long-term synaptic plasticity, long-term memory, and the underlying molecular and synaptic changes. This could be important for intervening with memory disorders and pathologies carrying memory or cognitive deficits in general including neurodegenerative conditions as AD, aging and dementia. Drawing attention to re-establishing or enhancing normal astrocytic functions could be a great strategy to enhance neuroprotection in various central nervous system (CNS) disorders (Suzuki et al, 2011).

A strong evidence that astrocytes play a pivotal role in maintaining and nourishing normal brain function is clearly seen in neurological disorders that are caused by dysfunction of these cells. Also some pathologies are observed due to a secondary malfunction of other cell types that depends on astrocytes for support as neurons, microglia and oligodendrocytes (Belanger and Magistretti, 2011).

Examples of pathologies caused due to malfunction of Astrocytes:

- *Hepatic encephalopathy* (HE), high concentrations of ammonia accumulate in the brain, which is mainly detoxified in astrocytes by the glutamine synthetase (GS) enzyme, accordingly the intracellular concentration of glutamine is increased which is osmotically active glutamine and leads to astrocytic swelling (Haussinger et al, 2008; Felipo et al, 2002),

- Alexander disease (AXD), mutations in the gene encoding glial fibrillary acidic protein (GFAP) which is found in Astrocytes were confirmed in most patients (Brener et al, 2001; Li et al, 2005).

- Neuroinflammatory disease, Astrocytes play a neuroprotective and/or neurotoxic effects in modulating neuroinflammatory processes. This occurs via their release of various mediators, including pro- and anti-inflammatory cytokines neurotrophic factors, chemokines, complement factors and reactive oxygen species (ROS) (Sofroniew et al, 2010).

- Alzheimer's disease, Astrocytes are believed to have a role in the clearance of Aβ in human AD brains. This was suggested after observing large amounts of Aβ in activated astrocytes [38], More recently, in vivo studies in a transgenic mouse showed the ability of astrocytes to migrate to and internalize deposited Aβ (Pihalaja et al, 2008).

- Amyotrophic lateral disease (ALS), a fatal neurodegenerative disease principally characterized by the loss of motor neurons in leading to paralysis and muscle atrophy. Astrocytes are involved in this disease as they fail to clear glutamate at the synapse leading to the degeneration of motor neurons via excitotoxic mechanisms (Ilieva et al, 2009; Raoul et al 2006).

1.4 Molecular mechanism of plasticity and LTP (Long Term Potentiation)

New learning initiates short and long-term memories through a cascade of events in the brain. While short-term memories involve post-translational modifications, the stabilization of long-term memories involves the activation of a gene cascade and downstream changes in neurons that store the acquired information (Dudai, 2004; Kandel, 2001). One of the early markers of memory consolidation is the translation of the immediate early gene Arc (activity-regulated cytoskeletal protein) at activated synapses. The role of increased Arc is believed to modulate the actin cytoskeletal dynamics and regulate the membrane expression of AMPA receptors (Bramham et al., 2008). LTP is a leading cellular model for memory formation (Whitlock et al., 2006)

1.5 Structure and function of different types of Glutamate receptors

Glutamate receptors are located in neuronal and non-neuronal cells and they mediate fast synaptic transmission in the central nervous system. The ionotropic glutamate receptors are integral membrane proteins that consist of four large subunits (>900 residues), creating the central ion channel pore. There is a sequence similarity among glutamate receptor subunits, within the AMPA (α-amino-3-hydroxy-5-methyl-4-isoxazolepropionic acid), kainate, NMDA (N-Methyl-D-aspartate) and sigma receptors. Glutamate receptor subunits consists of four domains: the extracellular amino terminal domain (ATD), the extracellular ligand binding domain (LBD), the trans-membrane domain (TMD), and an intra-cellular carboxyl domain (CTD). The Glutamate receptors

are assembled as tetrameric complexes of subunits (Laube et al., 1998; Mano and Teichberg, 1998). Based on pharmacology and structural homology, glutamate receptors are grouped into four distinct classes: the AMPA receptors, the kainate receptors, the NMDA receptors and the sigma receptors (Partin et al., 1993,1995).

NMDA receptors are co-localized with AMPA receptors at virtually all central synapses to from the functional synaptic unit, so that the pre-synaptically released glutamate can co-activate both receptors. (Petralia and Wenthold, 2008). Functional NMDA receptors require the assembly of two GluN1 subunits with either two GluN2 subunits or a combination of GluN2 and GluN3 subunits (Monyer et al., 1992) as shown in Fig 2. For the activation of NMDA receptors, simultaneous binding of glutamate and glycine are needed (Johnson and Ascher, 1987). Glycine binding sites are found on GluN1 and GluN3 (Furukawa and Gouaux, 2003), while the glutamate binding sites are found on the GluN2 subunit (Furukuwa et al, 2005). Another possible combination of subunits is GluN1 subunit with two different GluN2 subunits, to form triheteromeric receptors (Brothwell et al., 2008). The initial step in the activation of the glutamate receptor is the binding of the agonist to the LBD, which is followed by a conformational change of the LBD (ligand binding domain) (Armstrong and Gouaux, 2000). This triggers subsequent transition of the ion channel domain into an open state.

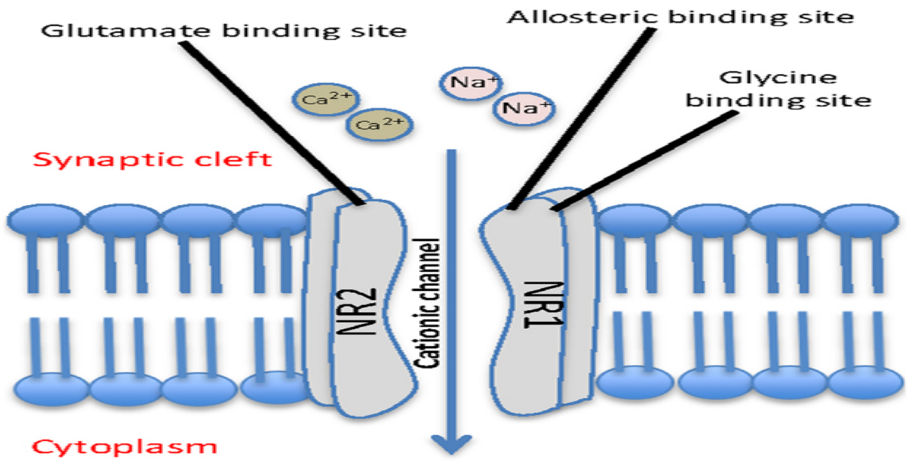

Figure 2 **Tetrameric structure of NMDAR**. S-E Lakhan et al., Frontiers in Psychiatry, 2015

1.6 Redox modulation of NMDAR

The extracellular redox state regulates NMDA receptors. NMDA receptor activity can be enhance NMDA generated currents by the formation of free thiol groups, whereas oxidizing agents inhibit currents by the formation of disulfide bonds. This occurs through decreasing frequency of channel opening and hence decreased NMDA receptor activity (Aizenman et al., 1989) as shown in Fig 3.

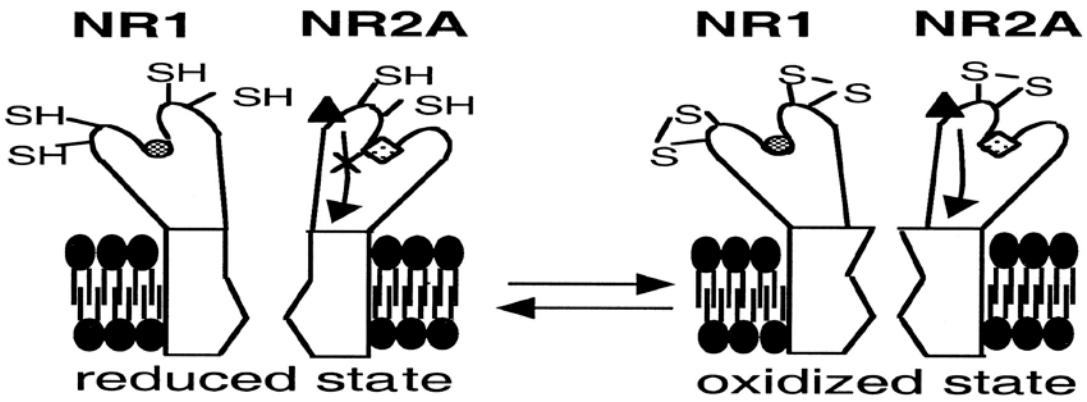

Figure 3 **Redox sensitivity of NMDAR**. In the left panel, reducing conditions where free thiol groups confer a conformation with larger opening. In the right panel, oxidizing conditions where disulfide bridges confer a conformation with smaller opening. Y-B Choi et al., Journal of Neuroscience, 2011

Multiple cysteine residues located in different NMDA receptor subunits have been identified as molecular determinants underlying redox modulation. The subunits which are responsible for redox modulation are GluN1 and GluN2. The intermediate and slow components of redox modulation for all GluN2 -containing NMDA receptors occur through the disulfide bonds formed between two pairs of cysteine residues within GluN1 (SVC79ED and RGC308VG within the ATD and Cys744 and Cys798 in the LBD) (Sullivan et al., 1994). As for the fast component of redox modulation, this occurs through a disulfide bond which had been proposed to from in the GluN2A subunit between Cys87 and Cys320 of the GluN2A ATD and also between Cys86 and Cys321 in GluN2B ATD (Karakas and Furukawa, 2009). Another mode of action of the previously mentioned disulfide bond would be a modification in the Zn+2 binding site and not only through mediating the fast component of redox modulation (Kohr et al., 1994). Zinc can be chelated by reducing agents and transient potentiation that occurs only in the presence of agents such as dithiothreitol (DTT) reflects in part the relief of zinc inhibition

through zinc chelation (Paoletti et al., 1997). Moreover, reduction of cysteine residues within GluN1/GluN2 NMDA receptors also reduces high affinity voltage-independent Zn+2 inhibition of NMDA receptors (Choi et al., 2001). The redox modulatory sites of NMDA receptors are clinically interesting as targeting of oxidizing agents to areas with excessive NMDA receptor activity can potentially inhibit the effects of high toxic levels of glutamate in the brain while saving normal neurotransmission in normal regions of the brain (Lipton et al, 1993; Chen et al, 1997).

Previous findings upon which this thesis is based

This research proposal is based upon the results obtained by (Suzuki, Magistretti, Alberinin et al., 2011) and also on some recent data generated. The main findings of the previously mentioned journal paper, were that learning leads to a significant increase in extracellular lactate levels derived from glycogen which is stored in Astrocytes. This was shown to be significantly important for long-term memory formation and for the maintenance of LTP in vivo. Moreover, disrupting the expression of lactate transporters on Astrocytes causes amnesia, which is rescued by lactate and not by equicaloric glucose. These transporters are also shown to be essential for the induction of molecular changes needed for memory formation as that of phospho-CREB, Arc and phosphor-cofilin. In addition, they showed that the expression of MCT1, a lactate transporter, was significantly higher in trained compared to untrained rats.

Regarding the current findings correlating the effect of L-lactate with NMDAR, these experiments were carried out using primary cultures of cortical neurons from embryonic mice. The first finding was that L-Lactate induces expression of selected plasticity genes in neurons such as Arc (activity regulated cytoskeleton-associated protein), c-fos (proto-oncogene), zif-268 (zinc finger protein 225) and BDNF (brain derived neurotrophic factor). Next, it was shown that L-Lactate triggers a specific inward current (I lac) through electrophysiological recordings. Finally, the most important result obtained was that NMDA receptors generate the (I lac) and are responsible for the effects of L-Lactate on plasticity genes expression. This was shown by blocking the NMDA receptors using MK801, where the L-lactate induced Arc and zif268 expression at both mRNA and protein levels was completely vanished (Yang et al., 2014)

Objectives of dissertation

Given the above results, the main aim of this proposal is to dig deeper into the interaction between L-Lactate and NMDA receptor and find out the molecular and signaling pathways underlying this interaction. This was achieved by creating a cellular model expressing NMDARs either wild type or mutated on selected redox sensitive sites. The effect of L-Lactate on wild type NMDARs versus mutated was assessed to identify the key important redox sensitive site location and its localization in terms of subunits.

Chapter 2

Introducing mutations to NMDAR subunits at sites modulated by redox state

2.1 Significance

It was shown previously that the NMDAR evoked responses of NMDARs containing different subunit are affected by the redox state of their environment. In order to better understand the molecular details involved in NMDARs responses to redox states, this chapter is focused on introducing targeted mutations in NMDAR subunits at sites that are responsible for modulating the redox sensitivity. The targeted amino acids in all the mutations performed were cysteine residues. The idea is to disrupt the disulfide bridges formed between neighboring cysteine residues. These disulfide bridges are formed and dismantled according to the redox state of the surrounding environment to the NMDAR subunit.

Some key neighboring cysteine residues on NMDAR subunits had been well investigated in single-channel studies. Those studies revealed that NMDA induced responses can be potentiated by sulfhydryl reducing agents such as dithiothrietol (DTT) and can be attenuated by sulfhydryl oxidizing agents such as 5,5’-dithio-bis-(2- nitrobenzoic acid) (DTNB) (Aizenman et al., 1989). The responses are enhanced by either increasing the opening time of the channel or the frequency of opening. Since both oxidizing and reducing agents can alter the NMDA evoked responses, it was suggested that the redox

sensitive sites on NMDAR responses are always present in an equilibrium; some being fully oxidized and some being fully reduced (Y-B Choi et al, 2000).

In this work, we hypothesize that L-Lactate potentiates the NMDAR evoked responses via creating a reducing environment (Jiangyan Yang and P.Magistretti, 2014). This happens through conversion of L-Lactate to pyruvate by lactate dehydrogenase, which is accompanied by conversion of NAD+ to NADH. The accumulation of the latter is what is believed to cause the reduction of the sulfhydryl groups of the cysteine residues on NMDAR subunits and enhancing the NMDA evoked responses. In order to confirm the previously suggested mechanism of action of L-Lactate on modulating NMDAR activity, we aimed to mutate some of the key cysteine residues that are well known to regulate the NMDAR activity based on the redox state. Afterwards, we will check whether the modulatory effects of L-Lactate on NMDAR evoked responses persisted after introducing the mutations or not.

2.2 Materials and methods

2.2.1 Plasmid amplification

Transformation

Top10 one shot supercompetent cells stored at -80 C were used for amplification of constructs. The cells were allowed to thaw completely on ice, then 5 ng of DNA was added to cells were both cells and DNA were mixed together by flickering. The cell/DNA mixture was left on ice for 15-20 minutes. Afterwards, a heat shock was introduced to

the cell/DNA mixture by placing the cells in a thermo block at 42C for 45 seconds then moving them back quickly to ice for 2 minutes. 500 µl of SOC (super optimal broth catabolite repression). The cells were then shaken in a thermoblock at 37C for 1 hour at 500 rpm.

80 µl of the cells were spread on an agar plate containing Ampicillin at a concentration of 100 µg/ml using a sterile loop. The agar plate was then incubated at 37C upside down to prevent condensation overnight.

Picking colonies and growing mini cultures

The next day, single bacterial colonies were picked using sterile pipette tips and grown in 3ml LB (Lysogeny broth) media containing ampicillin (50 µg/ml) in a shaker at 37C overnight. The cell culture was then incubated in a shaking incubator overnight at 37C.

Growing midi cultures

The next day, cultures were diluted 1:500 and then grown in a shaking incubator overnight at 37C again in 50 ml media to obtain a higher amount of the amplified construct.

Extracting amplified plasmids

The next day, the cultures were centrifuged in a high speed centrifuge at 6000 x g for 15 minutes at 4C. The supernatant was discarded and the cell pellet was used to extract the amplified DNA construct using a Qiagen HiSpeed Midi kit. The extracted DNA was dissolved in molecular grade water and kept at a final volume of 1000 µl.

DNA concentration

The extracted DNA concentration was measured using the Nanodrop machine. Afterwards, it was concentrated using isopropanol to a final concentration of 1 µg/µl. The DNA precipitation and concentration was done as follows; 100 µl NaOAc (concentration: 3M, pH: 5.4) and 700 µl isopropanol were added to the 1000 µl of extracted DNA. The previous mixture was then centrifuged at maximum speed for 20 minutes at 4C. The supernatant was then discarded and the DNA pellet was washed with 1000 µl ethanol (70%) and centrifuged at maximum speed for 5 minutes at 4C. The supernatant was then removed and the DNA pellet was air dried then re-suspended in molecular grade water at a final concentration of 1 µg/µl

2.2.2 Introducing targeted mutations

Fig 4 shows a summary of the concept of introducing targeted mutations. For this end, we used QuikChange II XL Site-Directed Mutagenesis Kit by Agilent technologies. Basically, the procedure involves a supercoiled double stranded DNA containing an insert (NMDAR subunits), PfuUltra high-fidelity (HF) DNA polymerase, two synthetic primers containing the targeted mutations and a mixture of deoxynucleotides (dNTP). The primers which are complementary to opposite strands of the vector, are elongated by the DNA polymerase during thermocycling without primers detachment producing mutated strands with staggered nicks. The PCR product is then treated with Dpn I endonuclease which is specific against digesting methylated and hemi-methylated DNA

(produced by Dam^{+} E.coli), in order to digest the parental DNA template and keep only the mutated copies. The treated DNA is then transformed to supercompetentent E.Coli cells to repair the nick and propagate the vector containing the mutated insert.

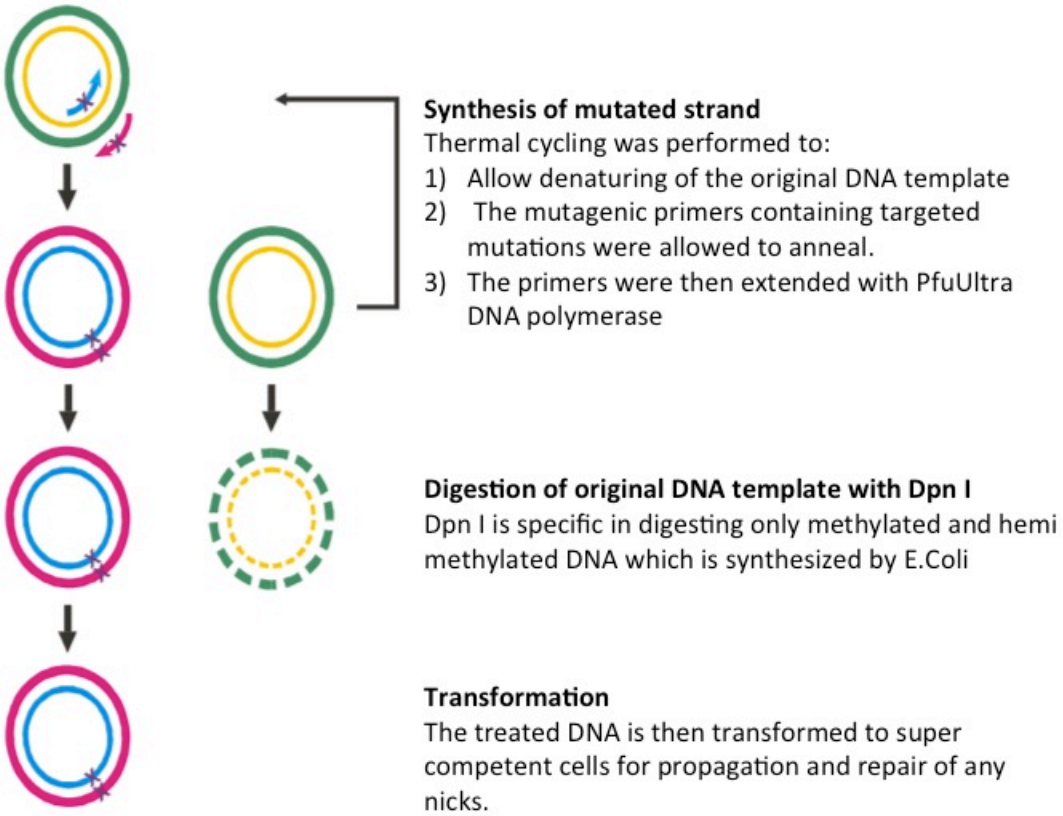

Figure 4 **summary of the steps used to introduce site directed mutations**

Designing primers for directed mutagenesis

Primers were designed using Quick change primer design tool by Agilent technologies. Care was given to select primers with melting points higher than 78 and a length ranging from 25 to 40 bases with the mutation lying in the middle (preceded and followed by 10-15 bases of correct sequence). Both forward and reverse primers for the same mutation were designed to bind to the same sequence on opposite strands of the vector. The primers were synthesized by Sigma and purified using PAGE technique. The primers were stored at stock concentration of 100uM at -80 C and working concentration of 5 uM at -20 C. Table 1 shows the sequence of the designed primers which targeted changing cysteine residue to either Alanine or Serine residues. For NR1 subunit, primers were aimed to introduce the following point mutation; C79S, C308S, C744A and C798A. For NR2B subunit, primers were aimed to introduce the following point mutation; C86S and C321S. For NR2A subunit, primers were aimed to introduce the following point mutation; C87A and C320A. Sequences of mutagenic primers are shown in table 1.

Table 1 sequence of mutagenic primers for NR1, NR2B and NR2A subunits

Name			Sequence (5’-3’)	Length
NR1	C79S	Forward	CAGATGGCCCTGTCAGTGAGTGAGGACCTCATCTC	35
		Reverse	GAGATGAGGTCCTCACTCACTGACAGGGCCATCTG	35
	C308S	Forward	GATCCACCGCGGGGTAGCGTGGGCAACACCAAC	33
		Reverse	GTTGGTGTTGCCCACGCTACCCCGCGGTGGATC	33
	C744A	Forward	GAGGCTTCACAGAAGGCCGATCTGGTGACCACG	33
		Reverse	CGTGGTCACCAGATCGGCCTTCTGTGAAGCCTC	33
	C798A	Forward	GTTCGGTATCAAGAAGCTGACTCCCGCAGCAATG	34
		Reverse	CATTGCTGCGGGAGTCAGCTTCTTGATACCGAAC	34
NR2B	C86S	Forward	CATAATCACCCGCATCTCCGATCTTATGTCTGACCG	36
		Reverse	CGGTCAGACATAAGATCGGAGATGCGGGTGATTATG	36
	C320S	Forward	GAGCCCAAGAGCAGTTCCTACAACACCCACGAG	33
		Reverse	CTCGTGGGTGTTGTAGGAACTGCTCTTGGGCTC	33
NR2A	C87A	Forward	CCGGACATGAGGTCGGCCACATGCGTGATGAG	32
		Reverse	CTCATCACGCATGTGGCCGACCTCATGTCCGG	32

	C320A	Forward	GGCCAAGGCCAGCGCCTACGGGCAGACA	28
		Reverse	GTCTGCCCGTAGGCGCTGGCCTTGGCC	27

Thermal cycling to synthesize mutagenic strand

One site directed mutation was done at a time using both forward and reverse primers designed for that mutation. Another mutation would be added in the following mutation cycle to obtain a construct with multiple mutations and so on. A thermo blocker was used for that end. The PCR reaction mix was prepared on ice and was composed of the following:

- 5 µl of 10X Reaction buffer
- 1 µl ds DNA template (50ng/µl) = 50ng
- 2 µl of Fwd primer (5µM) = 125ng
- 1 µl dNTP mix
- 3 µl QuickSolution reagent
- 35 µl H2O
- 2 µl of Rev primer (5µM) = 125ng
- 1µl PfuUltra HF DNA polymerase (2.5 U/µl)
- final reaction volume is 50 µl

The above reaction mixture then went through PCR cycles using a thermocycler with the parameters mentioned in table 2

Table 2 Cycling parameters for introducing targeted mutations

Repeats	Temp	Time
1	95°C (hot start)	1 min
18	95°C	50sec
	60°C	50 sec
	68°C	1min/ kb of plasmid
1	68 °C	7 mins

At the end of the PCR, the samples were chilled on ice for about 2 minutes till their temperature reached < 37 °C. Afterwards, 1ul of Dpn1 (10U/ul) was added to the sample to destroy the non-mutated template (parental strand), it was mixed by pipetting up and down, then the sample was incubated at 37 °C for 1 hour in a thermoblock.

Transformation of the mutated construct

The Dpn I treated DNA was then used to be transformed into super competent Top 10 cells or XL 10 Gold ultracompetent cells to repair the nicks and to propagate the DNA. Some colonies were picked to prepare a miniculture as detailed earlier. The DNA was extracted using Qiagen miniprep kit and eluted using Molecular biology grade water.

2.2.3 Sequencing for mutated construct verification

In order to validate that the desired targeted mutation was accomplished and that no other random mutation happened, the extracted DNA was sent for Sanger sequencing in KAUST core lab facilities. Sequencing primers were designed every 400 bases to span the whole length of the NMDAR subunit insert using the GenScript DNA sequencing primers design tool. Sequence of primers for NR1, NR2B and NR2A subunits are shown in tables 3, 4 and 5 consequently. Verified mutated constructs were then used to either introduce another mutation or to propagate and amplify the construct in midi cultures as detailed before or both.

Table 3 Sequence of primers used for sanger sequencing of NR1 subunit

Sequencing primers for NR1 PCEP4 construct	
Primer direction	Sequence (5’-3’)

Reverse	CGCCGATGTTGACAATCTT
Forward	CTCCCACCCCTGTCTCCTAC
Forward	TCATCATCCTTTCTGCAAGC
Forward	CTGTCAGTTCATGTGGTGGC
Forward	CCCAGTGCTGTTATGGCTTC
Forward	GAAGACCTGGATAAGACATGGG
Forward (binds to PCEP4)	AGCAGAGCTCGTTTAGTGAACCG
Reverse (binds to PCEP4)	GTGGTTTGTCCAAACTCATC

Table 4 Sequence of primers used for sanger sequencing of NR2B subunit

Sequencing primers for NR2B PCEP4 construct	
Primer direction	Sequence (5'-3')
Forward	TGCGATCTTATGTCTGACCG

Forward	AGCTGAAGAAGCTGCAGAGC
Forward	AAAAATGCTGCAAGGGGTTT
Forward	CAATGGCAGCACAGAGAGG
Forward	CAGAGTGCCCTGGACTTCAT
Forward	CGTGGACTTGACTGACATTTACA
Forward	TAATTCCAAGGCCCAGAAGA
Forward	ACCCTTTCATCCCCACTTTT
Forward (binds to PCEP4)	AGCAGAGCTCGTTTAGTGAACCG
Reverse binds to PCEP4	GTGGTTTGTCCAAACTCATC

Table 5 Sequence of primers used for sanger sequencing of NR2A subunit

Sequencing primers for NR2A PCDNA 3 construct	
Primer direction	Sequence (5'-3')
Forward	CATCCAGCAGCAAGCCAC
Forward	CTACGGGCAGACAGAGAAGC
Forward	GGAAGCATGGGAAAAAGGTT
Forward	ATCCAGGAGGAGTTTGTGGA
Forward	TGGCAGGAGTTTTCTACATGC
Forward	CTCTCAATGAGTCCAACCCC
Forward	TCACAATGAGAATTTCCGCA
Forward	AGGCTACTGGAGGGCAACTT
Reverse	TCTGTAGCCAGGGAAGATG

Reverse	AAATCCAGCATCTGAGCC
Reverse	CCGTAAATACTCCACCCATTG

2.3 Results

The NMDAR subunits were purchased from GenScript cloned into either the pCEP4 or pcDNA3.1 mammalian vectors. These constructs were propagated to generate a midi culture using Top 10 supercompetent E. coli cells. The propagated DNA was then used to generate targeted mutations one after the other to generate the following constructs:

pCEP4 NR1 C744A, C798A

pCEP4 NR1 C744A, C798A, C79S, C308S

pCEP4 NR2B C86S, C320S

pcDNA3.1 NR2A C87A, C320A

Chapter 3

Finding a model system suitable for expressing functional NMDARs

3.1 Significance

Since our main goal in this work is to characterize the modulation of NMDAR by L-lactate, we aimed to create a simple model where the interaction between L-lactate and NMDAR can be studied. In this chapter we focused on optimizing the conditions for creating such a model where functional NMDARs are expressed either as wild type or mutated subunits. Such a tailored model has the advantage of controlling the subunit composition of NMDAR, either NR1/NR2A or NR1/NR2B. We can also control which subunit contains a mutation and at which site, the level of expression of NMDARs, etc.

3.2 Materials and methods

3.2.1 Cell Culture

HEK 293/T17 was purchased from ATCC (ATCC® CRL11268™) and CHO-K1 cells were kindly provided to us by Prof. Jasmeen Merzaban research group. Upon receipt of the cells, they were stored in their original vial at -140 C to ensure the highest level of viability. Upon need, the vial of frozen cells was thawed at 37 C in a water bath by gently moving the vial in water for no more than 2 minutes. During that time, care was taken not to immerse the cap or O-ring in water to minimize the probability of contamination. Once the vial content was thawed, it was sterilized by spraying 70 % ethanol then moved inside a sterile biosafety cabinet where all the following steps were carried out.

The vial content was then added in a drop wise manner to a centrifuge tube containing 9.0 ml DMEM high glucose media supplemented with 10% HI-FBS and 1% penicillin/Streptomycin mix in addition to 1% Non-essential amino acids (NEAA) in the case of CHO cells. The tube was centrifuged for 7 min at 100X g to pellet the cells. The supernatant was then aspirated and the cells were re-suspended in 12 ml of the fore mentioned DMEM media and then dispensed into a T75. Care was taken to pre-equilibrate the added media in the incubator (humidified, 37C, 5%CO_2) for at least 30 minutes before adding it to the cells to adjust pH and avoid excess alkalinity or acidity.

Cells were maintained in the aforementioned DMEM media and were split twice a week as follows. When cells were about 80% confluent in the T75 flask, the media was aspirated and discarded. The cells were then washed one time with 1X PBS to remove any traces of serum which can hinder the action of Trypsin. Afterwards, 2ml of 0.05% Trypsin were added to the T75 flask containing the confluent cells. The flask was then incubated at 37C and 5% CO_2 for 2 minutes in the case of HEK cells and for 5 minutes in the case of CHO-K1 cells. After examination of the cells under the microscope to ensure that the cells were detaching already, 8 ml of the fore mentioned DMEM was added to the cells to inactivate the action of Trypsin. The cell suspension was then centrifuged at 100X g to pellet the cells and the supernatant was discarded. The cell pellet was then re-suspended in 5 ml DMEM media. 20 µl of the cell suspension was mixed with 80 µl Tryptan blue at a dilution of 5X. 10 µl of the Trptan blue/cell mix was loaded to a hemocytometer and the cell count was determined accordingly (no of cells/ml= average

no of counted cells x 5 x 10,000). The desired number of cells (usually 1 million cells on the bases of a twice per week splitting) was mixed with 11 ml media and added to a T75 flask then incubated at 37C and 5%CO_2.

Unused cells from early passages were frozen with 5%DMSO and kept at -140 C for future use.

3.2.2 Seeding cells on glass coverslips

12 mm glass coverslips were coated with 0.1 mg/ml poly-D-lysin for 20 mins at 37C to enhance cell attachment and prevent detachment during perfusion conditions. The poly-D-Lysine was stored in aliquots of stock solution at a concentration of 10g/L then diluted to working solution at a concentration of 0.1 mg/ml which was stored at 4C for a maximum of two weeks.

The coating solution was then aspirated and the coverslips were washed twice with autoclaved water then twice with 1X PBS. The coated and washed coverslips were placed in 24 well plates, one coverslip per well. Cells were then seeded on the coverslips at a density of 0.3 millions per well in 0.5 ml DMEM media.

3.2.3 Transfection using Lipofectamine method

The DNA was diluted in OPTIMEM media and vortexed gently to mix. Lipofectamine was also diluted in equal volume of the same OPTIMEM media. FBS and antibiotics were eliminated to avoid hindrance of the formation of lipofectamine/DNA complexes. The diluted lipofectamine solution was then incubated for 5 minutes at RT after which the DNA solution was added to it slowly and vortexed gently to mix. The DNA/lipofectamine

mix was incubated for 20 mins at RT then added to cells in culture. The cells were allowed to sit in the transfection mix for some time to enable the expression of NMDAR at 37 °C and 5% CO_2 humidified incubator.

3.2.4 Immunocytochemistry

HEK Cells were grown on 12 mm glass coverslips as described earlier. The cells were seeded at a density of 0.3 mio in 0.5 ml media. 24 hours after seeding, the cells were fixed on the coverslips by adding 166 µl paraformaldehyde (PFA) (16% solution in 1xPBS) to get a final concentration of 4%. The cells were incubated in the fixation solution for 10 minutes at room temperature (RT). The PFA was then aspirated and the cells were washed twice with 1x PBS containing Ca^{+2} and Mg^{+2}. A solution of 0.1% triton in PBS was added to the cells for 10 min at RT in order to permeabilize the cells. The reason for this permeabilization step is that the epitopes of both the antibodies used against the NR1 and NR2B subunits are intracellular (lie on the C-terminal of the protein). The cells were then washed 2 times with 2ml PBS while shaking each wash for 2-3 minutes on a rocking platform. To block non-specific antibody binding, fixed cells were incubated with 1ml PBS-1% BSA for 30min at room temperature. The coverslips were then transferred on a parafilm sheet and 80ul of first antibody (against either NR1 or NR2B) diluted in PBS-1% BSA was added to it and incubated for 2 hours at RT. Afterwards, the coverslip was transferred in a 24-well plate containing 500 µl PBS / well. Three more washes with 1ml PBS were carried out with each wash lasting 2 to 3 minutes on a rocking platform. The coverslip was moved back on the parafilm sheet and Add

80ul of the second fluorescent antibody diluted in PBS-0.25% BSA for 1 hour at RT then moved back to the 24 well plate to be washed 3x with 1ml PBS where each wash was shaken 2-3minutes on a rocking platform. The nuclei was then stained with Hoechst 1:1000 in PBS for 1min. Afterwards, cells were washed 2x with 1ml PBS and the glass coverslip was mounted on glass slides using 5 µl Fluoromount and kept at 4°C till microscopes analysis.

3.2.5 Western blot

Collection of cell lysate

Cells were splitted and plated in a non-coated 6 well plate, 0.8 mio cells/ well in 2 ml media (DMEM #31966-021+10%HI FBS+ 1% Pen-strep). 24 hours after plating, cells were transfected with NMDAR subunits using Lipofectamine 2000 as described earlier, without changing the media. 24 hours after transfection, the media was aspirated and the cells were washed using 2ml PBS per well. The cells were then collected by adding 1 ml PBS and pipetting up and down to detach cells. The detached cells were then collected in an eppendorf tube, centrifuged at 4C for 10min at 10 rcf. The supernatant was discarded and pellets were stored at -20C or following steps were carried out.

The pellets were thawed on ice, then resuspended in 100 µl lysis buffer + Protease inhibitor (PI) by pipetting up and down and then put on ice. The composition of the Lysis buffer is detailed in table 6.

Table 6 Lysis buffer composition

Lysis buffer	stock	Volumes needed to make 2 ml
50 mM Tris-HCL (PH 7.5)	1M	100 µl
150 mM NaCl	1M	300 µl
1% Triton x-100	10%	200 µl
10% Glycerol	50%	400 µl

The above was sonicated for 10 seconds and then centrifuge at 4C for 20 minutes at 10,000 rcf.

The supernatant was kept and the pellet was discarded.

Electrophoresis

20 µl of the supernatant was mixed with 10 µl of homemade loading dye (3x). The composition of the loading dye is detailed in table 7.

Table 7 Loading buffer composition

Loading buffer:	
Tris HCl (PH 6.8)	62.5 mM

DTT	50 mM
SDS	5.4 %
Glycerol	30%
Bromophenol blue	0.3% w/v

The above mixture was heated at 99C for 10 minutes, then loaded to ready-made SDS-PAGE gradient gel by Biorad (4 %-20%). The gel was run at 50 v in the beginning to enhance separation for 15 minutes, then at 100 v for 75 minutes.

Transfer

PVDF membrane was immersed in 100% methanol for 15 minutes, then soaked in transfer buffer for another 15 min. 1x transfer buffer was prepared using the ready-made 25x buffer+ 20% methanol)

After assembling the sandwich of the gel and the PVDF membrane, wet protein transfer took place at 50v for 2 hours.

Blocking and antibody

The membrane was rinsed in PBS + 0.1% Tween20 (PBST), then incubated in 10% skimmed milk at 4C overnight. The next day the membrane was incubated in the appropriate dilution of the primary antibody in 5% skimmed milk (solubilized in PBST)

for 2 hours. The membrane was then washed 2 times for 5min with PBST then 1 more time for 10 minutes. Afterwards, the membrane was incubated in the appropriate dilution of the secondary antibody in 5% skimmed milk (solubilized in PBST) for 1 hour. The membrane was then rinsed with PBST 2 times, then washed 3 times for 5minutes each in PBST in an addition to a final wash for 15 minutes in PBST. Incubation with a chemiluminescence visualization solution took place in the dark for 5 minutes. Afterwards, the membrane was visualized using image Quanta for 10 sec of exposure.

3.3 Results

3.3.1 Optimization of Transfection conditions

The first step to generate a model expressing functional NMDAR was to transfect the desired NMDAR subunits into CHO (Chinese hamster ovary) and HEK (human embryonic kidney) cells which are easy to grow and maintain and are easily transfectable with high efficiency. The transfection reagent used was lipofectamine 2000 which facilitates the delivery of DNA into the cells (Chesnoy and Huang, 2000; Hirko et al., 2003; Liu et al., 2003). This reagent is composed of cationic lipids which interact with the phosphate backbone of the DNA to form Lipofectamine/DNA complexes, the positive charge on the liposomes also interacts with the negatively charged cell membrane allowing the entrance of the Lipofectamine/DNA complex by endocytosis. Complexes that diffuse through the cytoplasm and reach the nucleus successfully should result in gene expression.

In order to determine the effect of different concentrations of DNA, Lipofectamine and FBS on transfection efficiency, we used two vectors expressing fluorescent proteins so that we can evaluate the transfection efficiency based on the number of cells showing expression of those fluorescent proteins. We used two proteins in order to assess the co-transfection efficiency as well, because the main target is to express functional NMDARs which consists of two subunits, so our goal is to have the same cell express two proteins. The vectors used for transfection in this experiment were pCAG-GFP and pCAG-tdTomato in a 1:1 ratio, the transfection host used was CHO-k1 cells.

CHO-K1 cells were seeded in 24 well plates at a density of $6x10^4$ cells/well in DMEM media described earlier containing 10% FBS. Twenty four hours later, the cells were about 70 % confluent where the media was changed to DMEM containing 1 % FBS for half of the wells and DMEM containing 10% FBS for the other half of wells. In both conditions, the media was antibiotic free. Two hours later transfection was carried out as described earlier. For both conditions (1% and 10%FBS), two concentrations of DNA were used (0.8 µg DNA and 2 µg DNA) along with four different volumes of Lipofectamine 2000 (1 µl, 1.5 µl, 2 µl, 2.5 µl). The media used to dilute both DNA and lipofectamine was Optimem. The composition of the transfection mix is shown in Table 8. Twenty four hours after transfection, cells at the different conditions were imaged using bright field, illumination with UV lamp and use of green filter to visualize GFP and illumination with UV lamp and use of red filter to visualize tdTomato. The GFP and tdTomato fluorescence showed similar expression levels and a high degree of co-

localization, hence the images of tdTomato only are shown for simplicity. Bright field images of control non-transfected cells grown in media containing 1% and 10% FBS are shown in Fig 5. In both conditions, cells looked healthy with a spindle shape that is characteristic of CHO-K1 cells. However, with the 10%FBS condition, cells started to get over confluent and grow on top of each other.

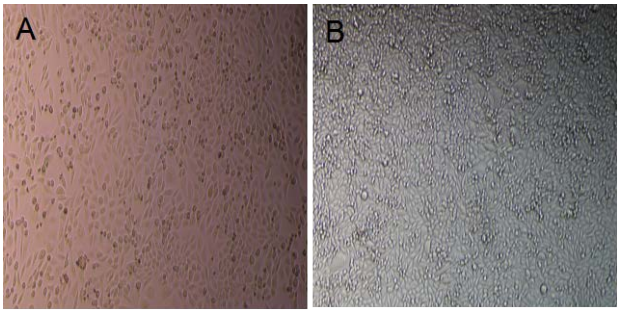

Figure 5 **Control non-transfected cells after 24 hours of transfection**. Panel A shows cells grown in DMEM media supplemented with 1% FBS. Panel B shows cells grown in DMEM media supplemented with 10% FBS

Table 8 composition of transfection mixture in different conditions

Condi -tion	Lipo mix	DNA mix	Serum
1	1µl+50µl opti	0.4µg GFP in PCAGG+ 0.4µg dTomato in PCAGG +50µl opti	1% or 10% FBS
2	1.5µl +50µl opti	0.4µg GFP in PCAGG +0.4µg dTomato in PCAGG +50µl opti	
3	2 µl+50µl opti	0.4µg GFP in PCAGG +0.4µg dTomato in PCAGG +50µl opti	

4	2.5 µl+50µl opti	0.4µg GFP in PCAGG +0.4µg dTomato in PCAGG +50µl opti	
5	1 µl+50µl opti	1µg GFP in PCAGG +1µg dTomato in PCAGG +50µl opti	
6	1.5 µl+50µl opti	1µg GFP in PCAGG +1µg dTomato in PCAGG +50µl opti	
7	2 µl+50µl opti	1µg GFP in PCAGG +1µg dTomato in PCAGG +50µl opti	
8	2.5 µl+50µl opti	1µg GFP in PCAGG +1µg dTomato in PCAGG +50µl opti	

The transfection results of cells grown in 1% FBS media and transfected with a total DNA amount of 0.8 µg is shown in Fig 6. From the bright field images of all different volumes of Lipofectamine, we can see that the cells are in a healthy state and tolerated these transfection conditions. By inspecting the tdTomato panel, we can see that its level of expression decreases with increasing the Lipofectamine volume i.e in panel A with 1 µl Lipofectamine, the transfection efficiency was the highest while in panel D with 2.5 µl the transfection efficiency was the lowest.

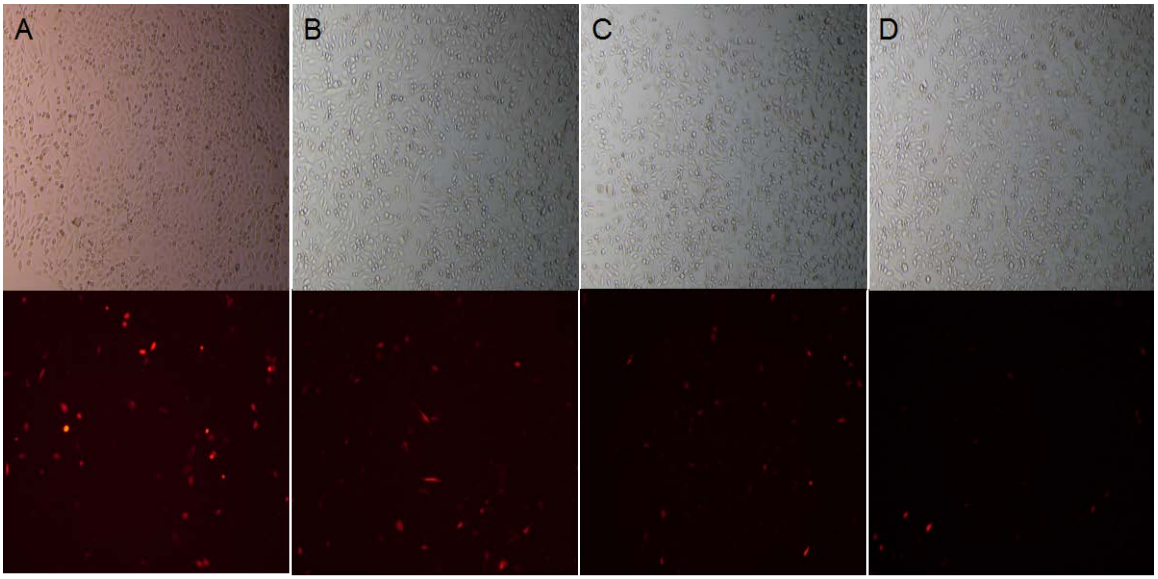

Figure 6 Images of CHO-K1 cells grown in media containing 1% FBS during transfection time and transfected with a total DNA (pCAG-GFP and pCAG-tdTomato) amount of 0.8 µg and different volumes of lipofectamine 2000. The top panel shows the bright field images of the cells, the bottom panel shows the fluorescence of tdTomato expressed protein. The volume of lipofectamine used was 1 µl, 1.5 µl, 2 µl, 2.5 µl, in panels A,B,C,D correspondingly.

The transfection results of cells grown in 1% FBS media and transfected with a total DNA (pCAG-GFP and pCAG-tdTomato) amount of 2 µg (shown in Fig 7) and those grown in 10% FBS media and transfected with a total DNA amount of 2 µg (shown in Fig 9) were comparable. From the bright field images, we can see that with 2 µl and 2.5 µl Lipofectamine (panels C and D), the cells are showing some dead clumps indicating that these transfection conditions are moderately stressful to the cells. However, the latter conditions (panels C and D) show the highest transfection efficiency in terms of tdTomato expression, in particular panel D showed striking expression levels.

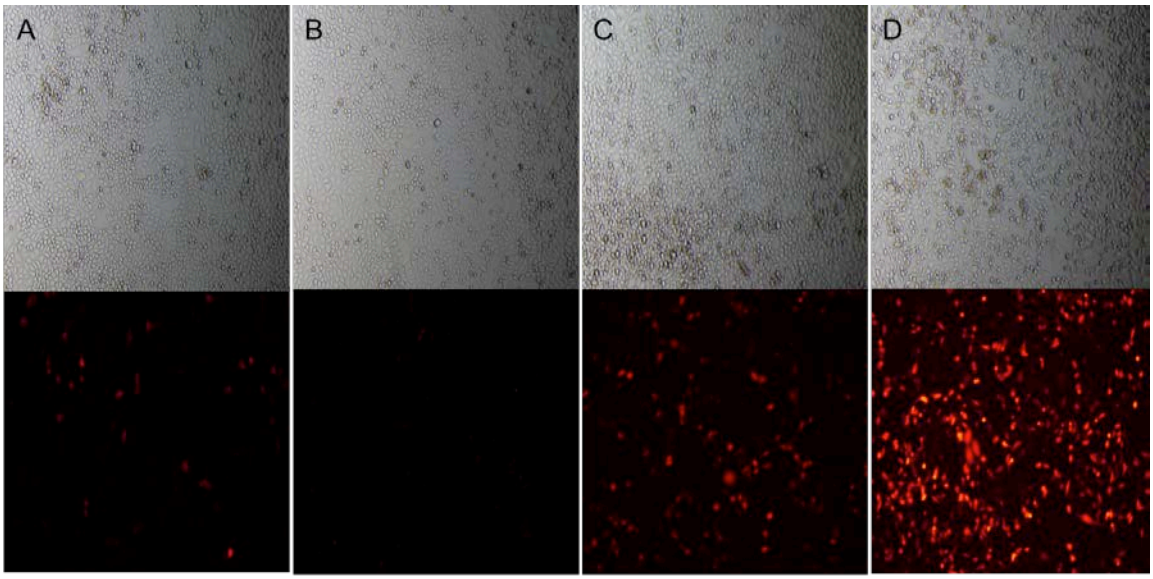

Figure 7 Images of CHO-K1 cells grown in media containing 1% FBS during transfection time and transfected with a total DNA (pCAG-GFP and pCAG-tdTomato) amount of 2 µg and different volumes of lipofectamine 2000. The top panel shows the bright field images of the cells, the bottom panel shows the fluorescence of tdTomato expressed protein. The volume of lipofectamine used was 1 µl, 1.5 µl, 2 µl, 2.5 µl, in panels A,B,C,D correspondingly.

The transfection results of cells grown in 10% FBS media and transfected with a total DNA amount of 0.8 µg is shown in Fig 8. From the bright field images of all different volumes of Lipofectamine, we can see that the cells are in a healthy state and tolerated these transfection conditions. By inspecting the tdTomato panel, we can see that the level of expression is highest when a volume of 1.5 µl or 2 µl of Lipofectamine is used (panels B and C). Using 1 µl of Lipofectamine (Panel A) showed the weakest expression of tdTomato in these conditions.

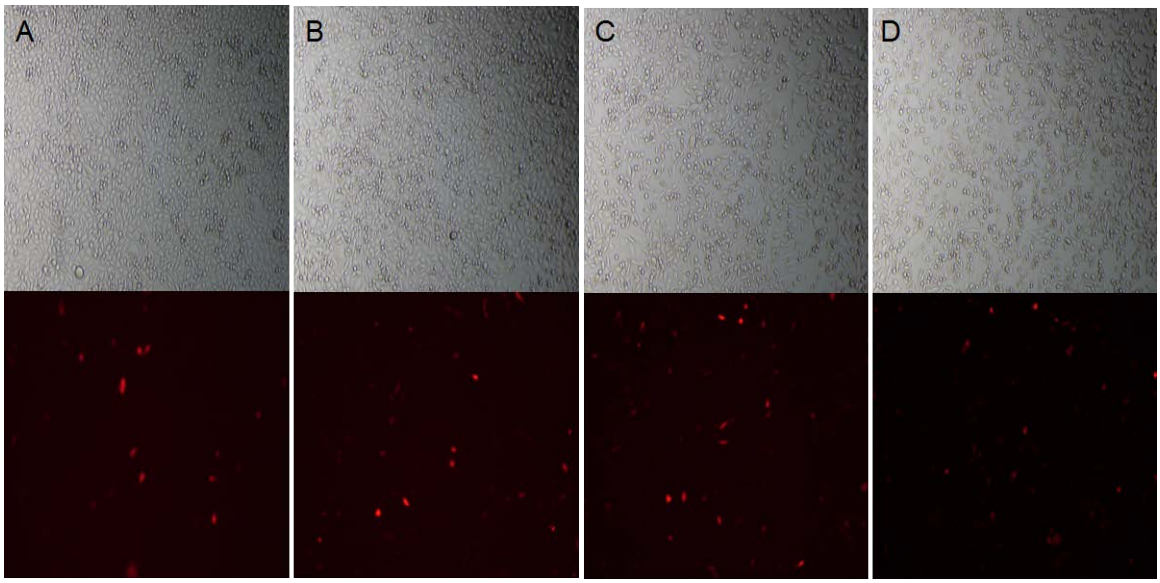

Figure 9 Images of CHO-K1 cells grown in media containing 10% FBS during transfection time and transfected with a total DNA (pCAG-GFP and pCAG-tdTomato) amount of 0.8 µg and different volumes of lipofectamine 2000. The top panel shows the bright field images of the cells, the bottom panel shows the fluorescence of tdTomato expressed protein. The volume of lipofectamine used was 1 µl, 1.5 µl, 2 µl, 2.5 µl, in panels A,B,C,D correspondingly.

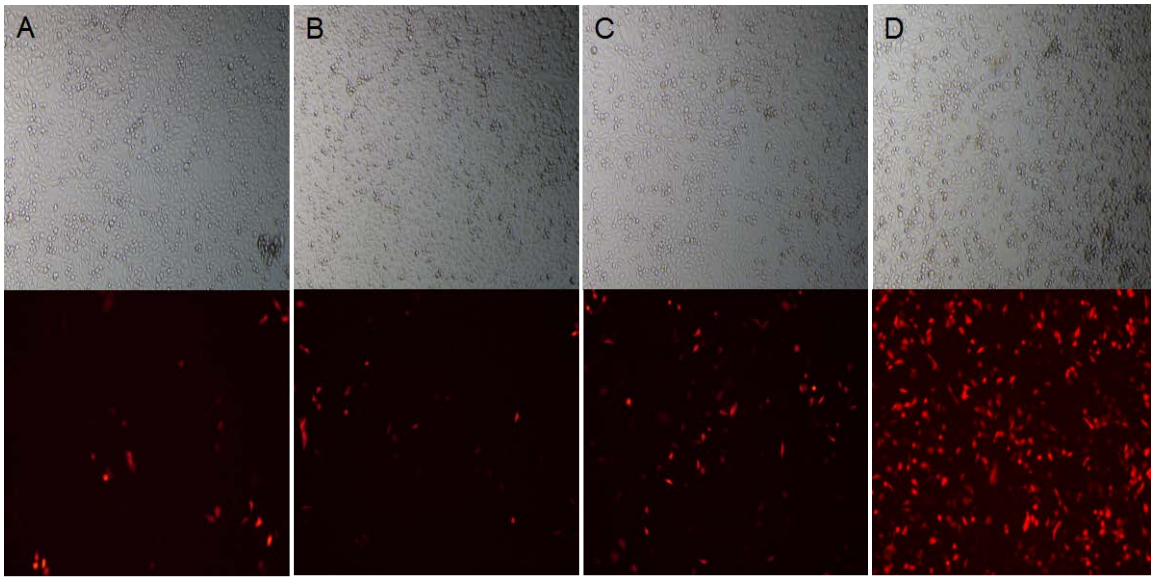

Figure 8 Images of CHO-K1 cells grown in media containing 10% FBS during transfection time and transfected with a total DNA (pCAG-GFP and pCAG-tdTomato) amount of 2 µg and different volumes of lipofectamine 2000. The top panel shows the bright field images of the cells, the bottom panel shows the fluorescence of tdTomato expressed protein. The volume of lipofectamine used was 1 µl, 1.5 µl, 2 µl, 2.5 µl, in panels A,B,C,D correspondingly.

In summary, the ratio between DNA and Lipofectamine concentration plays a significant role in determining the transfection efficiency. Very high concentrations of DNA and Lipofectamine can be stressful on the cells so a balance between the health of the cells and the transfection efficiency has to be taken into consideration.

3.3.2 Immunostaining of NR1 and NR2B subunits

Following the transfection of NR1 and NR2B subunits into HEK cells, validation for the expression of NMDAR subunits at the protein level was required. To this end, we did immunostaining to visualize the expression of these subunits and also to visualize the location of their expression. In this experiment, HEK cells were used as the host. Cells were seeded on 12 mm glass coverslips coated with poly D-Lysine at a density of $0.3x10^6$ cells per well in a 24 well plate containing DMEM 31966. Eighteen hours later, the media was changed to DMEM Sigma D3050 and transfection was done two hours after the media change in the presence of D-AP5 as described earlier in the materials and methods section. Transfection was done using NR1 and NR2B subunits as detailed in table 9.

Table 9 composition of transfection mix

Transfection mix per well	20 µl sigma D3050 w/o serum or antibiotics + 0.25 µg NR1 in pCEP4+ 0.25 µg NR2B in pCEP4	20 µl D3050 w/o serum+ 1 µl lipofectamine 2000	D-AP5 at a final concentration of 500 µM

After eighteen hours, cells were fixed using paraformaldehyde in preparation for immunostaining. The cells were incubated with two primary antibodies; mouse anti NR1 at a dilution of 1:100 and rabbit anti NR2B at a dilution of 1:500. Two secondary antibodies were used; anti mouse Alexa Fluor 488 (green against NR1) and anti-rabbit Alexa fluor 563 (red against NR2b), both at a dilution of 1:500 along with Hoechst nuclei stain at a dilution of 1:1000. Images were taken using an inverted confocal microscope under 40x magnification using the appropriate filters as shown in Fig 10.

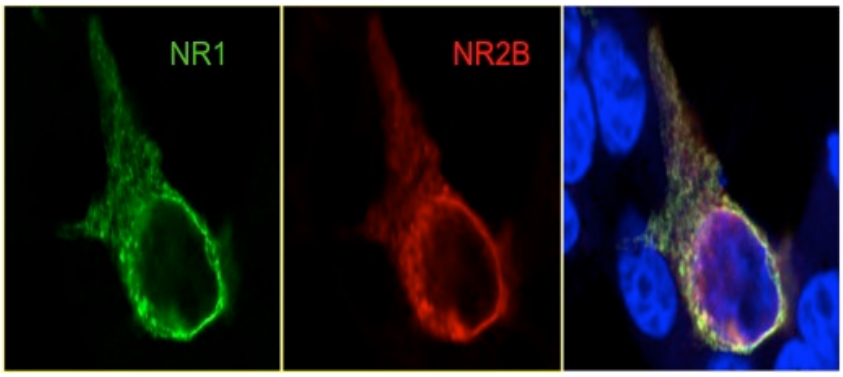

Figure 10 Immunostaining of HEK cells transfected with both NR1 and NR2B subunits. Two sets of antibodies were used to stain the cells; mouse anti NR1, anti-mouse Alexa Fluor 488 and rabbit anti NR2B, anti-rabbit Alexa Fluor 563. On the left panel, the image was taken using the green filter to visualize the expression of NR1 subunit. In the middle panel, the image was taken using the red filter to visualize the expression of NR2B subunit. In the right panel, a merge of green, red and blue filters. Blue color represents Hoechst, the nuclei stain.

By inspecting the images, we can see that both the NR1 and NR2B subunits are expressed in the same cell. We can also see that not all cells are successfully transfected or successfully express the NMDAR subunits. About the localization of the expressed receptor, it is apparent that the receptor subunits are expressed on the periphery of the cell meaning that they are displayed on the cell membrane, however this is not

conclusive because the epitopes of the primary antibodies lie intra-cellularly on the C terminus, so we had to permeabilize the cells before adding the antibodies.

3.3.3 Western blot of wild type and mutated NR1, NR2B and NR2A

In the following experiment, HEK cells were used to validate the expression of the subunits NR1 and NR2B. Cells were seeded on uncoated 6 well plate in DMEM 31966 media then 24 hours later transfection was done as detailed earlier in the materials and methods section. tdTomato was used as a marker for transfection efficiency. The different transfection conditions are shown below in Table 10.

Table 10 transfection conditions used to detect the expression of NR1 and NR2B on the protein level

Condition	Lipofectamine	DNA
Control non transfected (NT)		
tdTomato	2 µl Lipofectamine 2000+ 40 µl Optimem	0.25 µg tdTomato pCAG+ 40 µl Optimem
NR1	2 µl Lipofectamine 2000+ 40 µl Optimem	0.5 µg NR1 pCEP 4+ 40 µl Optimem
NR2B	2 µl Lipofectamine 2000+ 40 µl Optimem	0.5 µg NR2B pCEP + 40 µl Optimem
NR1+NR2B	2 µl Lipofectamine 2000+ 40 µl Optimem	0.5 µg NR1 pCEP +0.5 µg NR2B pCEP4+ 40 µl Optimem

NR1+NR2B+tdTomato	2 µl Lipofectamine 2000+ 40 µl Optimem	0.5 µg NR1 pCEP4+0.5 µg NR2B pCEP4+ 0.25 µg tdTomato pCAG+ 40 µl Optimem

The cell lysate was used to prepare two western blots. The first blot was used to detect the expression of the NR1 subunit using NR1 mouse monoclonal primary antibody at a dilution of 1:10,000 and goat anti mouse antibody at dilution of 1: 20,000 as a secondary antibody. The second blot was used to detect the expression of the NR2B subunit using NR2B rabbit polyclonal primary antibody at a dilution of 1:5000 and goat anti rabbit antibody at dilution of 1:10,000 as a secondary antibody. As shown in Fig 11, expression of the NR1 subunit, which has a protein size of 112.69 kDa, and the NR2B subunit, which has a protein size of 167 kDa, was detected by western blot. The subunits were successfully expressed either as single subunits or co-existing in the same cells or even coexisting with tdTomato. Control cells that didn't undergo any transfection and cells transfected with tdTomato only didn't show any bands for NR1 or NR2B confirming the specificity of the antibodies used.

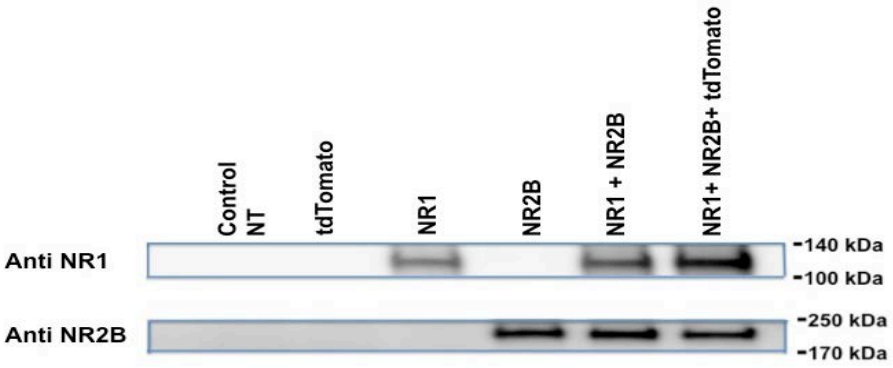

Figure 11 Western blots showing the expression of WT NR1 (upper panel) and WT NR2B subunits (lower panel) in transfected HEK cells.

In another independent experiment, the expression of the WT NR2A subunit was tested also by using HEK cells as the transfection host. Transfection conditions are shown in Table 11.

Table 11 transfection conditions used to detect the expression of NR2A on the protein level

Condition	Lipofectamine	DNA	NMDAR anatagonist
Control non transfected (NT)			none
NR2A	2 µl Lipofectamine 2000+ 40 µl Optimem	0.5 µg NR2A pCDNA 3.1+ 0.125 µg tdTomato pCAG+ 40 µl Optimem	none

NR2A mouse monoclonal primary antibody was used at a dilution of 1:1000 and goat anti mouse antibody at dilution of 1:20,000 as a secondary antibody, results are shown in Fig 12. Results confirmed the expression of the WT NR2A subunit which has a protein size of 167 kDa. The subunit was successfully expressed as a single subunit. Control cells that didn't undergo any transfection didn't show any bands for NR2A confirming the specificity of the antibodies used.

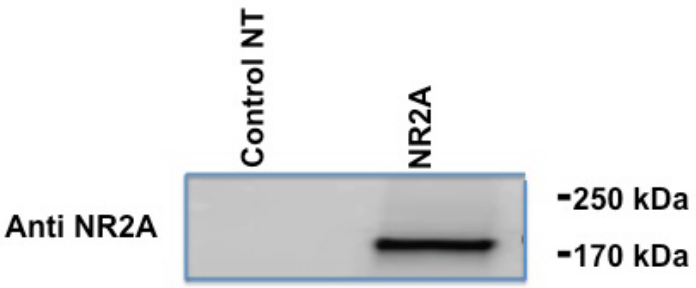

Figure 12 Western blots showing the expression of WT NR2A in transfected HEK cells

Since we had confirmed the successful expression of the wild type subunits of NMDAR, we went further and validate the expression of the mutated subunits. A western blot for each of the subunits, WT and mutants, was prepared using the same antibody conditions as detailed earlier. As seen in Fig 13A, successful detection of the mutated NR1 C79.320S was shown, however the mutated NR1 C79.320S, C744.798A was not detected. In Fig 13B, the expression of the mutated NR2B C86.320S was not detected. In Fig 13C, the expression of all NR2A mutants (NR2A C320.87A, NR2A C87A and NR2A C320A) were successfully detected. For the constructs that we weren't successfully able to detect (NR1 C79.320S, C744.798A and NR2B C86.320S), these were already fully sequenced before and no alterations were found. We speculate that the failure to detect them might be due to alterations in the epitope of the primary body caused by the mutations; hence the antibody cannot recognize the protein. However, this is not conclusive as it might also be due to a failure in their expression.

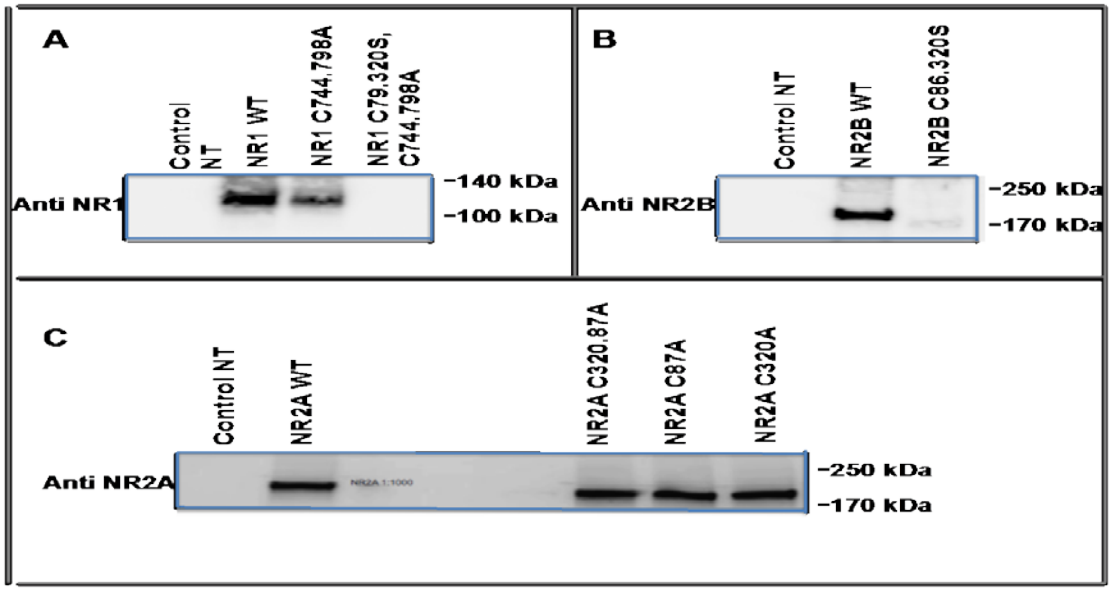

Figure 13 Western blot showing the expression of different mutants of NMDAR subunits. Panel A shows the expression of WT NR1, mutated NR1 C744.798A and mutated NR1 C79.320S, C744.798A in HEK cells. Panel B shows the expression of WT NR2B and mutated NR2B C86.320S in HEK cells. Panel C shows the expression of WT NR2A, mutated NR2A C320.87A, NR2A C87A and NR2A C320A. panel C is adapted from Ohood Al Zahrani master thesis

Chapter 4

Validating that the model system is functional and that the expressed NMDARs can be activated in a reliable manner.

4.1 Significance

In previous chapters, we had established a model where we were able to detect the expression of various NMDAR subunits. However, the characterization and functionality of those expressed NMDARs were not investigated yet. The aim of this chapter is to show that the expressed NMDARs are functional and to characterize their biophysical properties. The technique we focused on is fluorescent calcium imaging.

4.2 Materials and methods

4.2.1 Cell culture

Explained earlier in chapter 3

4.2.2 Seeding cells on glass coverslips

12 mm glass coverslips were coated with 0.1 mg/ml poly-D-lysin for 20 mins at 37C to enhance cell attachment and prevent detachment during perfusion conditions. The poly-D-Lysine was stored in aliquots of stock solution at a concentration of 10g/L then diluted to working solution at a concentration of 0.1 mg/ml which was stored at 4C for a maximum of two weeks.

The coating solution was then aspirated and the coverslips were washed twice with autoclaved water then twice with 1X PBS. The coated and washed coverslips were placed in 24 well plates, one coverslip per well. HEK 293/T17 cells were then seeded on the coverslips at a density of 0.3 millions per well in 0.5 ml DMEM media.

18 hours post seeding, the cells were about 80 % confluent and that's when the media was aspirated, cells washed once with 1X PBS and then media was replaced with 0.5 ml of DMEM (Sigma D3050). The latter media was prepared by adding glucose to a final concentration of 5 mM, $NaHCO_3$ to a final concentration of 3.7 g/L and 10% FBS. The logic behind using this custom made media was to; 1- reduce glucose concentration to 5 mM in an attempt to decrease the L-lactate production by the cells, to increase the chances of L-lactate entering the cells when added extracellular. 2- Avoid Glutamax and Glutamine which are potential sources of Glutamate that can case excitotoxicity to the cells through the expressed NMDARs. 3- Avoid addition of antibiotics which can hinder the transfection process.

4.2.3 Transfection

Two hours post changing the media to the above described DMEM media (Sigma D3050). The transfection transfection mix was prepared as in table 12.

Table 12 composition of transfection mix used for calcium imaging

Mastermix for 6	120 µl sigma D3050 w/o serum or antibiotics + 1.5 µg NR1 in pCDNA3.1+	120 µl D3050 w/o serum+ 6 µl lipofectamine 2000	D-AP5 at a final concentration of

coverslips.	1.5 µg NR2A in pCDNA 3.1		500 µM

The DNA was diluted in DMEM media (Sigma # D3050) and vortexed gently to mix. Lipofectamine was also diluted in the same DMEM media. Again FBS and antibiotics were eliminated to avoid hindrance of the formation of lipofectamine/DNA complexes. The diluted lipofectamine solution was then incubated for 5 minutes at RT after which the DNA solution was added to it slowly and vortexed gently to mix. The DNA/lipofectamine mix was incubated for 20 mins at RT. The DNA concentration for the two NMDAR subunits NR1 and NR2A/NR2B was always kept at a 1:1 ratio. The DNA: Lipofectamine ratio was always kept at 1:2. 40 µl of the latter mix was then added to each well in a drop wise manner with gentle movement of the plate for mixing. D-AP5 a competitive NMDA receptor glutamate site antagonist was then added to the cells to a final concentration of 500 µM to block the to be expressed NMDARs and avoid excitotoxicity. The above mentioned quantities in the table were used for a master mix to transfect 8 wells in a 24 well plate and the quantities were either scaled up or down depending on the size of the experiment. Cells were allowed to sit in the transfection mix for 20-24 hours to enable the expression of NMDAR at 37C and 5%CO_2 humidified incubator.

4.2.4 Calcium imaging

Preparation of HBS

1X HBSS with 1mM Glucose, 295 mOsm

NaCl 150 Mm

KCl 3 mM

HEPES 10 mM

Glucose 1 mM

$CaCl_2$ 2 mM

NaOH to adjust pH to 7.4

Split the 1X HBSS into 2 bottles:

Bottle 1, Add stimulants as required according to the experimental aim.

Bottle 2: Add $MgCl_2$ to a final concentration of 2 mM. Magnesium binds tightly to the pore of NMDAR blocking it and preventing other ions like Calcium from passing through the pore, thus avoiding excitotoxicity.

Staining cells with Fluo-4 AM

After 20-24 hours of transfection of cells, the cells were stained with the cell permeable Calcium sensitive fluorescent dye (Fluo4- AM) (Invitrogen #F14201) at a final

concentration of 5 µM. To prepare the staining solution, a vial of Fluo4-AM was solubilized in DMSO to prepare a stock solution. The desired amount of Dye stock solution was then vortexed with an equal amount of 20% w/v solution of pluronic acid (Sigma # P2443) to facilitate the entrance of the dye into solution. The dye/pluronic acid mix was then mixed into HBSS by vortexing to a final concentration of 5 µM. D-AP5 was added to the staining solution to a final concentration of 500 µM to prevent excitotoxicity during the staining time. To stain the cells, they were taken out of the incubator, DMEM media aspirated and discarded then replaced with the staining solution. The cells were incubated with the staining solution for 20 minutes at room temperature. Incubation was done at RT to reduce the possibility of dye compartmentalization. The dye solution was then discarded and the cells were washed once with HBSS to wash off excess dye. The cells were then incubated with HBSS with D-AP5 (500 µM) at RT for another 10 minutes to allow time for cleavage of all the AM moieties by intracellular esterases to make sure the dye is trapped inside the cell and minimize the chances of dye leakage during imaging.

Fluorescent Imaging

An upright Zeiss fluorescence microscope was used for imaging. A chamber (describe) was used where the coverslips were placed and perfused and a 40x water immersion objective (catalogue no) was used to acquire the images. A time course series was recorded using a Fluo-4 filter (λ_{ex} 495 nm; λ_{em} 516 nm) with an image taken every 2

seconds at a gain of 200 ms and a mercury lamp intensity of 15 %. The software used was Zen pro imaging system.

A reliable perfusion system operated by gravity was used to perfuse the cells at a rate of 1ml/min throughout the time series recording. The experiment is usually initiated by recording the fluorescence intensity of Fluo4 while perfusing the cells with HBSS containing 2 mM $MgCl_2$. The aim of this step is to collect information about the basal Calcium levels in the cells, which will then be, used a reference for normalization of data. The base line recording is followed by a stimulation period where desired stimulants (ex: Glutamate, Glycine, L-lactate, etc.) is perfused to stimulate the cells. Finally, the cells are perfused with HBSS containing 2 mM $MgCl_2$ again to wash out the stimulants to get an idea about the kinetics of the fading out of the stimulation. Also this washing step helps us differentiate live healthy cells (show a decrease in fluorescence upon washout and tend to return to basal Calcium levels) from dead cells (doesn't respond to washout and the fluorescence signal keeps in increasing).

4.2.5 Analysis of images

Image J was used for analysis. One hundred random cells were manually selected from the field of view using the ROI tool. The average fluorescence per ROI was then measured in each image over the time series recorded. The average fluorescence of the baseline (F_0) for each cell was then calculated and the rest of the fluorescence

measurements (F) throughout the time series were normalized against that average (F/F0) using a custom made MATLAB script. Afterwards cells were filtered using Excel based on a predefined filter and the cells that passed the filter were averaged to collect data about the fold change of Calcium fluorescence upon stimulation. In addition, Graphpad prism was used to analyze the frequency distribution of the peak value among cells expressed in percentage of total number of cells analyzed. Graphpad prism was also used to run the statistical measurements and tests.

4.3 Results

4.3.1 Reliability of Fluo-4Am in establishing a graded response

In order to validate the choice of Fluo-4 AM as a calcium dye indicator and that it's compatible with the changes in the amounts of calcium we want to spot, a dose response experiment was carried out using 10 µM, 1 µM, 0.1 µM, 0.01 µM of glutamate. Again the cell line of choice was HEK293 T/17 expressing recombinant NR1 WT/NR2A WT.

By analyzing Fig 14, we can see that the change in glutamate concentration used for stimulation reflects very well in the increase of the fluorescence signal by Fluo4-AM. In Fig 14A, there is a clear distinction between the average amplitude of response in the case of using 10 µM glutamate (maximum peak value is 5.0 ±0.16) as when compared to the other concentrations (1 µM, 0.1 µM, 0.01 µM) whose maximum peak values were 2.9 ± 0.1, 3.1 ± 0.16, 3.3 ± 0.35 respectively. However, there is no clear distinction

between the average amplitude of response when using lower concentrations of glutamate. Also, the speed of initiation of the response differs with changes in the concentration of glutamate, with 10 μM providing the fastest initiation (time to peak value is 10 seconds) and 0.01 μM resulting in the slowest initiation (time to peak value is 64 seconds). In Fig 14B, the percentage of cells showing peak values ≥ average of baseline+ 3 times standard deviation of baseline decreased gradually with decreasing concentration of glutamate from 10 μM to 0.1 μM (65% in case of 10 μM glutamate, 41 % incase of 1 μM glutamate, 23.5 in the case of 0.01 μM glutamate and 6.5 % in the case of 0.01 μM glutamate). In Fig 14C, we can see the peak value frequency distribution of cells that passed our specified criteria, it is obvious that the percentage of cells showing the highest peak values increases with increasing the concentration of glutamate. For the 0.01 μM concentration, the highest percentage of cells have peak values which lie between 1.5 and 2.5, also the maximum peak value is around 6. On the other hand, for the 10 μM concentration, the highest percentage of cells have peak values which lies between 4.5 and 6.5, and the maximum peak value is around 9.

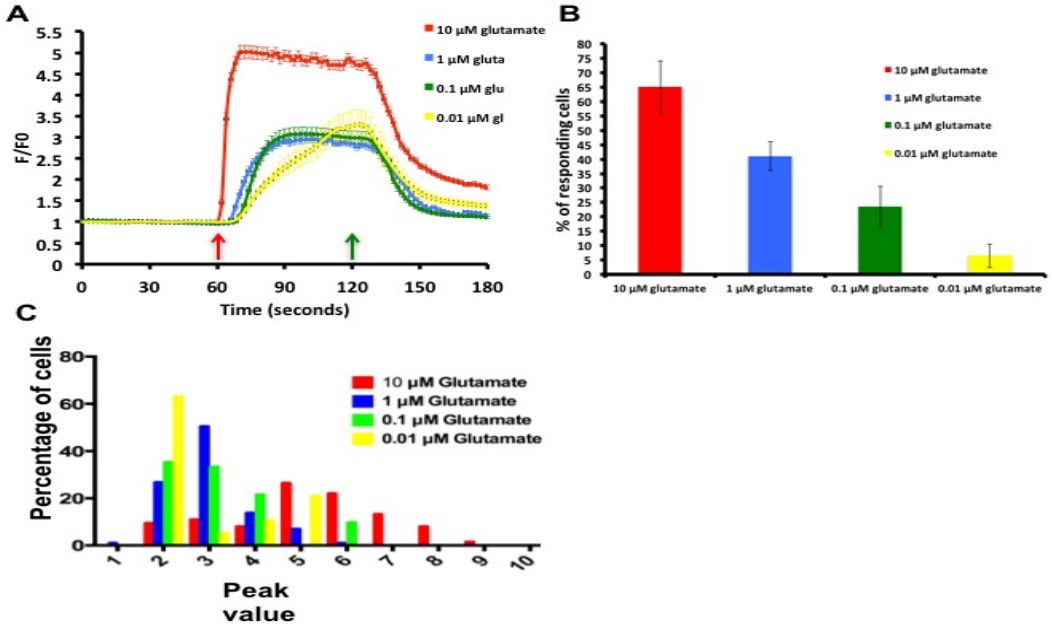

Figure 14 Stimulation of HEK 293T/17, transfected with NR1WT/NR2AWT, with different doses of Glutamate; 10 µM (red), 1 µM (blue) , 0.1 µM (green) , 0.01 µM (Yellow). A) Average of fold increase in fluorescence of single cells upon stimulation. Red arrow signals the start of stimulation, green arrow signals the start of wash off. Error bars are expressed as SEM. Cells analyzed were from two different coverslips from the same experiment for each condition. Number of cells analyzed expressing NR1/NR2A and showing peak values >= average of baseline+ 3 times standard deviation of baseline in response to 10 µM , 1 µM, 0.1 µM, 0.01 µM were 130, 82, 47, 13 respectively from two different coverslips from the same experiment for each condition. B) A bar graph showing the quantity of cells whose peak values is >= average of baseline+ 3 times standard deviation of baseline. The quantity of cells is expressed as a percentage of the total number of analyzed cells. C) Peak value distribution as a percentage of total cells whose peak values is >= average of baseline+ 3 times standard deviation of baseline. The width of each bin is 1.

In conclusion, the average amplitude of response, speed of initiation of response, percentage of responding cells that satisfy our pre-set criteria and frequency of peak value distribution are all measures that can be used to differentiate the characteristics of the response of recombinant NR1/NR2A when stimulated with 10 µM glutamate versus 1 µM Glutamate or any lower concentration. On the other hand, care should be taken when comparing responses to 1 µM glutamate and lower concentrations. When comparing those low concentrations, we shouldn't rely on the average amplitude of response as this seems to be comparable among all tested concentrations (1 µM, 0.1

μM, 0.01 μM). However, the percentage of responding cells that satisfy our preset criteria and frequency of peak value distribution show robust changes among these low concentrations and should be relied on in future experiments when working with that range of low concentrations of glutamate.

4.3.2 Use of Ionomycin on HEK 293T/17 led to rapid influx of Calcium

Ionomycin is an ionophore that facilitates the passage of Ca^{+2} across the cell membrane. It was used in this experiment as a positive control to ensure that our calcium imaging protocol was reliable. Upon addition of 1 μM Ionomycin, a rapid immediate increase in the Fluo4 fluorescence was seen (Fig.15) with a peak value of 4.5 ± 0.023 fold increase compared to the baseline. This experiment assured us that our calcium imaging protocol was a functional reliable one. HEK cells were seeded on glass coverslips coated with poly-D-Lysine at a density of 0.3 millions in DMEM media containing Glutamax and supplemented with FBS. After 24 hours, cells were stained and imaged as detailed earlier. By analyzing the difference in fluorescence between Fig 15 B and Fig 15 C, we can see that all the cells showed an increase in their fluorescence intensity after the addition of ionomycin as it targets all the cell membranes without any distinction.

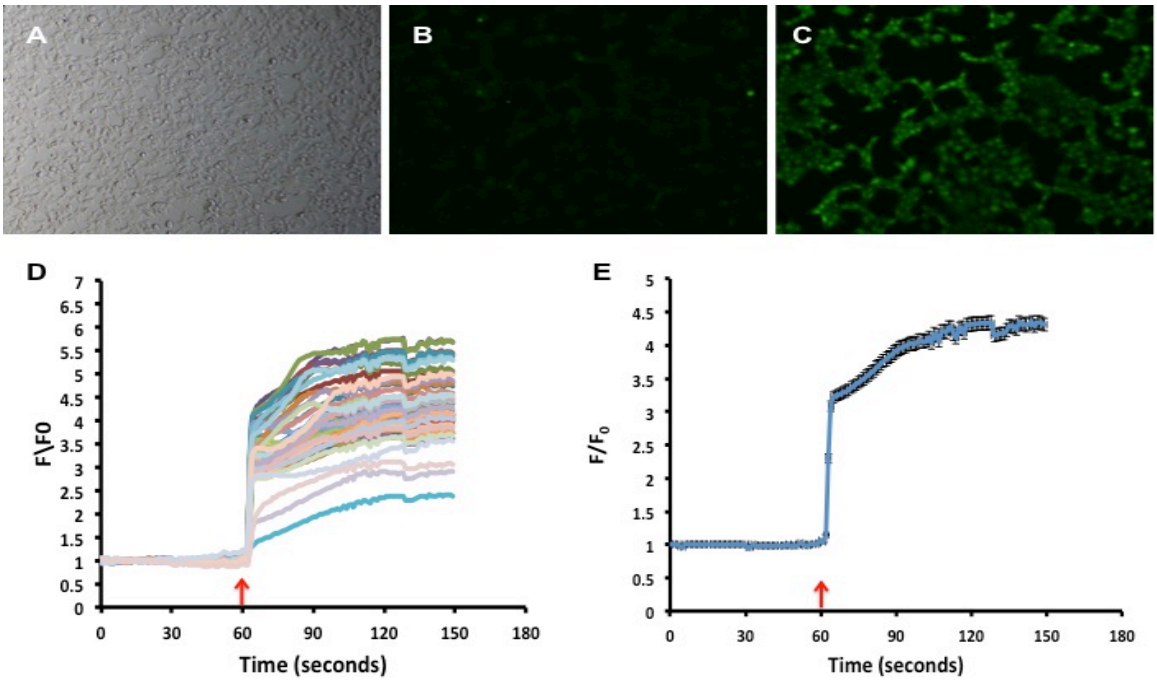

Figure 15 Effect of stimulation of HEK 293T/17 cells with 1 µM Ionomycin. A) Bright field image of HEK cells before imaging. B) cells after staining with Fluo-4 and before stimulation with Ionomycin. C) cells stained with Fluo-4 after stimulation with Ionomycin showing the rapid increase in fluorescence. D) Normalized fluorescence intensity traces of single cells. A baseline was recorded for 1 minute then stimulation with Ionomycin was done for 1.5 minutes. Number of analyzed cells n= 50 randomly selected from one coverslip. The red arrow shows the beginning of stimulation. E) Average of normalized fluorescence intensity traces shown in D with error bars shown as SEM.

4.3.3 Activation of recombinant NMDA receptors by glutamate and glycine

We showed in previous chapters that the expression of NMDAR subunits (NR1, NR2A, NR2B) was detectable both by immunocytochemistry and by Western blotting. However, the functionality of the recombinant receptor where both subunits come together to form a channel that opens and closes in response to different stimuli wasn't assessed. Here, we used calcium imaging as a means to show the functionality of the receptor. Fig 16 is an explanatory illustration of how cells transfected with NR1/NR2A subunits responded to the addition of glutamate. Only some of the cells showed an increase in their fluorescence upon addition of glutamate indicating that they are

expressing both NR1 and NR2A subunits as a functional receptor. On the other hand, some other cells didn't show any change in their fluorescence intensity level upon addition of glutamate. We hypothesize that that those cells are either not expressing any NMDAR subunits, expressing only a single subunit, or expressing functional NMDARs with low expression levels where the added amount of glutamate is below its activation threshold. Fig 16 A shows how ROIs are selected by manually drawing circles on the periphery of the cells, Fig 16 B shows the change in fluorescence intensity after addition of glutamate and Fig 16 C shows the normalized fluorescence intensity of those selected cells over time.

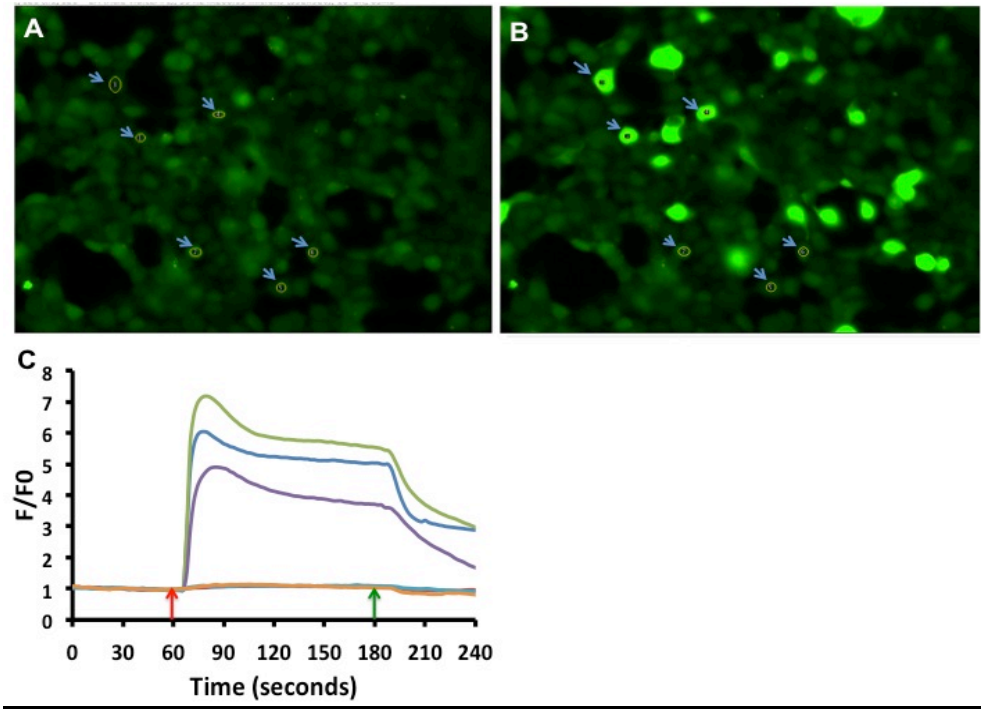

Figure 16 Explanatory figure showing selection of ROI and analysis method using HEK cells transfected with NR1/NR2A. A) Cells stained with fluo-4 before stimulation and selection of ROI. B) Fluorescence intensity of cells after stimulation with 1 µM Glutamate and 1 µM Glycine. C) Normalized fluorescence intensity of corresponding ROI over time, red arrow indicates the beginning of stimulation, green arrow indicates the beginning of washout.

4.3.4 Effect of 1 µM Glutamate on NR1WT/NR2AWT and NR1WT/NR2BWT

In order to test the functionality of the expressed NMDAR, different doses of glutamate and glycine were used for stimulation of NR1/NR2A and NR1/NR2B. Furthermore, we wanted to characterize the properties of both NMDAR types relative to each other and see how they match with previous studies. In the following experiment we used 1 µM glutamate and 1 µM glycine for stimulation.

As shown in Fig 17A, the kinetics of the initiation of response in the case of NR1WT/NR2AWT is faster than in the case of NR1 WT/NR2BWT, for the NR1/NR2A the time to peak value was 16 seconds and for the NR1/NR2B was 24 seconds. Also, the maximum peak value shows a bigger fold change in case of NR1WT/NR2AWT compared to NR1WT/NR2BWT (4.3 ± 0.13 versus 3.6 ± 0.2 correspondingly). When inspecting the number of cells that passed the filtering criteria (peak values is >= average of baseline+ 3 times standard deviation of baseline), we found that it was higher in case of NR1WT/NR2AWT compared to NR1WT/NR2BWT as shown in Fig 17 B (39 ± 5.5 versus 26 ± 0 correspondingly). Finally looking at the peak value frequency distribution in Fig 17 C, we found that the percentage of cells whose peak values are between 0.5 and 2.5 are higher in NR1WT/NR2BWT compared to NR1WT/NR2A WT. On the contrary, the percentage of cells whose peak values are between 3.5 and 8.5 are higher in NR1WT/NR2AWT compared to NR1WT/NR2BWT. To summarize, the overall response of NR1WT/NR2AWT in terms of average of increase in fluorescence, number of responding

cells and the shift of peak values towards bigger values was higher in NR1WT/NR2AWT compared to NR1WT/NR2BWT.

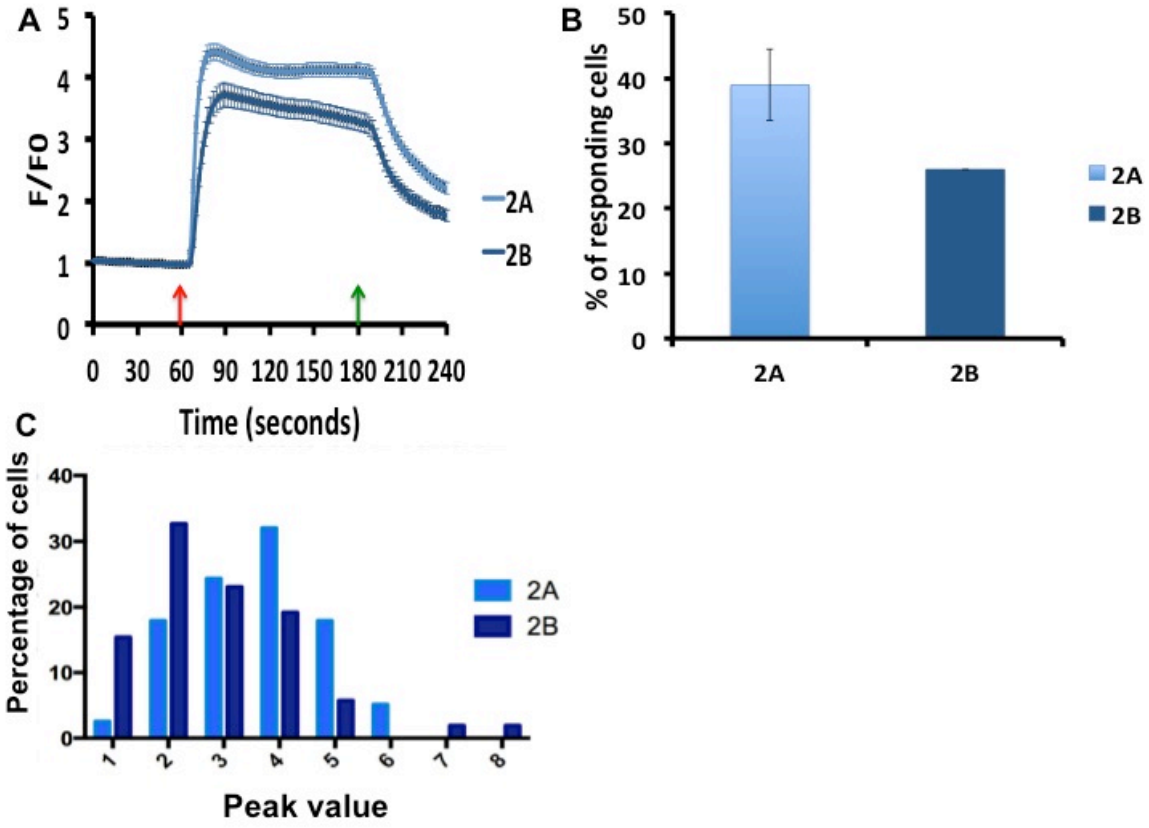

Figure 17 Stimulation of HEK 293T/17 cells transfected with either NR1WT/NR2AWT or NR1WT/NR2BWT with 1 µM Glutamate and 1 µM Glycine. Light blue color represents cells transfected with NR1/NR2A, dark blue color represents cells transfected with NR1/NR2B A) Average of fold increase in fluorescence of single cells upon stimulation. Red arrow signals the start of stimulation, green arrow signals the start of wash off. Error bars are expressed as SEM. Number of cells analyzed expressing NR1/NR2A was 78, number of cells analyzed expressing NR1/NR2B was 52. Cells analyzed were from two different coverslips from the same experiment for each condition B) A bar graph showing the quantity of cells whose peak values is >= average of baseline+ 3 times standard deviation of baseline. The quantity of cells is expressed as a percentage of the total number of analyzed cells. Error bars are shown as SEM. C) Peak value distribution as a percentage of total cells whose peak values is >= average of baseline+ 3 times standard deviation of baseline. The width of each bin on the x-axis is 1.

4.3.5 Effect of 0.25 µM Glutamate on NR1WT/NR2AWT and NR1WT/NR2BWT

As shown in Fig 18A, the kinetics of the initiation of response in case of NR1WT/NR2AWT is much faster than in case of NR1 WT/NR2BWT, for the NR1/NR2A the time to peak value was 28 seconds and for the NR1/NR2B it was 68 seconds. Also, the maximum peak value shows a much bigger fold change in the case of NR1WT/NR2AWT compared to NR1WT/NR2BWT (4.9 ± 0.2 versus 3.1 ± 0.17 correspondingly). When inspecting the number of cells that passed the filtering criteria (peak values is >= average of baseline+ 3 times standard deviation of baseline), we found that it was much higher in the case of NR1WT/NR2AWT compared to NR1WT/NR2BWT (37.5 % versus 8% correspondingly, almost 4.6X increase) as shown in Fig 18B. Finally looking at the peak value frequency distribution in Fig 18C, we found that the percentage of cells whose peak values are between 0.5 and 3.5 are much higher in NR1WT/NR2BWT compared to NR1WT/NR2A WT. On the contrary, the percentage of cells whose peak values are between 3.5 and 9.5 are much higher in NR1WT/NR2AWT compared to NR1WT/NR2BWT. In addition, the maximum peak value for the NR1WT/NR2BWT didn't exceed 3.5, however for the NR1WT/NR2AWT it went up to 9.5. To summarize, the overall response of NR1WT/NR2AWT in terms of average of increase in fluorescence, number of responding cells and the shift of peak values towards bigger values was significantly higher in NR1WT/NR2AWT compared to NR1WT/NR2BWT.

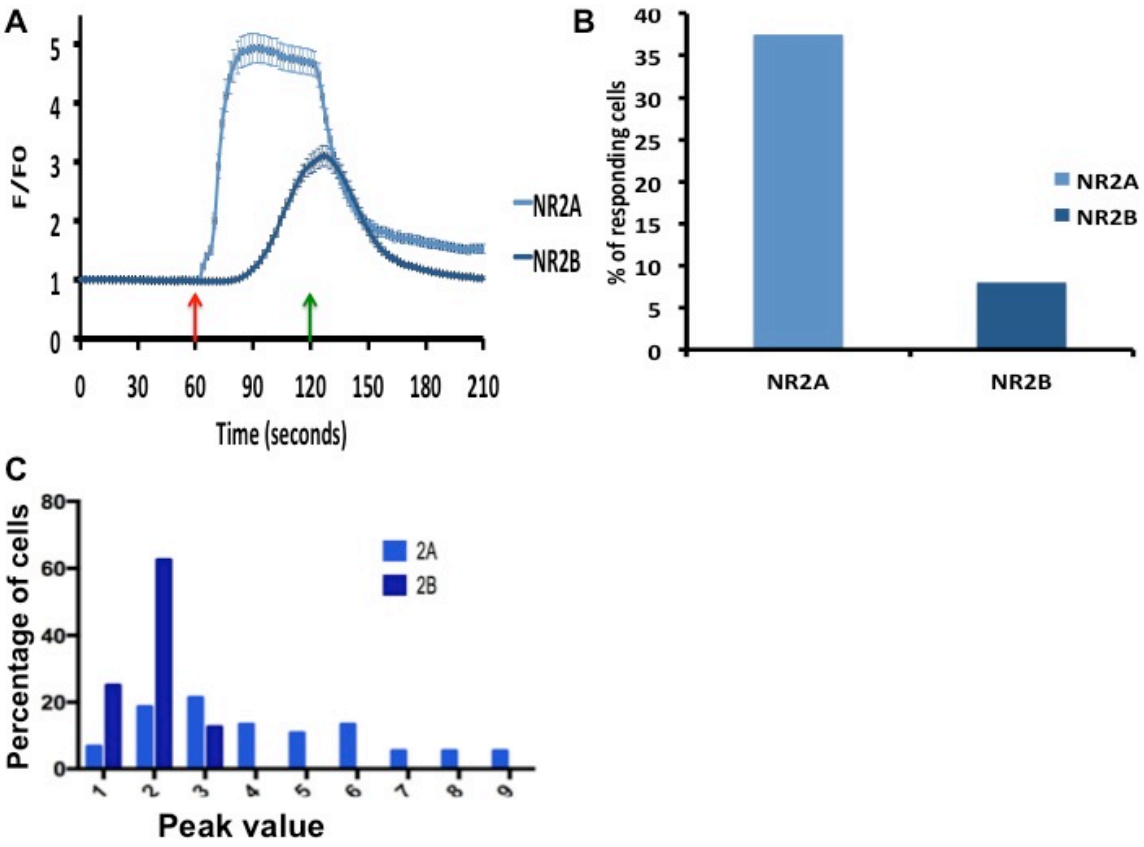

Figure 18 Stimulation of HEK 293T/17 cells transfected with either NR1WT/NR2AWT or NR1WT/NR2BWT with 0.25 µM Glutamate and 0.25 µM glycine. Light blue color represents cells transfected with NR1/NR2A, dark blue color represents cells transfected with NR1/NR2B A) Average of fold increase in fluorescence of single cells upon stimulation. Red arrow signals the start of stimulation, green arrow signals the start of wash off. Error bars are expressed as SEM. Number of cells analyzed expressing NR1/NR2A was 75, number of cells analyzed expressing NR1/NR2B was 16. Cells analyzed were from two different coverslips from the same experiment for each condition. B) A bar graph showing the quantity of cells whose peak values is >= average of baseline+ 3 times standard deviation of baseline. The quantity of cells is expressed as a percentage of the total number of analyzed cells. C) Peak value distribution as a percentage of total cells whose peak values is >= average of baseline+ 3 times standard deviation of baseline. The width of each bin is 1.

4.3.6 Effect of 0.1 µM Glutamate on NR1WT/NR2AWT and NR1WT/NR2BWT

As shown in Fig 19 A, only cells transfected with NR1WT/NR2AWT were able to show some response upon stimulation with 0.1 µM glutamate and 0.25 µM glycine (time to peak value is 50 seconds, maximum peak value is 3.19 ± 0.19). However, cells expressing NR1WT/NR2BWT showed very minimal response with none of the cells satisfying the

criteria of peak values >= average of baseline+ 3 times standard deviation of baseline, hence no data are shown for the latter cells in Fig 19. Moreover, the number of cells transfected with NR1/NR2A that passed the filtering criteria (peak values is >= average of baseline+ 3 times standard deviation of baseline) which was 12.5% out of 200 total analyzed cells, was much less than that in Fig 16 B or Fig 19 B. To summarize, only cells expressing NR1WT/NR2AWT were able to show responses that satisfied our criteria in response to 0.1 μM glutamate and 0.25 μM glycine, while those expressing NR1WT/NR2BWT were not.

Overall, we demonstrated that the responses of NMDARs composed of NR1/NR2A is higher than those composed of NR1/NR2B when exposed to the same concentration of glutamate. However, it is worth noting that these differences might be due to different transfection efficiencies in both conditions. Based on results shown in Fig 17, Fig18 and Fig 19, the ideal minimal concentration of glutamate that can be used to stimulate recombinant NR1WT/NR2BWT is 1 μM and 0.25 μM for NR1WT/NR2AWT so that we obtain a minimal response that could be amplified when adding L-lactate later.

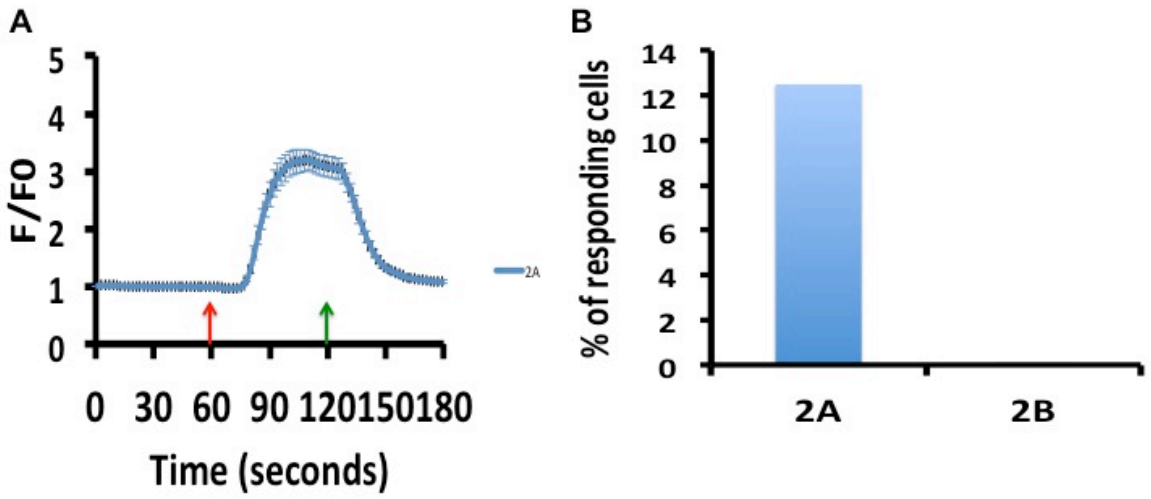

Figure 19 Stimulation of HEK 293T/17 cells transfected with either NR1WT/NR2AWT or NR1WT/NR2BWT with 0.1 µM Glutamate and 0.25 µM Glycine. Light blue color represents cells transfected with NR1/NR2A, dark blue color represents cells transfected with NR1/NR2B A) Average of fold increase in fluorescence of single cells upon stimulation. Red arrow signals the start of stimulation, green arrow signals the start of wash off. Error bars are expressed as SEM. Number of cells analyzed expressing NR1/NR2A was 25, none of the cells analyzed expressing NR1/NR2B showed peak values >= average of baseline+ 3 times standard deviation of baseline. Cells analyzed were from two different coverslips from the same experiment for each condition. B) A bar graph showing the quantity of cells whose peak values is >= average of baseline+ 3 times standard deviation of baseline. The quantity of cells is expressed as a percentage of the total number of analyzed cells.

4.3.7 Sensitivity of NR1WT/NR2AWT to redox changes

The main hypothesis of this thesis is that L-Lactate modulates the NMDAR activity by changing the redox state of the cell. It was shown previously that NMDARS are sensitive to redox changes (Min Li, 1999) and show an enhanced response when reduced and a diminished response when oxidized. To test that our recombinant NMDARs exhibit this sensitivity, we used the reagents DTT (reducing agent) and DTNB (oxidizing agent) (Tang LH,1993)

4.3.7.1 Effect of 4 mM DTT on the response of NR1WT/NR2AWT to 0.25 µM Glutamate and 0.25 µM Glycine

In this experiment, 4mM DTT (1,4-Dithiothreitol) was used based on previously published data (Yang et al., 2014). Cells expressing NR1/NR2A were stimulated with 0.25 µM glutamate and 0.25 µM glycine and their responses were recorded. In a parallel condition response from cells stimulated with 4mM DTT in addition to 0.25 µM glutamate and 0.25 µM glycine was also recorded.

By examining Fig 20 A, 4 mM of DTT didn't cause a detectable increase in the average of Amplitude of response. When cells were stimulated with glutamate and glycine only, the maximum peak value was 3.72 ±0.18 and the time to peak value was 28 seconds. On the other hand, when cells were stimulated with DTT in addition to glutamate and glycine, the maximum peak value was 4.0 ±0.2 and the time to peak value was 32 seconds. When examining the number of responding cells that satisfy our pre-set criteria in Fig 20 B, we find that DTT increased the percentage of those cells compared to when the cells were stimulated with glutamate and glycine only (30.5 % versus 21 % correspondingly). In Fig 20 C, we can see that cells stimulated with DTT, glutamate and glycine show a higher percentage of cells with high peak values as compared to their counterparts stimulated with glutamate and glycine only. In Fig 20 D, the cells showing peak values between 5.5 and 8.5 in both conditions were added up and show that when cells were stimulated with DTT and glutamate, the percentage of those cells was about 6.5%. However, when cells were stimulated with glutamate and glycine only, none of their peak values reached 5.5.

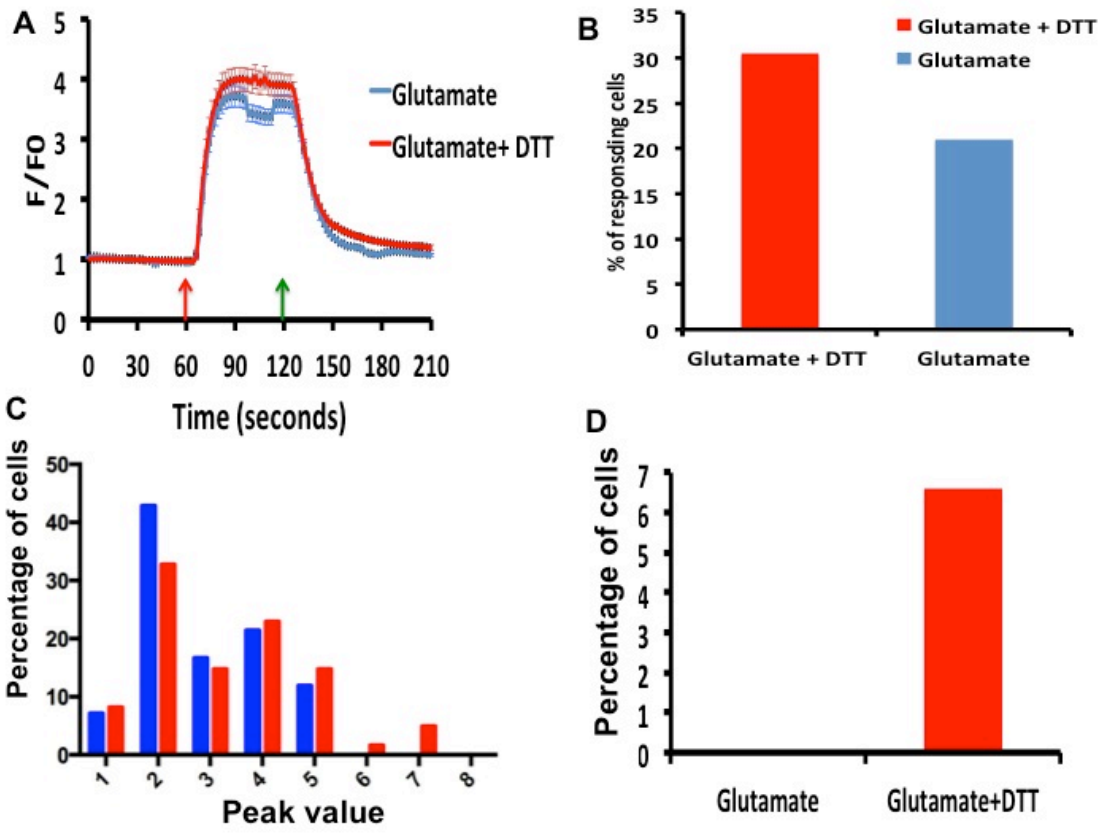

Figure 20 Stimulation of HEK 293T/17 cells transfected with NR1WT/NR2AWT with 0.1 µM Glutamate and 0.25 µM Glycine (Blue) or 0.25 µM Glutamate and 0.25 µM Glycine + 4 mM DTT (red). A) Average of fold increase in fluorescence of single cells upon stimulation. Red arrow signals the start of stimulation, green arrow signals the start of wash off. Error bars are expressed as SEM. Number of cells analyzed expressing NR1/NR2A and showing peak values >= average of baseline+ 3 times standard deviation of baseline in case of stimulation with Glutamate and Glycine was 42 and in case of Glutamate and Glycine + 4 mM DTT was 61, Cells analyzed were from two different coverslips from the same experiment for each condition.. B) A bar graph showing the quantity of cells whose peak values is >= average of baseline+ 3 times standard deviation of baseline. The quantity of cells is expressed as a percentage of the total number of analyzed cells. C) Peak value distribution as a percentage of total cells whose peak values is >= average of baseline+ 3 times standard deviation of baseline. The width of each bin is 1. D) A bar graph showing the percentage of cells whose peak values lies between 5.5 and 8.5 in both conditions.

4.3.7.2 Effect of 10 mM DTT and 0.5 mM DTNB on the response of NR1WT/NR2AWT to 0.25 µM Glutamate

In an attempt to see a graded response corresponding to different doses of DTT, the concentration of DTT was increased. Also DTNB was used to examine the oxidizing effect. For condition 1, cells were stimulated with 0.25 µM glutamate and 0.25 µM glycine. For condition 2, cells were stimulated with 0.25 µM glutamate and 0.25 µM glycine + 10 mM DTT. For condition 3, cells were stimulated with 0.25 µM glutamate and 0.25 µM glycine + 0.5 mM DTNB**.** By examining Fig 21 A, 10 mM DTT didn't cause a significant increase in the average of amplitude of response (maximum peak value for glutamate, glutamate+ DTT, glutamate+ DTNB was 4.0 ± 0.16, 3.99 ± 0.12, 3.9 ±0.11 respectively). However, during the initiation of stimulation, kinetics in case of the presence of DTT was faster compared to the other two conditions where the fluorescence intensity increased to 1.5 folds in 14 seconds in the case of stimulation with glutamate, 12 seconds in the case of stimulation with glutamate+ DTNB and 6 seconds in the case of stimulation with glutamate and DTT. When examining the number of responding cells that satisfy our pre-set criteria in Fig 21 B, we find that DTT increased the percentage of those cells compared to when the cells were stimulated with glutamate and glycine only (50.7% versus 40%). On the contrary, DTNB led to a reduction in the number of responding cells compared to when cells were stimulated with glutamate and glycine only (36% versus 40%). In Fig 21 C, we can see that cells

stimulated with DTT and glutamate show a higher percentage of cells with high peak values as compared to their counterparts stimulated with glutamate and glycine only and vice versa in the case of DTNB. In Fig 21 D, the cells showing peak values between 5.5 and 8.5 in all conditions were added up and it shows that when cells were stimulated with DTT and glutamate, the percentage of those cells was higher than when cells were stimulated with glutamate and glycine only (11.2% versus 6.3%). On the other hand, when cells were stimulated with DTNB and glutamate, the percentage of those cells was lower than when cells were stimulated with glutamate and glycine only (2.8 % versus 6.3 %).

In summary, our expressed recombinant NR1WT/NR2AWT is responsive to redox changes. The changes in response can be detected through examining the percentage of responding cells that satisfy our pre-set criteria and the frequency of peak value distribution. On the contrary, examining the average amplitude of cells doesn't reflect those changes

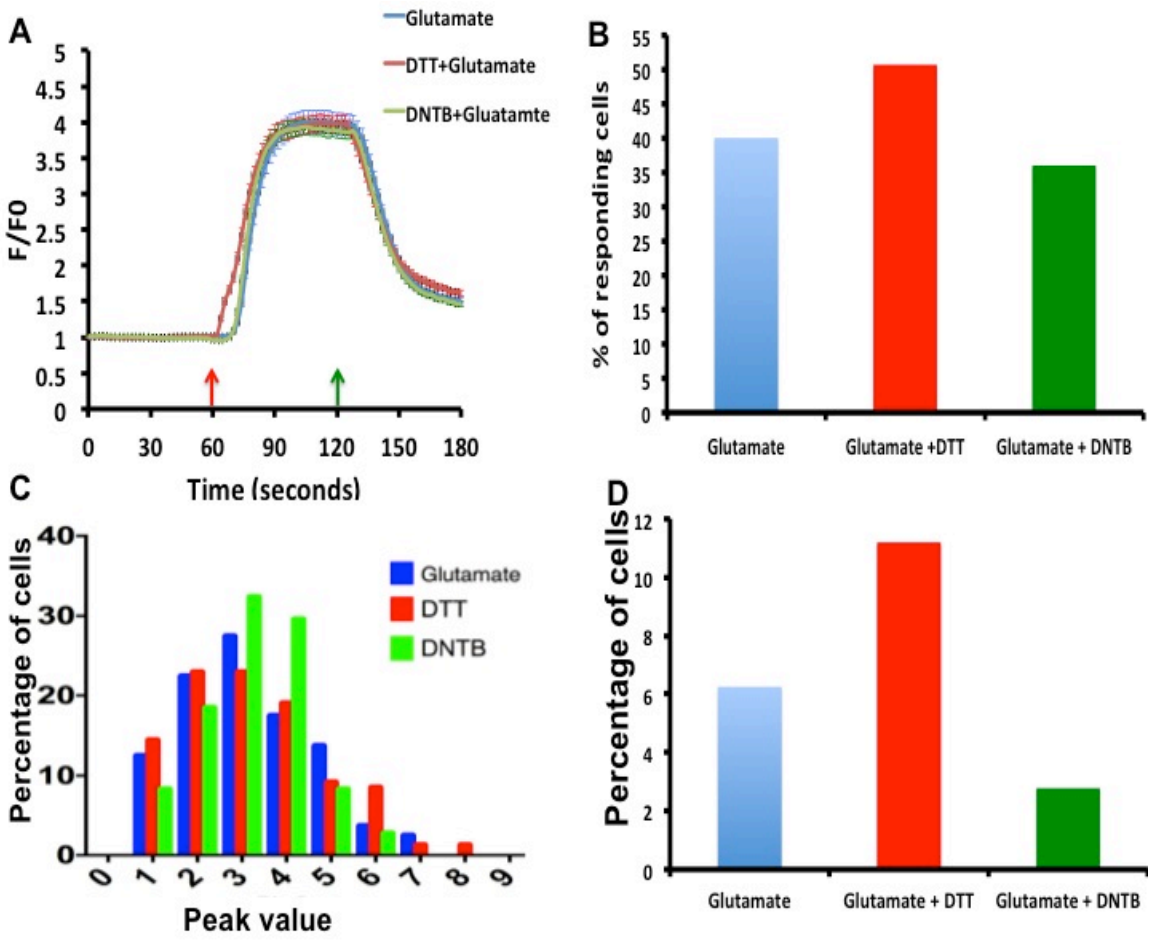

Figure 21 Stimulation of HEK 293T/17 cells transfected with NR1WT/NR2AWT with 0.25 µM Glutamate and 0.25 µM Glycine in the presene of either DTT and DTNB. HEK cells transfected with NR1WT/NR2AWT were stimulated with condition 1) 0.25 µM Glutamate and 0.25 µM Glycine (Blue) or condition 2) 0.25 µM Glutamate and 0.25 µM Glycine + 10 mM DTT (red) or condition 3) 0.25 µM Glutamate and 0.25 µM Glycine + 0.5 mM DTNB. In all 3 conditions, the cells were perfused for 5 minutes with HBSS containing the following stimulants for 5 minutes; HBSS with no additives for condition 1, 10 mM DTT for condition 2, 0.5 mM DTNB for condition 3. A) Average of fold increase in fluorescence of single cells upon stimulation. Red arrow signals the start of stimulation, green arrow signals the start of wash off. Error bars are expressed as SEM. Number of cells analyzed expressing NR1/NR2A and showing peak values >= average of baseline+ 3 times standard deviation of baseline in case of stimulation with Glutamate and Glycine was 82 from two different coverslips and in case of Glutamate and Glycine + 10 mM DTT was 152 from three different coverslips and in case of Glutamate and Glycine + 0.5 mM DTNB was 108 from three different coverslips from the same experiment for each condition B) A bar graph showing the quantity of cells whose peak values is >= average of baseline+ 3 times standard deviation of baseline. The quantity of cells is expressed as a percentage of the total number of analyzed cells. C) Peak value distribution as a percentage of total cells whose peak values is >= average of baseline+ 3 times standard deviation of baseline. The width of each bin is 1. D) A bar graph showing the percentage of cells whose peak values lies between 5.5 and 8.5 in among all conditions.

Chapter 5

Global effects of L-lactate on HEK239 T/17 independent of NMDAR

5.1 Significance

In this chapter we aimed to investigate the effects of adding L-Lactate to non-transfected HEK cells. The main target of this thesis is to investigate the modulatory effect of L-Lactate on NMDAR, however prior to that it's important to investigate its effects on the system in which NMDARs are expressed, which is the HEK cells in our studies.

5.2 Materials and Methods

HEK cells were seeded on glass coverslips coated with poly-D-Lysine at a density of 0.3 million in DMEM 31966 media. After 24 hours of seeding, the media was changed to DMEM D3050, then calcium imaging was done 20-24 hours later. Detailed steps were mentioned earlier in the materials and methods section of Chapter 4.

5.3 Results

5.3.1 Effect of L-Lactate on non-transfected HEK293 T/17

Upon stimulation of HEK293 T/17 cells with 20 mM L-lactate only, we noticed a minor increase in the fluorescence intensity, about 1.3 ± 0.03 fold as shown in Fig 22. The variability across cells was minimal as shown by the SEM error bars. This is also shown by examining the single cells' responses in Fig 22 A, where all the responses range between 1.1 to 1.5 fold increase. In order to do this analysis, 100 cells were randomly

selected for analysis as representatives while in fact all the cells in the visualized field view had the same response. It is worth mentioning that the cells were initially seeded on glass coverslips in DMEM media containing 25 mM glucose, 17-19 hours post seeding, the DMEM media was changed to another one containing 5 mM glucose. During imaging, HBSS buffer containing 1 mM glucose was used. This gradual decrease in the glucose concentration was meant to decrease the intrinsic Lactate production by cells. This increases the probability that the L-Lactate that we add extracellularly finds its way to the inside of the cells. This hypothesis was built on the finding that HEK cells profoundly express functional MCT1 (Ahlin, 2009). MCTs are monocarboxylate transporters that carry molecules containing one carboxylate group as in L-Lactate and pyruvate. It had also been shown that MCT transport of lactic acid is associated with the release of calcium from intracellular stores (Cheeti, 2010). The latter finding explains the global effect that we see here in this experiment indicating that the source of the increase of calcium intracellularly upon addition of L-Lactate is the intracellular stores.

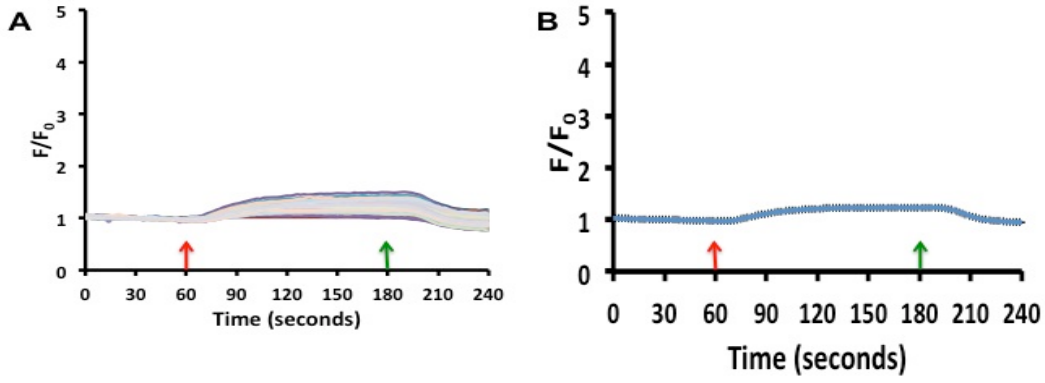

Figure 22 Effect of 20 mM L-lactate on non-transfected HEK 293 T/17. A) Fold increase in fluorescence of single cells upon stimulation. Red arrow signals the start of stimulation, green arrow signals the start of wash off. Number of cells analyzed was 100 from one coverslip. B) Average of the single cells' responses shown in panel A. Error bars are expressed as SEM.

5.3.2 Effect of pyruvate on non-transfected HEK293 T/17

In this experiment we aimed to investigate whether the global L-Lactate dependent, NMDAR independent increase in intracellular calcium can be seen when using other substrates that are also transported via MCTs. Pyruvate was chosen to investigate whether this effect that we observe is specific to L-lactate or is a general phenomenon due to monocarboxylate containing molecules. Upon stimulation of HEK293 T/17 cells with 20 mM Pyruvate, we noticed a similar global effect with the same characteristics as those shown and described in the previous figure. The maximum peak value was 1.3 ± 0.02. This effect was seen in all examined cells with very small variations as shown in the SEM bars as sown in Fig 23. The finding that pyruvate was able to produce a global effect similar to that produced by L-Lactate strengthens our hypothesis that this response is related to the MCT transport.

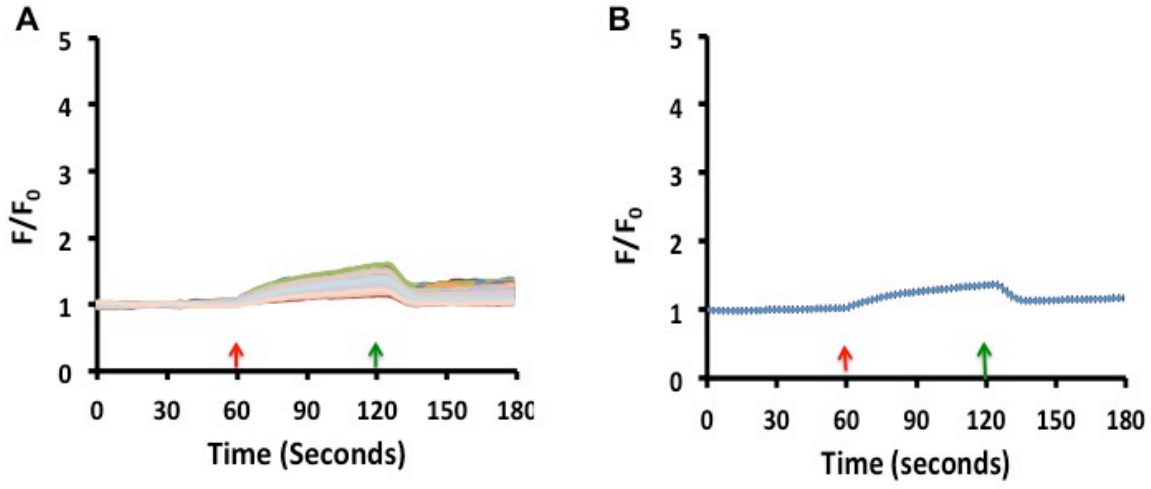

Figure 23 Effect of 20 mM Pyruvate on non-transfected HEK 293 T/17. A) Fold increase in fluorescence of single cells upon stimulation. Red arrow signals the start of stimulation, green arrow signals the start of wash off. Number of cells analyzed was 100 from one coverslip. B) Average of the single cells' responses shown in panel A. Error bars are expressed as SEM.

5.3.3 Effect of D-Lactate on non-transfected HEK293 T/17, a negative control.

To further characterize the global effect seen by L-Lactate on non-transfected HEK cells, we used D-Lactate as a negative control. MCT-1 exhibits an uptake coefficient for L-lactate twice that for D-lactate (Ewaschuk, 2005). Hence, we should expect a decreased global response of HEK cells to D-Lactate when compared to L-Lactate.

Upon stimulation of HEK293 T/17 cells with 20 mM D-lactate, we noticed a very minor increase in the fluorescence intensity, maximum peak value is 1.097 ± 0.01 as shown in Fig 24 B. Again, the variability across cells was minimal as shown by the SEM error bars. This is also shown by examining the single cells' responses in Fig 24 A, where all the maximum peak value ranges between 1.05 to 1.097 times. In order to do this analysis, 100 cells were randomly selected for analysis as representatives while in fact all the cells in the visualized field of view had the same response. This finding coincides with our hypothesis that this global effect is correlated to the MCT transport, since MCT transporters have higher affinity to the L- isoform of lactate than the D-isoform. Also, the initiation of the global effect in the case of D-Lactate is slower than in the case of L-lactate or pyruvate again indicating that this global effect is correlated to the MCT transport. In summary, D-Lactate leads to a minimized global effect compared to L-lactate and pyruvate in terms of maximum peak value and time to peak value. This further strengthens our hypothesis that the global effect is related to MCT transport.

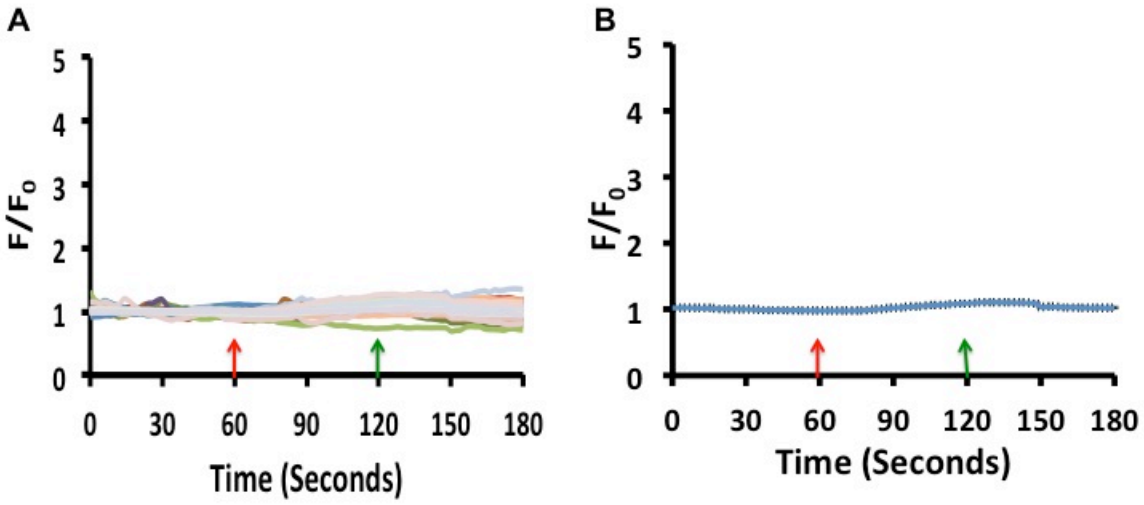

Figure 24 Effect of 20 mM D-lactate on non-transfected HEK 293 T/17. A) Fold increase in fluorescence of single cells upon stimulation. Red arrow signals the start of stimulation, green arrow signals the start of wash off. Number of cells analyzed was 100 from one coverslip. B) Average of the single cells' responses shown in panel A. Error bars are expressed as SEM.

5.3.4 Effect of UK5099 on the global effect

In order to confirm that the global effect seen in the case of L-lactate and pyruvate and to a lesser extent in the case of D-lactate is mediated through MCT, we used UK5099 (Yang et al., 2014). UK 5099 is a general blocker of MCTs. The cells were perfused with 50 µM UK5099 for 1 minute to allow blockage of MCTs, then the cells were perfused with a combination of 50 µM UK5099 and 20 mM L-lactate, then washed out with HBSS for 1 minute. It was noticed that UK5099 abolished the global effect upon addition of L-lactate as seen in Fig 25. This indicates that the MCT transport is highly correlated with the global effect seen.

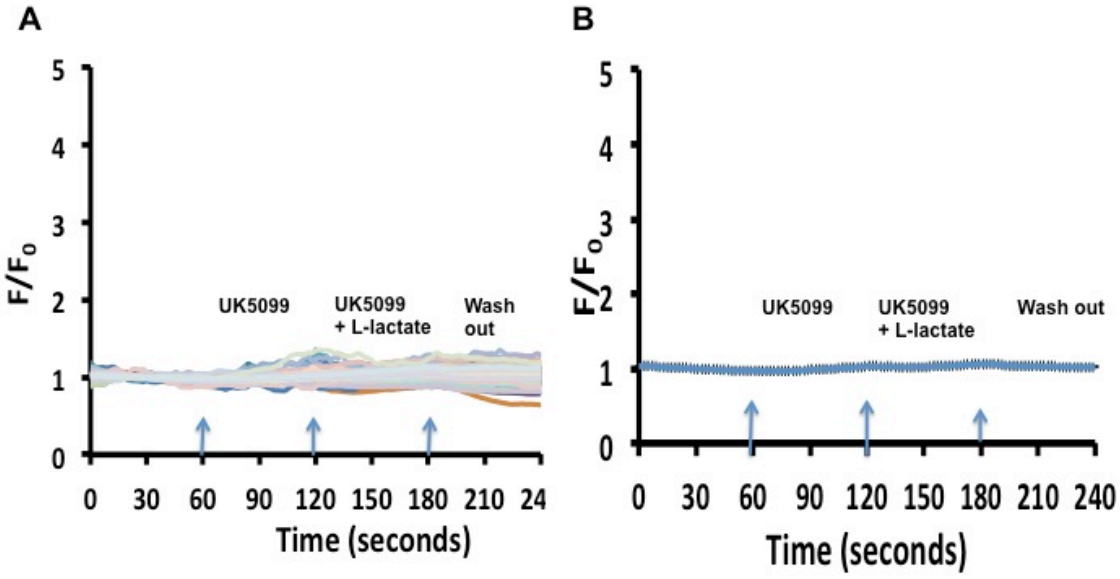

Figure 25 Effect of UK5099 on the global effect initiated by L-Lactate. Non-transfected HEK 293 T/17 were perfused with HBSS and the fluorescence of Fluo4-AM was recorded for 1 minute as a baseline, the cells were then perfused with 50 µM UK5099 for 1 minute, followed by 1 minute of perfusion with 50 µM UK5099 and 20 mM L-lactate and eventually 1 minute of wash out.. A) Fold increase in fluorescence of single cells upon stimulation. Number of cells analyzed was 100 from one coverslip. B) Average of the single cells' responses shown in panel A. Error bars are expressed as SEM.

In summary, both L-lactate and pyruvate caused a global effect on non-transfected HEK293 T/17 cells. The global effect was defined as 1.3X folds increase in the Fluo4, AM fluorescence upon addition of L-lactate or pyruvate in all cells displayed in the field of view. D-Lactate also caused a global effect, but to a lesser extent (1.1 X). MCT transport is associated with release of Calcium from intracellular stores. In order to confirm that, we used UK5099 (MCT blocker), which abolished the global response.

Chapter 6

Solo effects of L-lactate without Glutamate, NMDAR dependent

6.1 Significance

In the previous chapter, we characterized the solo effect of L-Lactate on HEK cells which are used as the host system for expressing NMDARs in HEK cells. In this chapter, the solo effect of L-Lactate on expressed NMDARs was investigated. The reason behind this is that there might be a possibility that L-Lactate binds directly to NMDARs as an agonist or co-agonist and stimulate them, hence we aimed to test for that.

6.2 Materials and Methods

Culturing of cells and calcium imaging protocol was detailed earlier in chapter 4.

6.3 Results

6.3.1 L-lactate leads to initiation of single events in case of NR1/NR2A but not NR1/NR2B.

We wanted to test the pure effect of L-lactate on cells expressing NMDAR receptors. The main idea of the project is to add L-lactate to glutamate to see how the cells would react compared to when they are stimulated with glutamate only. However, before doing this, we wanted to examine the pure effects of L-lactate on cells expressing NMDAR as a control. When cells expressing the NMDAR subunits NR1/NR2A were stimulated with 20 mM L-lactate, single events of cell responses were observed as seen

in Fig 26 A. The timing of the initiation and termination of these events coincided with the timing of initiation and termination of the global response. Due to this observation, we assumed that these single events are also directly correlated to L-lactate. In Fig 26 A, responses from 100 single cells transfected with NR1/NR2A are displayed. We observed the percentage of these single events compared to the total number of analyzed cells and calculated that the percentage lies in the range of 5%-7% of total analyzed cells in 3 independent experiments. When examining Fig 26 B, responses from 100 cells transfected with NR1/NR2B are displayed. No single events were seen, only the global response was detected. By examining the literature, we found out that glycine was reported to stimulate NR1/NR2A NMDAR on its own without glutamate (Jones KS, 2002), however this stimulation was to a lesser extent compared to that with glutamate. The mechanism of that stimulation with glycine was unknown. So maybe in our case L-lactate binds to the glycine site and stimulates the NR1/NR2A NMDAR by a similar mechanism. Recent docking studies in lab showed that L-lactate has high binding affinity to the glycine binding site on NMDAR. So literature review combined with our findings suggest that L-lactate can activate NR1/NR2A in the same way glycine does. The other possibility would be that there are traces of glutamate produced by the cells which when combined with L-lactate lead to those single events. However, this possibility is ruled out because those single events are only characteristic to NMDARs containing NR1/NR2A and not NMDARs containing NR1/NR2B. To further exclude the possibility of the presence of glutamate traces, future experiments should be done in the presence of glutamate dehydrogenase.

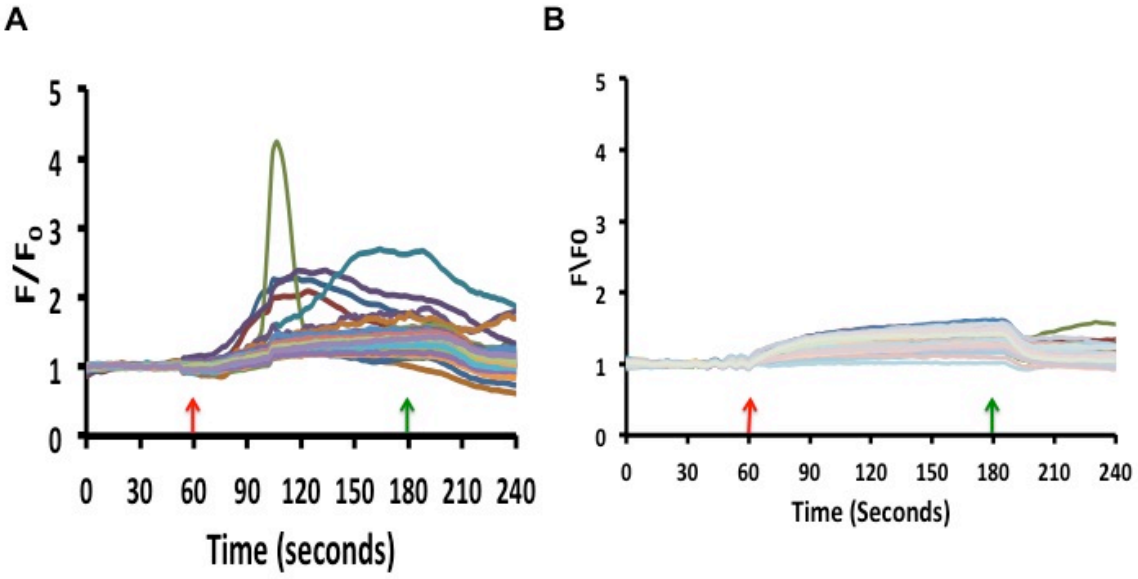

Figure 26 Effect of 20 mM L-lactate on HEK 293 T/17 either expressing NR1/NR2A (panel A), or NR1/NR2B (panel B). The graphs are representatives of fold increase in fluorescence of single cells upon stimulation. Red arrow signals the start of stimulation, green arrow signals the start of wash off. Number of cells shown is 100 from one coverslip.

6.3.2 Effect of D-AP5 on the single events

In order to characterize the single events and confirm that they are related to NMDA receptors, we used D-AP5, a competitive NMDA receptor glutamate antagonist. In Fig 27, cells transfected with NR1/NR2A were perfused with a mix of 20 mM L-lactate and 500 µM D-AP5. Although we observed single events, they exhibited different characteristics. The initiation was delayed compared to the initiation of the global response, also those events died earlier than the global response and independent of the wash out start time. Since D-AP5 is a competitive antagonist of NMDAR, one explanation could be that 500 µM of D-AP5 is able to block all the expressed NMDARs at

the beginning of initiation, but when the concentration of L-lactate builds up in the chamber, that's when L-lactate is able to find its way in producing some single events, but then D-AP5 shuts down those events making them short lived and causing them to fade out independently following the initiation of the wash out

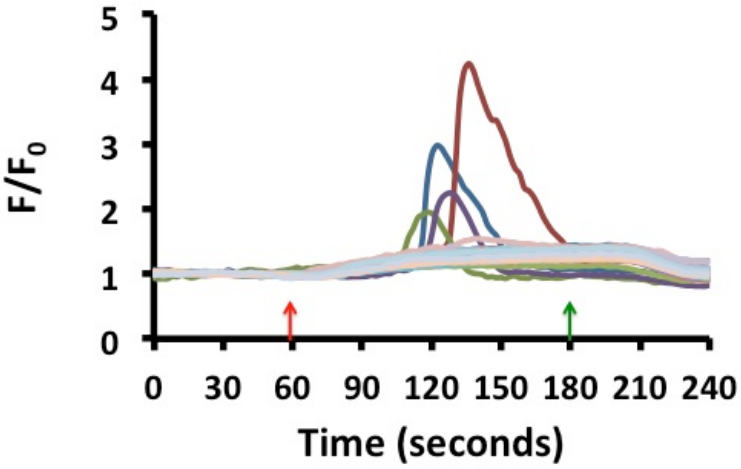

Figure 27 Effect of 20 mM L-lactate + 500 µM D-AP5 on HEK 293 T/17 transfected with NR1/NR2A subunits. The graphs is a representative of fold increase in fluorescence of single cells upon stimulation. Red arrow signals the start of stimulation, green arrow signals the start of wash off. Number of cells analyzed was 100.

6.3.3 Effect of MK-801 on the single events

To further characterize the single events and confirm that they are related to NMDA receptors, we used MK-801. MK-801 is a non-competitive, potent and selective NMDA receptor antagonist. It binds to the receptor only in its open state, since its binding site is in the pore of the channel. When blocking the pore of the NMDAR channel, it inhibits

the Calcium influx. In Fig 28, cells transfected with NR1/NR2A were perfused with a mix of 20 mM L-lactate and 40 µM D-AP5. We noticed that although single events did appear, they again exhibited different characteristics. The initiation time matched the global response, however those events died earlier than the global response, independent of the wash out start time. Since MK-801 binds to NMDAR only when it is in its open state, those changes in the characteristics of the response make perfect sense. When L-lactate is added to the cells, it initiates the opening of some of the expressed NMDARs in what we call “single events”. When the channels are open, MK-801 is able to enter the pore and block it, hence making the single events short lived and fade away independent of the wash out timing.

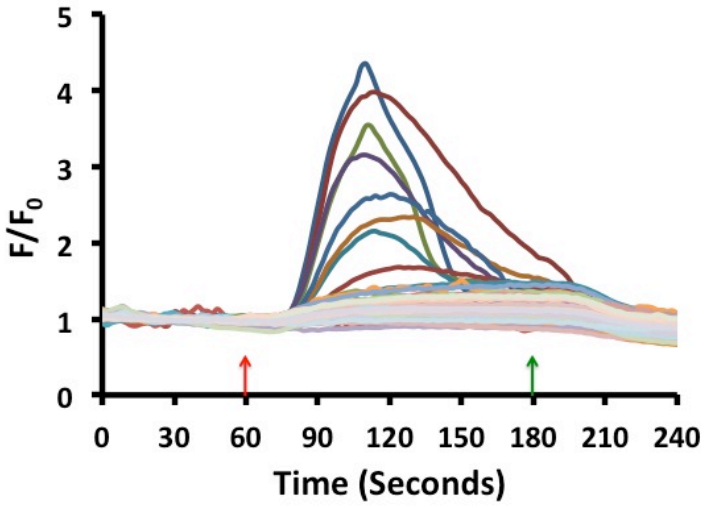

Figure 28 Effect of 20 mM L-lactate + 40 µM MK-801 on HEK 293 T/17 transfected with NR1/NR2A subunits. This graphs is a representative of fold increase in fluorescence of single cells upon stimulation. Red arrow signals the start of stimulation, green arrow signals the start of wash off. Number of cells analyzed was 100.

Chapter 7

Modulatory effect of L-Lactate on the response of NR1WT/NR2AWT to glutamate.

7.1 Significance

In this chapter we aimed to characterize the modulatory effect of NMDAR response to glutamate. Since we had seen single events stimulated in the case of NR1/NR2A in response to L-Lactate, we decided to focus on the modulatory effect of L-Lactate on NMDAR response to glutamate mainly on NR1/NR2A rather than NR1/NR2B. In the latter, no single events were seen when stimulated with L-Lactate. In previous research (Yang et al, 2014), it was mentioned that L-Lactate potentiated the response of NMDAR to glutamate in primary neuronal cultures, however detailed mechanisms of this potentiation were not explored. Also, they didn't explore whether this potentiation is specific to NMDARs containing certain subunits or a general effect on NMDARs composed of any subunits. In this chapter, we aimed to explore some of these details.

7.2 Materials and methods

Mentioned earlier in chapter 4

7.3 Results

7.3.1 Effect of L-lactate on NR1/NR2A response to glutamate

In this experiment we used a very low concentration of glutamate (0.1 μM) in order to stimulate the expressed NMDARs, which composed of the subunits NR1WT and

NR2AWT. The idea was to use the lowest concentration that could activate the receptor to allow room for detection of the L-Lactate potentiation. Cells were stimulated with a solution containing 20 mM L-Lactate and 0.1 µM glutamate and 0.25 µM glycine for one minute then followed by 1.5 minutes of washout with HBSS buffer. Stimulation with 0.1 µM glutamate and 0.25 µM glycine only was used on another set of cells as a control.

As shown in Fig 29 A, the kinetics of the initiation of response in case of stimulation with L-lactate+ glutamate+ glycine was slower than when cells where stimulated with glutamate + glycine only (maximum peak value reached in 50 seconds in case of stimulation with glutamate and glycine only and in 58 seconds in the case of the presence of L-Lactate). Also, the average of the maximum peak amplitude shows a bigger fold change in the case of glutamate + glycine only (3.19 ± 0.18) compared to when L-Lactate was present (2.7 ± 0.15). The measurement that showed a significant difference between the two conditions was the kinetics of the washout. The washout kinetics in the case of the presence of L-Lactate was slower compared to the control. A multiple t-test as carried out for the washout period and significance was found between the time points 148 seconds and 158 seconds with p values ranging from 0.028 to 0.05 using the Holm Sidak method. When inspecting the number of cells that passed the filtering criteria (peak values is >= average of baseline+ 3 times standard deviation of baseline), we found that it was lower in case of the presence of L-Lactate (7.5 % ± 1.5) compared to the control (12.5 % ± 0.5) as shown in Fig 29 B, however with no significance (p value = 0.127) using a paired t-test. Finally looking at the peak value

frequency distribution in Fig 29 C, we found that in the presence of L-Lactate, the peak values tend to shift to lower numbers compared to the control. On the contrary, when cells are stimulated with glutamate and glycine only, the peak values of cells tend to shift towards higher values. To summarize, the presence of L-Lactate under these conditions led to significant slower kinetics of the washout and peak value distribution shifted towards lower values.

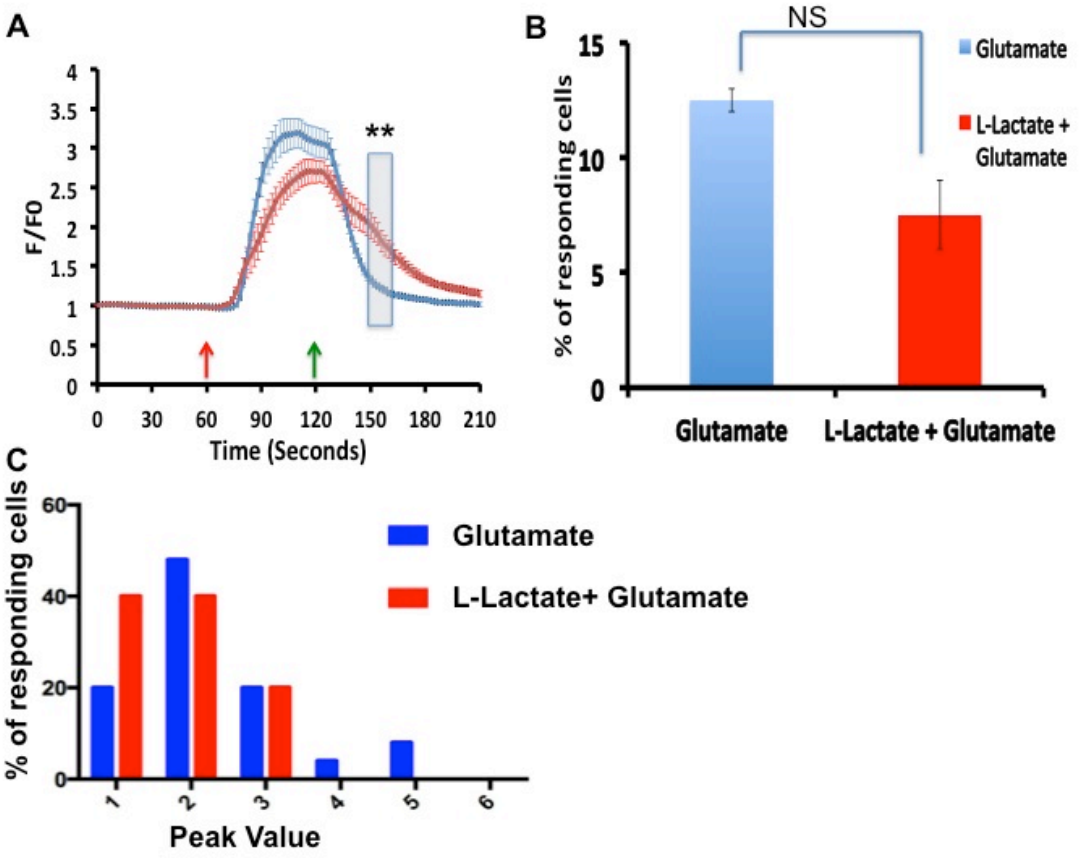

Figure 29 HEK 293T/17 cells transfected with NR1WT/NR2AWT were stimulated with 0.1 µM Glutamate and 0.25 µM Glycine (represented in blue) or 0.1 µM Glutamate and 0.25 µM Glycine + 20 mM L-lactate (represented in red). Cells treated with L-Lactate were incubated in 20 mM L-Lactate for 1 hour prior to imaging. A) Average of fold increase in fluorescence of single cells upon stimulation. Red arrow signals the start of stimulation, green arrow signals the start of wash off. Error bars are expressed as SEM among individual cells. Number of cells analyzed in case of treatment with Glutamate + Glycine only was 70 cells, cobined from 3 different coverslips form 1 experiment, number of cells analyzed in case of treatment with Glutamate + Glycine+ L-lactate was 140

cells, combined from 3 different coverslips form 1 experiment. B) A bar graph showing the quantity of cells whose peak values is >= average of baseline+ 3 times standard deviation of baseline. The quantity of cells is expressed as a percentage of the total number of analyzed cells (300 cells for each condition). C) Peak value distribution as a percentage of total cells whose peak values is >= average of baseline+ 3 times standard deviation of baseline. The width of each bin is 1.

7.3.2 Effect of incubation of HEK cells expressing NR1/NR2A with L-Lactate for 1 hour

We further wanted to examine the long term effects of L-Lactate as opposed to the immediate effects that were investigated earlier. Hence, HEK cells expressing NR1WT/NR2AWT were incubated with 20 mM L-Lactate for 1 hour prior to imaging. The imaging process was then carried out as explained earlier withone minutes recording of baseline where cells were perfused with HBS, followed by a stimulation phase were cells were perfused with 20 mM L-Lactate, 0.25 µM Glutamate and 0.25 µM Glycine. Finally, a washout phase where cells were perfused with HBS for 1.5 minutes. On the other hand, control cells didn't undergo any incubation and were stimulated with 0.25 µM glutamate and 0.25 µM glycine only. As shown in Fig 30 A, the kinetics of the initiation of response in case of the presence of L-Lactate is faster towards the last part of initiation than when glutamate + glycine only are used for stimulation (54 seconds to reach maximum peak amplitude in the case of L-Lactate presence versus 44 seconds in its absence). The average amplitude in both cases is quite similar (3.4 ± 0.07 fold change in the case of incubation with L-Lactate versus 3.32 ± 0.13 fold change in the case of the control). By examining the washout kinetics in both conditions, we find that it was slower in the condition where cells were incubated with L-Lactate and also stimulated with L-Lactate + Glutamate+ Glycine compared to when cells where stimulated with Glutamate+ Glycine only. In Fig 30 B, when inspecting the number of cells that passed

the filtering criteria (peak values is >= average of baseline+ 3 times standard deviation of baseline), we found that it was doubled in case of the presence of L-Lactate (46.6 % ± 5.54) compared to when cells were stimulated with glutamate and glycine only 23.3 % ± 5.9). Finally looking at the peak value frequency distribution in Fig 30 C, the peak value distribution percentage was comparable, however in the case of L-Lactate some cells had peak values that lied within the bin 7, while in the control condition, the maximum peak values lied within the bin 6. To summarize, the effect of incubating HEK293 T/17 cells with 20 mM L-Lactate was evident in two aspects. First, the washout kinetics were slower in the presence of L-Lactate. Second, the percentage of responding cells out of analyzed cells doubled up in the case of L-Lactate compared to control (absence of L-Lactate).

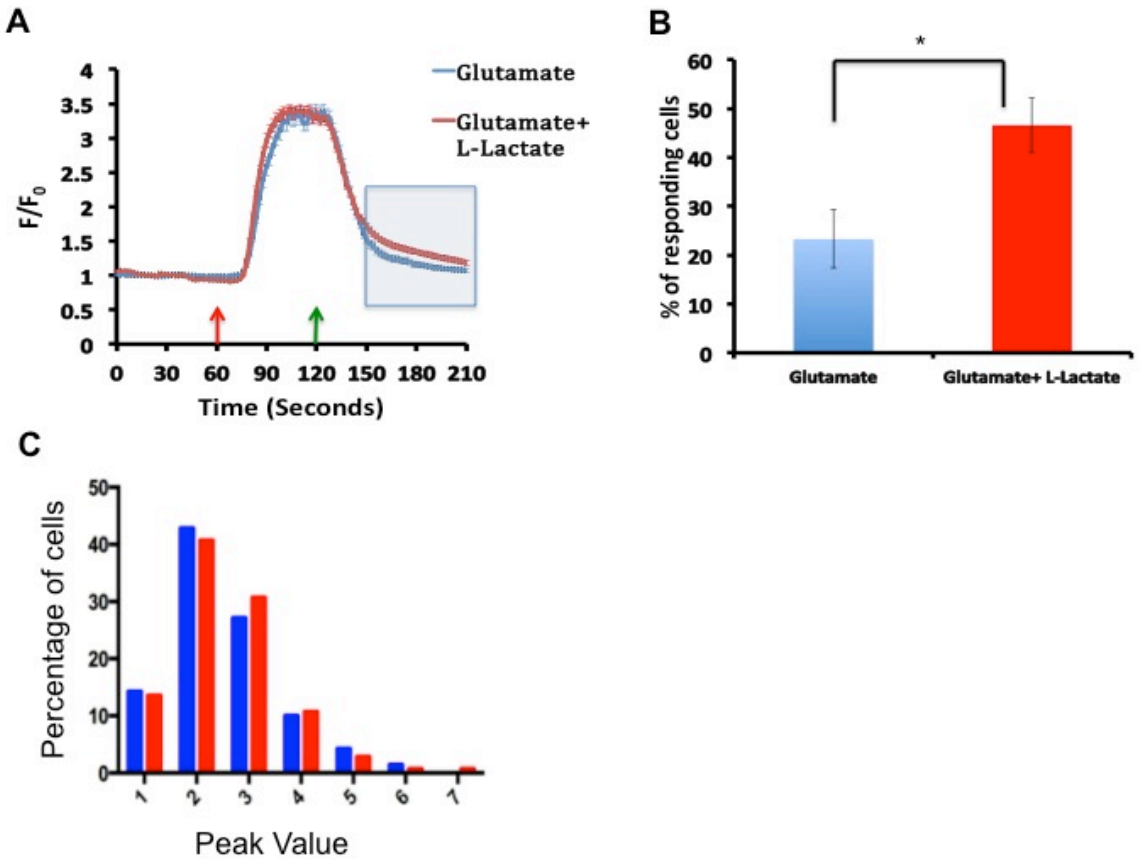

Figure 30 Effect of 1 hour incubation of HEK 293 T/17 expressing NR1/NR2A with 20 mM L-Lactate. HEK 293T/17 cells transfected with NR1WT/NR2AWT were stimulated with 0.25 µM Glutamate and 0.25 µM Glycine (represented in blue) or 0.25 µM Glutamate and 0.25 µM Glycine + 20 mM L-lactate (represented in red). Cells treated with L-Lactate were incubated in 20 mM L-Lactate for 1 hour prior to imaging. A) Average of fold increase in fluorescence of single cells upon stimulation. Red arrow signals the start of stimulation, green arrow signals the start of wash off. Error bars are expressed as SEM among individual cells. Number of cells analyzed in case of treatment with Glutamate + Glycine only was 70 cells, combined from 3 different coverslips form the same experiment, number of cells analyzed in case of treatment with Glutamate + Glycine+ L-lactate was 140 cells, combined from 3 different coverslips form the same experiment. B) A bar graph showing the quantity of cells whose peak values is >= average of baseline+ 3 times standard deviation of baseline. The quantity of cells is expressed as a percentage of the total number of analyzed cells (300 cells for each condition). C) Peak value distribution as a percentage of total cells whose peak values is >= average of baseline+ 3 times standard deviation of baseline. The width of each bin is 1.

7.3.3 Effect of L-lactate on NR2A, successive stimulation on same set of cells

In this experiment, the extended effect of L-Lactate was investigated. We aimed to test whether the effects of L-Lactate on NMDARs (NR1WT/NR2AWT) we observed previously would last after the washout or not. Accordingly, experiments were designed where the same set of HEK cells transfected with NR1WT/NR2AWT would undergo two successive

stimulations with one washout in between. In all three conditions, a baseline was recorded for 1 minute during which cells were perfused with HBSS, followed by 1 minute of stimulation with stimulants of choice, followed by 1.5 minutes of washout with HBSS, followed by 1 minute of second stimulation and eventually 1 minute of washout with HBSS. In the control condition, both stimulations were carried out using 0.25 µM glutamate and 0.25 µM glycine (shown in blue in Fig 31). In the another condition, cells were stimulated with 20 mM L-Lactate + 0.25 µM glutamate and 0.25 µM glycine for the first time followed by a second stimulation with 0.25 µM glutamate and 0.25 µM glycine only (shown in red in Fig 31). The last condition was the reversible order of the latter condition where cells were stimulated with 0.25 µM glutamate and 0.25 µM glycine only for the first time followed by a second stimulation with 20 mM L-Lactate+ 0.25 µM glutamate and 0.25 µM glycine (shown in green in Fig 28). By examining Fig 31 A, the kinetics of the initiation of response after the first stimulation in case of the presence of L-Lactate (red line) is faster compared to the control (time to peak value was 48 seconds in the case of L-Lactate presence and was 56 seconds in the case of the control) . The average maximum peak amplitude in all 3 conditions were comparable (3.47 ± 0.07 fold change in the case of L-Lactate presence, 3.62 ± 0.23 fold change in the condition where cells were stimulated with glutamate only followed by glutamate and L-Lactate or 3.31 ± 0.19 fold change in the case of the control). In Fig 31 B, the condition where cells were stimulated with L-Lactate first followed by glutamate only was compared to the control. A multiple t-test was carried out using the Holm Sidak method and it was found that the washout kinetics were significantly slower that

the control in both stimulations. The p value ranged between 0.002 and 0.009 from time points 150 seconds till 198 seconds for the first washout. Moreover, the p value ranged between 0.04 and 0.05 from time points 278 seconds till 286 seconds for the second washout. In Fig 31 C, the frequency distribution of the maximum peak value amplitude of the first stimulation of cells that passed our filter was analyzed for the control condition and the condition where L-Lactate was present during the first stimulation. The maximum peak values tend to reach higher values in the case of L-Lactate compared to the control. When cells whose maximum peak value ranged between 7.5 and 11.5 were grouped as seen in Fig 31 D, the percentage of those cells were 8.4 % in the case of L-Lactate as compared to 1.8 % in the case of the control. To summarize, the effect of L-Lactate in slowing down the washout kinetics is significantly extended to the second stimulation, even though the second stimulation was done without any L-Lactate. This extended effect could be interpreted by assuming that the conformational changes conferred by L-Lactate to NMDARs is long lasting and cannot be reversed just by washing out. On the other hand, we should be cautious that some L-Lactate molecules could still be clinging to the receptors even after the washout, thus conferring this extended effect.

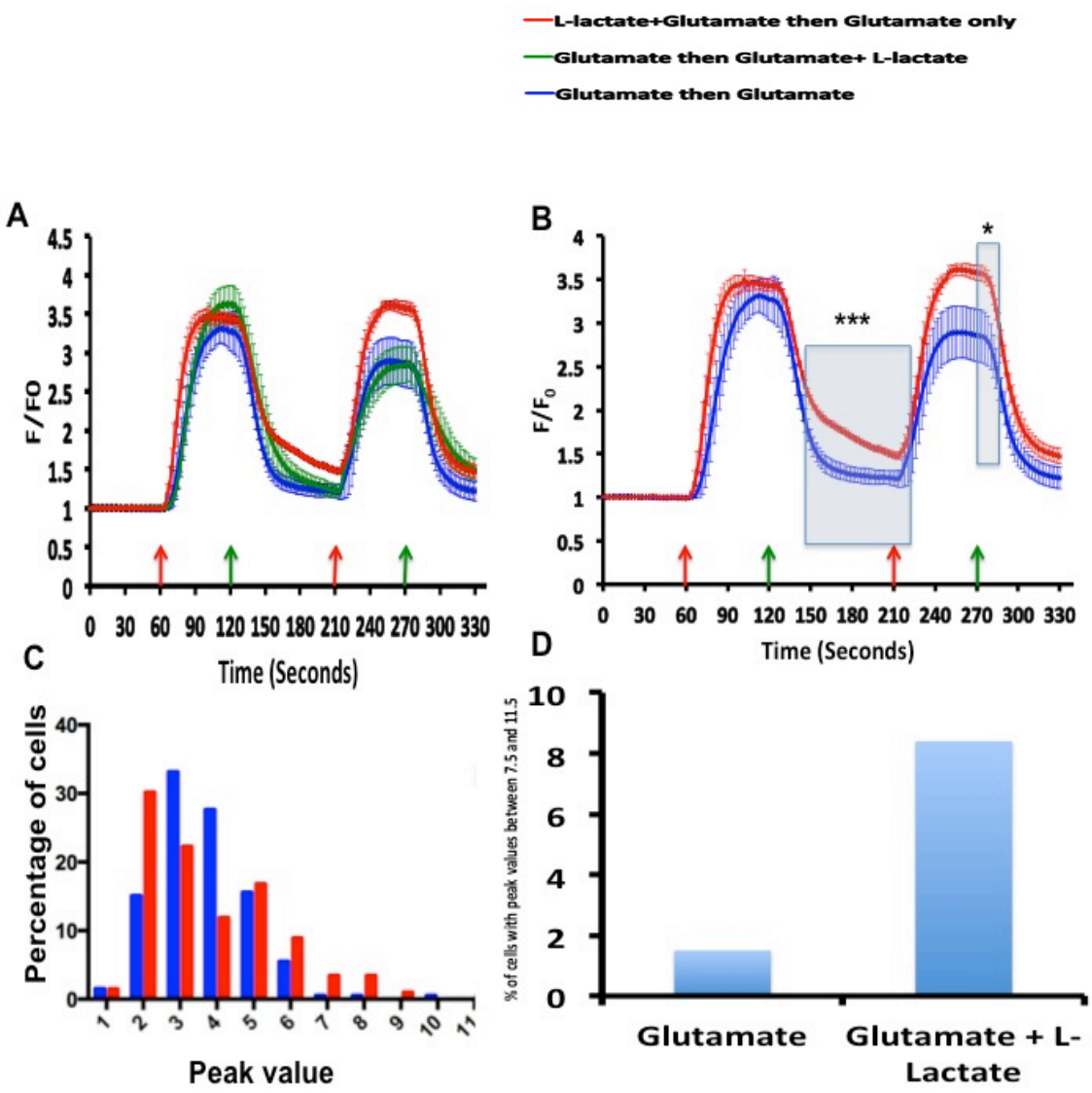

Figure 31 Extended effect of L-Lactate on HEK 293 T/17 expressing NR1/NR2A . Control : HEK 293T/17 cells transfected with NR1WT/NR2AWT were stimulated twice with 0.25 µM Glutamate and 0.25 µM Glycine (represented in blue). Treated condition 1: cells treated with 0.25 µM Glutamate and 0.25 µM Glycine + 20 mM L-lactate then 0.25 µM Glutamate and 0.25 µM Glycine successively (represented in red). Treated condition 2: cells treated with 0.25 µM Glutamate and 0.25 µM Glycine only then 20 mM L-Lactate+ 0.25 µM Glutamate and 0.25 µM Glycine successively (represented in green). A) Average of fold increase in fluorescence of single cells upon stimulation. Red arrow signals the start of stimulation, green arrow signals the start of wash off. Error bars are expressed as SEM among averages of independent experiments. Number of cells analyzed in case of control was 202 cells from 3 independent experiments , number of cells analyzed in case of treatment condition 1 was 202, no of cells analyzed in case of treated condition 2 was 205, from 3 independent experiments for each condition. C) Peak value distribution using the peaks from the first stimulation in control condition and treated condition 1, as a percentage of total cells whose peak values is >= average of baseline+ 3 times standard deviation of baseline. The width of each bin is 1. D) sum of the percentage of cells whose peak values (from first stimulation) lie between 7.5 and 11.5 in both control and treated condition.

Chapter 8

Investigating the effect of L-Lactate on NMDARs containing mutated subunits

8.1 Significance

In this chapter, the previously mutated NMDAR subunits were used. These subunits have mutations at redox sensitive sites to disrupt the disulfide bridge so that the receptor cannot respond to redox changes in its environment. It had been postulated before, that the potentiating effect seen by L-Lactate is attributed to its reducing power because when it is converted to pyruvate, NADH is released. Hence we mutated the key cysteine residues on NMDAR subunits that had been extensively studied in literature and found to affect the opening of the NMDAR channel based on the redox status of the environment and tested the effect of L-Lactate on such mutants.

8.2 Materials and methods

Mentioned earlier in chapter 4

8.3 Results

8.3.1 Effect of L-Lactate on NR1WT, NR2A C87,320A

In this experiment, HEK cells were transfected with NR1WT and NR2A C87,320S. A baseline was recorded for 1 minute during which cells were perfused with HBSS followed by a stimulation phase with either 0.25 µM glutamate and 0.25 µM glycine as

the control or 20 mM L-Lactate + 0.25 µM glutamate and 0.25 µM glycine**.** As shown in Fig 32 A, the kinetics of the initiation of response in the case of the presence of L-Lactate is slower than when Glutamate + Glycine only are used for stimulation (68 seconds to reach maximum peak amplitude in the case of L-Lactate presence versus 88 seconds in case of the control). These time differences were significant with a p value < 0.03 for the time points 74 seconds till 122 seconds. The average amplitude in both cases is quite similar (3.3 ± 0.17 fold change in the case of stimulation with L-Lactate versus 3.73 ± 0.19 fold change in the case of the control). By examining the washout kinetics in both conditions, we find that it was slower in the condition where cells were stimulated with L-Lactate compared to the control. This difference in the washout kinetics was significant with a p value lying between 0.01 and 0.03 for the time points 164 seconds till 208 seconds. In fig 32 B, when inspecting the number of cells that passed the filtering criteria (peak values is >= average of baseline+ 3 times standard deviation of baseline), we found that it was lower in case of the presence of L-Lactate (51 % ± 12.5) compared to the control (23 % ± 4), however this difference is not significant with a p value > 0.05. To summarize, introducing mutations on the NR2A subunit (NR2A C87, 320A) didn't affect the significant slowdown of the washout caused by L-Lactate that was seen earlier in the wild type. It is still significantly detectable in the mutated version of NR2A. This indicates that this effect is independent of the redox sensitivity of the receptor and is caused by some other mechanism that could be related to conformational changes. Another surprising observation was the significant slowdown of the initiation of the response when L-Lactate was added. We had observed the opposite in receptors

containing wild type subunits earlier where L-Lactate speeds up the initiation kinetics of the response. Hence, this effect (speeding up of the initiation of response) might be related to the redox changes caused by L-Lactate.

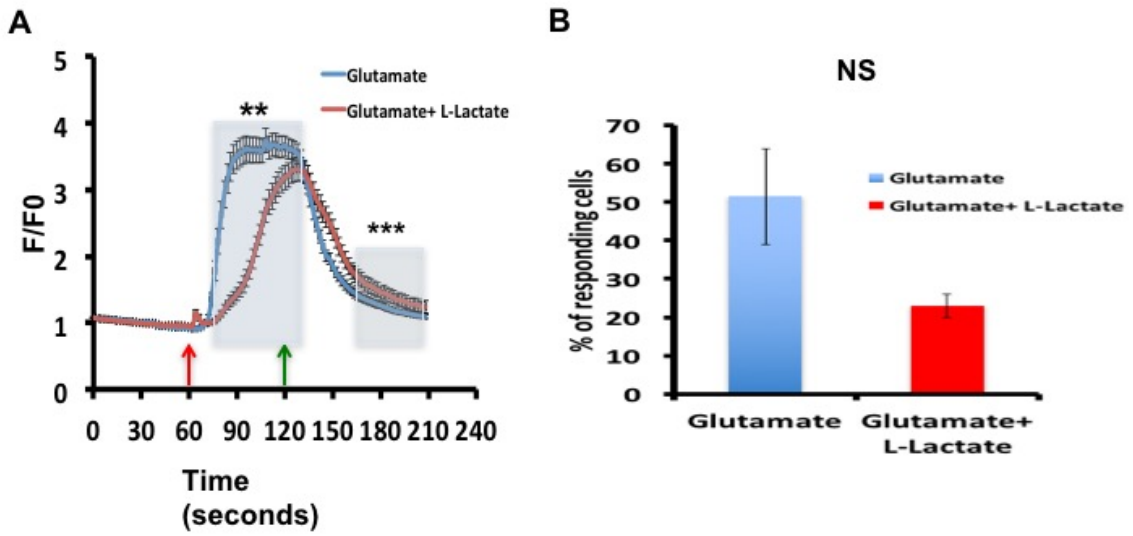

Figure 32 Effect of L-Lactate on HEK cells expressing NR1WT and NR2A C87, 320S. Cells were stimulated with 0.25 µM Glutamate and 0.25 µM Glycine (represented in blue) as a control. Treated condition were stimulated with 0.25 µM Glutamate and 0.25 µM Glycine + 20 mM L-Lactate (represented in red). A) Average of fold increase in fluorescence of single cells upon stimulation. Red arrow signals the start of stimulation, green arrow signals the start of wash off. Error bars are expressed as SEM among single cells. Number of cells analyzed in case of control was 103 cells, number of cells analyzed in case of treatment with L-Lactate was 46, from 2 independent experiments for each condition. B) A bar graph showing the quantity of cells whose peak values is >= average of baseline+ 3 times standard deviation of baseline. The quantity of cells is expressed as a percentage of the total number of analyzed cells (300 cells for each condition, error bars are shown as SEM.

8.3.2 Effect of L-Lactate on NR1 C744,798A, NR2A C87,320A

In this experiment, we aimed to further explore whether the redox sensitive sites on NR1 are involved in the effects of L-Lactate on NMDAR response. Therefore, cells transfected with NR1 C744,798A and NR2A C87,320A were used. Baseline was recorded for 15 seconds only. As shown in Fig 33 A, the kinetics of the initiation of response in the

case of the presence of L-Lactate is comparable to that of the control (51 seconds to reach maximum peak amplitude in both conditions). The average maximum peak amplitude for the control is 5.7 ± 0.44 fold change versus 4.7 ± 0.21 fold change in the case of stimulation with L-Lactate. By examining the washout kinetics in both conditions, we find that it was slower in the condition where cells were stimulated with L-Lactate compared to the control. The tau value for L-Lactate condition is 27.66 seconds while that for the control is 8.68 seconds. In fig 33 B, when inspecting the number of cells that passed the filtering criteria (peak values is >= average of baseline+ 3 times standard deviation of baseline), we found that it was higher in case of the presence of L-Lactate (33 %) compared to the control (24 %), however this difference is not significant with a p value > 0.05. To summarize, introducing mutations on both the NR2A subunit (NR2A C87,320A) and the NR1 subunit (NR1 C744,798A) didn't affect the significant slowdown of the washout caused by L-Lactate that was seen earlier in the wild type. It is still significantly detectable when both subunits (NR1 and NR2A) are mutated. This again indicates that this effect is independent of the redox sensitivity of the receptor and is caused by some other mechanism that could be related to conformational changes. Unlike the previous experiment where mutation on the NR2A subunit only led to a significant slowdown of the initiation of the response, when both the NR1 and NR2A subunits were mutated this was not seen any more. This could be interpreted by attributing the changes in the initiation kinetics to the redox sensitive sites. When redox sites are mutated on one subunit only, we see a slowdown in the initiation probably due

to conformational changes. However, when both subunits are mutated, they balance each other in a conformational manner and that delay is not seen anymore.

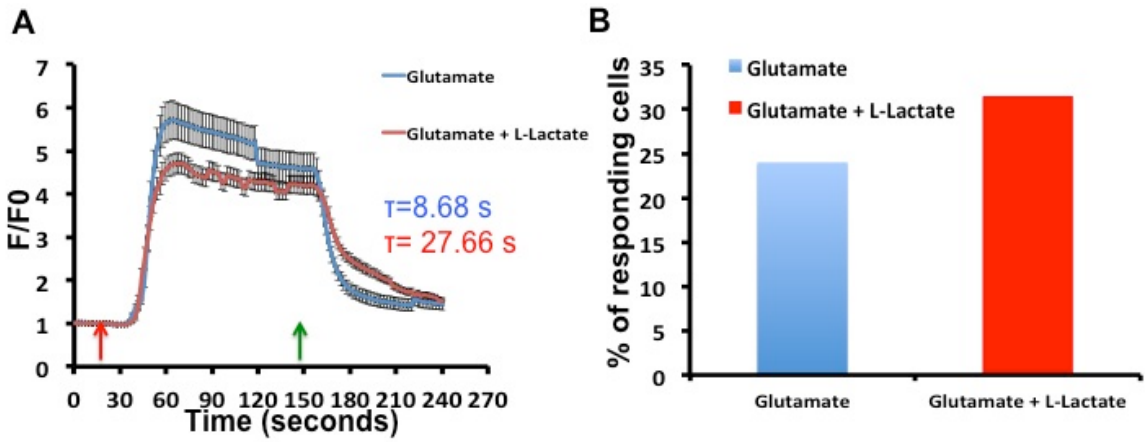

Figure 33 Effect of L-Lactate on HEK cells expressing NR1 C744,798A and NR2A C87,320S. Cells were stimulated with 0.25 µM Glutamate and 0.25 µM Glycine (represented in blue) as a control. Treated condition were stimulated with 0.25 µM Glutamate and 0.25 µM Glycine + 20 mM L-Lactate (represented in red). A) Average of fold increase in fluorescence of single cells upon stimulation. Red arrow signals the start of stimulation, green arrow signals the start of wash off. Error bars are expressed as SEM among single cells. Number of cells analyzed in case of control was 24 cells, number of cells analyzed in case of treatment with L-Lactate was 63, from 2 coverslips from the same experiment for each condition. B) A bar graph showing the quantity of cells whose peak values is >= average of baseline+ 3 times standard deviation of baseline. The quantity of cells is expressed as a percentage of the total number of analyzed cells.

Chapter 9

Discussion

The work addresses important questions regarding the role of lactate in the brain. Even though lactate has long been thought of as a waste product of metabolism to be eliminated, it is now recognized as a useful compound, serving the role of energy metabolic. However, over the past few years, several reports suggested that lactate may in addition act as a signaling molecule able to influence the functioning of neurons of the central nervous system. In particular, research performed in the Magistretti laboratory, led to the conclusion that lactate application to neurons caused the activation of plasticity genes of neurons. The mechanisms involve the activation of NMDA receptors that generate a lactate-mediated current. The mechanisms behind the modulation of NMDA receptors remain elusive. A good candidate mechanism is a redox-mediated modulation of the receptor/channel consecutive to the influx of lactate, its conversion into pyruvate, and the generation of NADH, a summary of the suggested model is shown in Fig 34. The purpose of the thesis work was to evaluate a potential redox-mediated NMDA receptor regulation operated by lactate and dissect the underlying molecular mechanism. This was performed by using site-directed mutagenesis of the protein (cysteine replacements) aimed at eliminating its sensitivity to redox challenges. The work consisted in generating these mutated genes, setting up the culture model and cell transfection, setting up the recording conditions, and

evaluating the redox sensitivity of the transfected mutated NMDA receptors. The approach chosen was intracellular calcium imaging in HEK cells, a technique chosen because opening of NMDA receptors includes the influx of calcium from the extracellular space. The experimental work led to the conclusion that lactate potentially potentiates NMDA receptors through an alteration of the redox state of the cell.

By combining earlier findings about the role of lactate in modulating NMDARs, we can see that it was reported earlier that L-Lactate potentiates the NMDAR current in primary neuronal cultures, this was revealed using both calcium imaging and electrophysiology (Yang et al, 2014). In addition, L-lactate increased the expression levels of memory related genes like Arc, Zif and P-Erk (Yang et al, 2014). However, the mechanism underlying this modulatory effect remained obscure. However, control compounds which cause similar pH, energy or osmotic changes did not result in similar potentiation in the NMDAR currents. The control compounds used were pyruvate, glucose and D-lactate (Yang et al, 2014). By comparing these compounds to L-lactate in terms of osmolarity, we can see that they all lead to similar changes in osmolarity. By examining the differences in pH that they cause, we can observe that the transport of L-lactate, D-lactate and Pyruvate leads to changes in intracellular pH unlike glucose. This is attributed to the different transporters involved in the transport of these compounds, L-lactate, D-lactate and Pyruvate are transported via the MCT where their transport is a companied with a proton unlike glucose which is transported via GLUT where no protons are involved. Moreover, in terms of energy production, L-lactate, pyruvate and

glucose all lead to the generation of the same amount of ATP unlike D-lactate which is not involved in the Kreb's cycle. We were trying to identify a characteristic that L-lactate did not share with all the control compounds and energy production, pH changes and osmolarity were not the answer. Interestingly, the increase in NADH/NAD ratio was the answer as L-lactate was the only one capable of causing such an increase upon its conversion to pyruvate by the lactate dehydrogenase enzyme (LDH). These comparisons are summarized in table 14. Moreover, NADH was shown to give similar results as those observed with L-Lactate in terms of potentiating NMDAR currents as revealed by using calcium imaging and electrophysiology (Yang et al., 2014). These findings suggest that the effects of L-Lactate are attributed to its reducing power where NADH is released upon its conversion to pyruvate. This hypothesis matches the established knowledge about NMDARs activity being potentiated when its environment is reduced.

In order to test for this correlation between the effect of L-Lactate on NMDAR and its reducing power, we introduced targeted mutations to different NMDAR subunits (NR1, NR2B, NR2A). The latter was then transfected into HEK cell which lack endogenous expression of NMDARs so acted as an excellent model for our experiment as it gives us the privilege of controlling the composition of the expressed NMDAR in terms of subunit composition and wildtype versus mutated subunits.

By stimulating HEK cells expressing wild type NMDARs with L-Lactate, glutamate and glycine, we noticed several effects compared to when cells were stimulated with

glutamate and glycine only (control). First, faster kinetics in the initiation of the response. Second a significant increase in the total number of responding cells when cells were incubated with L-Lactate for one hour. Third, the maximum peak values tend to shift towards higher peak values. Finally, a significant slowdown in the kinetics of washout, which was seen consistently in our experiments. In addition, L-Lactate on its own (without glutamate or glycine) was able to initiate some response in a few number of cells expressing NR1/NR2A. The latter effect might be explained by assuming that L-Lactate can bind directly to NMDARs as an agonist or co-agonist as observed recently using preliminary docking studies in our lab. This assumption is supported by literature where it was found out that glycine alone was able to activate a small percentage of NMDARs composed of NR1/NR2A without the addition of glutamate (Jones KS, 2002). However, this should be confirmed by destroying all the glutamate in the media that can be produced by cells using glutamate decarboxylase. Also one should be aware not to use glutamate dehydrogenase as it utilizes NAD+ as a co-factor leading to the generation of NADH.

Upon introducing mutations on the redox sensitive sites of NR2A only, we observed that the effect of L-Lactate had dramatically changed where it slowed down the initiation kinetics rather than speeding it up as observed earlier with the wild type. This confirms that the effect of L-Lactate on this component of the response is correlated to its reducing power. Also, L-lactate was no longer able to shift the maximum peak values

towards higher values. On the other hand, when mutations were introduced to the redox sites on the NR1 subunit as well where the cells express NMDARs with both subunits mutated, the slowing down effect on the initiation kinetics disappeared. This can be explained by assuming that when both subunits are mutated, they balance out each other in a conformational manner. In both cases either both subunits or only one subunit were mutated, the effect of L-Lactate on slowing down the washout kinetics resulting in a bigger Tau persisted significantly. The latter finding suggests that this effect is independent of the reducing power of L-Lactate and its ability to produce NADH upon its conversion to pyruvate. These results are summarized in table 13. Also, the finding that L-Lactate lost its potentiating power when the NR2A subunit only was mutated led us to conclude that the NR2A subunit is the key subunit involved in the modulatory effect of L-lactate on NMDAR through redox changes.

Table 13 Summary of the effects of L-Lactate on NR1/NR2A

Subunit composition	Effect of L-Lactate on calcium influx through NMDAR
WT NR1/NR2A	increases
Mutated NR1 and NR2A	decreases
Mutated NR2A only	decreases

Table 14 Comparison between L-lactate, D-lactate, pyruvate and NADH

Change osmolarity	YES	YES	YES	YES
Change pH	YES	YES	YES	NO
ATP prodcution	YES	YES	YES	YES
Increase NADH/NAD	YES	NO	NO	NO

Interestingly, the modulatory effect of L-lactate on NMDARs composed of NR1/NR2A subunits was different from its effect on NMDARs composed of NR1/NR2B subunits where it caused a potentiation in the first one and a depression in the second one. This was a thrilling finding as NR1/NR2A are believed to be involved in synaptic plasticity, whereas NR1/NR2B are believed to be involved in excitotoxicity. Calcium ions influx through activated postsynaptic NMDARs contribute to the long lasting changes in synaptic strength. It is exciting that both synaptic strengthening and weakening take place through Calcium influx through NMDARs. It was hypothesized that the magnitude of the change in Calcium concentration through its influx, determines the direction to which the synaptic efficacy is altered. The latter is also determined by the temporal properties of the changes in internal Calcium concentration (Lisman J., 1989).

Another hypothesis, is that the spatial change in internal Calcium concentration maybe spatially different. For example, NMDARs containing the subunit NR2B were shown to be found extra-synaptic (Brickley S.G. et al., 2003) although this is not exclusive (Thomas C.G., et al 2006). This spatial separation of NMDARs containing the NR2A subunit and those containing the NR2B subunit could lead to Calcium ions activating different signaling complexes and different pathways accordingly (Hardingham G.E. and Bading H., 2003; Vanhoutte P. and Bading H., 2003). Moreover, it was hypothesized that activation of NMDARs containing NR2A would lead to LTP and activation of those containing NR2B would lead to LTD (Liu L. et al., 2004; Massey P.V. et al, 2004). However, more work is needed to fully elucidate the molecular mechanisms underlying the response of NMDARs that are spatially separated and that are composed of different subunits.

The kinetics of activation, de-activation and de-sensitization of NMDARs determine their ability to decode and integrate synaptic signals and produce or maximize dendritic spines. It is worth mentioning that subunit composition is important to determine its kinetics, in particular during the deactivation phase. The amount of Calcium entering through NMDARs is also determined by pH, Zinc ions and polyamines.

Overall, this work provided a potential first molecular mechanism for the modulation of NMDAR through redox changes. L-lactate can open new doors for identifying pharmacologically active compounds that have a positive effect on memory through potentiating NR1/N2A and possibly neuroprotection through depressing NR1/NR2B.

For future directions, we suggest testing more mutants to further characterize the modulatory effect of L-Lactate on NMDAR. Additional experiments are also needed to fully understand the effect of L-Lactate on slowing down the washout kinetics. The most challenging part in this project was the variability among cells due to non-homogenous expression levels as we used transient transfection methods. Also, the size of NMDAR subunit DNA constructs was large which reduced transfection efficiencies. Hence, I strongly recommend establishing monoclonal stable cell lines expressing WT NMDARs and mutated ones of interest for future experiments. This will minimize the variability and allow easier comparisons to be made.

On another note, according to the findings by Yang et al., 2014, L-Lactate must go inside the cell in order to be able to detect its modulatory effect on NMDAR. This was shown by using MCT blockers where L-Lactate was incapable of exerting its modulatory effects. This could be also checked in HEK cells by measuring the pH changes associated with the

addition of L-lactate to the cells. However, it is worth mentioning that all the mutation sites that we targeted lied extracellular on the NMDAR subunits rather than intracellular. We hypothesize that the NADH generated by L-Lactate could be pumped by the cells to the outside to exert its reducing action possibly through pannexins. To further explore this, we recommend mutating some redox sensitive sites that lie intracellularly and compare their effects on the L-Lactate modulatory action. Also, block the pannexins and test whether the potentiation effect of L-lactate would last. To further confirm that the potention effect we observed was because of NADH production, blocking of LDH would be recommended for future experiments. In order to confirm our findings in vivo, mice expressing NMDARs with knocked out cysteine in the redox sensitive sites would be used.

It is also worth mentioning that the mechanism of action of L-Lactate as a neuromodulatory substance through NMDAR is not exclusive. There had been other hypothesis about how L-Lactate acts as a signaling molecule for the neurons. For example, it had been proposed that L-Lactate interacts directly with the HCA1 receptor which is a Gi protein coupled receptor (Bozzo and Chatton, 2013). In that study, it was reported that L-Lactate decreases the spontaneous Calcium spiking frequency in neurons (Bozzo and Chatton, 2013). The latter was correlated to HCA1 receptor because when they used pertussis toxin, which is a blocker of Gi protein, the effect of L-Lactate disappeared. Moreover, when they used 3,5 dyhydroxybenzoic acid, a specific agonist

for HCA1, they were able to reproduce the effect of L-Lactate (Bozzo and Chatton, 2013). In our study, we excluded the possibility that the effects of L-Lactate that we had seen could be related to HCA1, because we tested HEK cells for its expression and couldn't detect its presence (data not shown).

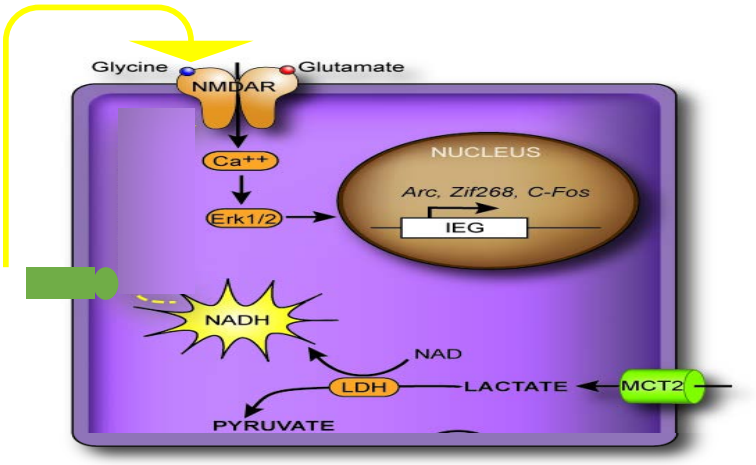

Figure 34 summary of the proposed model by which L-lactate modulates NMDAR

Conferences attended

The findings from this research project were presented in the annual meeting of the society for Neuroscience in November 2016 in San Diego, California.

BIBLIOGRAPHY

Ahlin G, Hilgendorf C, Karlsson J, Szigyarto CA, Uhlén M, Artursson P. Endogenous gene and protein expression of drug-transporting proteins in cell lines routinely used in drug discovery programs. Drug Metab Dispos. 2009;37:2275–83

Aizenman E., Lipton S. A., Loring R. H. (1989). Selective modulation of NMDA responses by reduction and oxidation. Neuron 2, 1257–1263. 10.1016/0896-6273(89)90310-3

Allaman I., Bélanger M., Magistretti P. J. (2011). Astrocyte-neuron metabolic relationships: for better and for worse. Trends Neurosci. 34, 76–87. 10.1016/j.tins.2010.12.001

Andriezen WL (1893) On a system of fibre-like cells surrounding the blood vessels of the brain of man and mammals, and its physiological significance. Int Monatsschr Anat Physiol 10:532–40

Armstrong, N. & Gouaux, E. Mechanisms for activation and antagonism of an AMPA-sensitive glutamate receptor: crystal structures of the GluR2 ligand binding core. Neuron 28, 165–181 (2000)

Barros LF, Courjaret R, Jakoby P, Loaiza A, Lohr C, Deitmer JW(2009) Preferential transport and metabolism of glucose in Bergmann glia over Purkinje cells: a multiphoton study of cerebellar slices. Glia 57:962–70

Bélanger, M., Allaman, I., & Magistretti, P. J. (2011). Brain energy metabolism: focus on astrocyte-neuron metabolic cooperation. Cell Metabolism, 14(6), 724–38.

Belanger, M. and Magistretti, P.J. (2009) The role of astroglia in neuroprotection. Dialogues. Clin. Neurosci. 11, 281 –295

Bittner CX, Loaiza A, Ruminot I, Larenas V, Sotelo-Hitschfeld T, Gutiérrez R, Córdova A, Valdebenito R, Frommer WB, Barros LF (2010) High resolution measurement of the glycolytic rate. Front Neuroenerg 2.pii:26.

Bouzier-Sore AK, Voisin P, Bouchaud V, Bezancon E, Franconi JM, Pellerin L (2006) Competition between glucose and lactate as oxidative energy substrates in both neurons and astrocytes: a comparative NMR study. Eur J Neurosci 24:1687–94

Bouzier-Sore AK, Voisin P, Canioni P, Magistretti PJ, Pellerin L (2003) Lactate is a preferential oxidative energy substrate over glucose for neurons in culture. J Cereb Blood Flow Metab 23:1298–306.

Bozzo L., Puyal J., Chatton J.Y. Lactate modulates the activity of primary cortical neurons through a receptor-mediated pathway. PLoS ONE. 2013;8:1450 doi: 10.1371/journal.pone.0071721.

Bramham CR, Worley PF, Moore MJ, Guzowski JF. 2008. The immediate early gene Arc/Arg3.1: regulation, mechanisms, and function. J Neurosci 28: 11760–11767.

Brickley S.G. et al., NR2B and NR2D subunits coassemble in cerebellar Golgi cells to form a distinct NMDAR subtype restricted to extrasynaptic sites, J. Neurosci., 23, 4958, 2003.

Brooks, G.A.(2009). Cell-cell and intracellular lactate shuttles. J.Physiol.587, 5591-5600

Brothwell S. L., Barber J. L., Monaghan D. T., Jane D. E., Gibb A. J., Jones S. (2008). NR2B- and NR2D-containing synaptic NMDA receptors in developing rat substantia nigra pars compacta dopaminergic neurones. J. Physiol. 586, 739–750. 10.1113/jphysiol.2007.144618

Cheeti S., Lee C.H (2010). The Involvement of Intracellular Calcium in the MCT-Mediated Uptake of Lactic Acid by HeLa Cells (2010). Mol Pharm 1; 7(1): 169.

Chen N., Moshaver A., Raymond L.A. Differential sensitivity of recombinant N-methyl-d-aspartate receptor subtypes to zinc inhibition. Mol. Pharmacol. 1997;51:1015–1023

Choi, Y., Chen, H.V., and Lipton, S.A. (2001). Three pairs of cysteine residues mediate both redox and zn2+ modulation of the nmda receptor. The Journal of neuroscience : the official journal of the Society for Neuroscience 21, 392-400.

Choi, Y. B., Tenneti, L., Le, D. A., Ortiz, J., Bai, G., Chen, H. S., and Lipton, S. A. (2000) Molecular basis of NMDA receptor-coupled ion channel modulation by S-nitrosylation. Nat. Neurosci. 3, 15–21

Dienel GA, Hertz L (2001) Glucose and lactate metabolism during brain activation. J Neurosci Res 66:824–38.

Dringen R., Gebhardt R., Hamprecht B. (1993). Glycogen in astrocytes: possible function as lactate supply for neighboring cells. Brain Res. 623, 208–214. 10.1016/0006-8993(93)91429-v

Dudai Y and Eisenberg M (2004) Rites of passage of the engram: reconsolidation and the lingering consolidation hypotheis. Neuron, 44, 93-100

Ewaschuk JB, Naylor JM, Zello GA. D-lactate in human and ruminant metabolism. J Nutr 2005; 135:1619 - 25; PMID: 15987839

Felipo, V. and Butterworth, R.F. (2002) Neurobiology of ammonia. Prog. Neurobiol. 67, 259 – 279

Furukawa, H., and Gouaux, E. (2003). Mechanisms of activation, inhibition and specificity: crystal structures of the NMDA receptor NR1 ligand-binding core. EMBO J. 22, 2873–2885.

Furukawa, H., Singh, S.K., Mancusso, R., and Gouaux, E. (2005). Subunit arrangement and function in NMDA receptors. Nature 438, 185–192

Gordon, G.R.et al. (2007) Astrocyte control of the cerebrovasculature. Glia 55, 1214 – 1221

Gordon GR, Choi HB, Rungta RL, Ellis-Davies GC, MacVicar BA (2008) Brain metabolism dictates the polarity of astrocyte control over arterioles. Nature 456:745–9

Hardingham G.E. and Bading H., The Yin and Yang of NMDAR signalling, Trends Neurosci., 26, 81, 2003.

Haussinger, D. and Schliess, F. (2008) Pathogenetic mechanisms of hepatic encephalopathy. Gut 57, 1156 – 1165

Herrero-Mendez A, Almeida A, Fernández E, Maestre C, Moncada S, Bolaños JP (2009) The bioenergetic and antioxidant status of neurons is controlled by continuous degradation of a key glycolytic enzyme by APC/C-Cdh1. Nat Cell Biol 11:747–52

Iadecola, C. and Nedergaard, M.(2007)Glial regulation of the cerebral microvasculature. Nat. Neurosci.10, 1369 –1376

Ilieva, H. et al. (2009) Non-cell autonomous toxicity in neurodegenerative disorders: ALS and beyond. J. Cell Biol. 187, 761 – 77253

Itoh Y, Esaki T, Shimoji K, Cook M, Law MJ, Kaufman E, Sokoloff L (2003) Dichloroacetate effects on glucose and lactate oxidation by neurons and astroglia in vitro and on glucose utilization by brain in vivo. Proc Natl Acad Sci USA 100:4879–84

Ivanov A, Mukhtarov M, Bregestovski P, Zilberter Y (2011) Lactate effectively covers energy demands during neuronal network activity in neonatal hippocampal slices. Front Neuroenerg 3:2.

Johnson, J.W., and Ascher, P. (1987). Glycine potentiates the NMDA response in cultured mouse brain neurons. Nature 325 , 529–531

Jones KS, VanDongen HM, VanDongen AM. The NMDA receptor M3 segment is a conserved transduction element coupling ligand binding to channel opening. J Neurosci. 2002;22:2044–2053

Kacem K, Lacombe P, Seylaz J, Bonvento G (1998) Structural organization of the perivascular astrocyte endfeet and their relationship with the endothelial glucose transporter: a confocal microscopy study. Glia 23:1–10.

Kadekaro M, Vance WH, Terrell ML, Gary H Jr., Eisenberg HM, Sokoloff L (1987) Effects of antidromic stimulation of the ventral root on glucose utilization in the ventral horn of the spinal cord in the rat. Proc Natl Acad Sci USA 84:5492–5

Kandel ER. The molecular biology of memory storage: a dialogue between genes and synapses. Science. 2001;294(5544):1030–8

Karakas, E., Simorowski, N., and Furukawa, H. (2009). Structure of the zincbound amino-terminal domain of the NMDA receptor NR2B subunit. EMBOJ. 28, 3910–3920.

Keller JN, Steiner MR, Mattson MP, Steiner SM (1996) Lysophosphatidic acid decreases glutamate and glucose uptake by astrocytes. J Neurochem 67:2300–5.

Kocharyan A, Fernandes P, Tong XK, Vaucher E, Hamel E (2008) Specific subtypes of cortical GABA interneurons contribute to the neurovascular coupling response to basal forebrain stimulation. J Cereb Blood Flow Metab 28:221–31.

Köhr G, Eckardt S, Lüddens H, Monyer H, Seeburg PH. NMDA receptor channels: Subunit-specific potentiation by reducing agents. Neuron. 1994;12(5):1031–1040

Laube B, Kuhse J, Betz H. Evidence for a tetrameric structure of recombinant NMDA receptors. J Neurosci 1998;18:2954–2961

Li, R.et al. (2005) Glial fibrillary acidic protein mutations in infantile, juvenile, and adult forms of Alexander disease. Ann. Neurol. 57, 310 –326

Lipton S. T., Choi Y.-B., Pan Z.-H., Lei S. Z., Chen H.-S. V., Sucher N. J., et al. . (1993). A redox-based mechanism for the neuroprotective and neurodestructive effects of nitric oxide and related nitroso-compounds. Nature 364, 626–632. 10.1038/364626a0

Lisman J., A mechanism for the Hebb and the anti-Hebb processes underlying learning and memory, Proc. Natl. Acad. Sci. USA, 86, 9574, 1989.

Liu L. et al., Role of NMDAR subtypes in governing the direction of hippocampal synaptic

plasticity, Science, 304, 1021, 2004.

Magistretti, P.J. (2006) Neuron –glia metabolic coupling and plasticity. J. Exp. Biol. 209, 2304 –2311

Magistretti, P.J.(2008). Brain energy metabolism. In Fundamental neuroscience, L.R. Squire, D. Berg, F.E. Bloom, S. du Lac, A. Ghosh, and N.C. Spitzer, eds. (San Diego: Academic Press), pp. 2771-293

Magistretti PJ, Allaman I (2007) Glycogen: a Trojan horse for neurons. Nat Neurosci 10:1341–2.

Magistretti, P.J., and Allaman, I. (2015). A Cellular Perspective on Brain Energy Metabolism and Functional Imaging. Neuron 86, 883-901.

Magistretti P.J., Chatton J.Y. Relationship between l-glutamate-regulated intracellular Na + dynamics and ATP hydrolysis in astrocytes. J. Neural Transm. 2005;112:77–85.

Magistretti PJ, Hof PR, Martin JL (1986) Adenosine stimulates glycogenolysis in mouse cerebral cortex: a possible coupling mechanism between neuronal activity and energy metabolism. J Neurosci 6:2558–62.

Magistretti PJ, Morrison JH (1988) Noradrenaline- and vasoactive intestinal peptide-containing neuronal systems in neocortex: functional convergence with contrasting morphology. Neuroscience 24:367–78.

Magistretti P.J., Pellerin L. Cellular mechanisms of brain energy metabolism and their relevance to functional brain imaging. Philos. Trans. R. Soc. Lond. B Biol. Sci. 1999;354(1387):1155–1163. doi: 10.1098/rstb.1999.0471.

Mangia S, Simpson IA, Vannucci SJ, Carruthers A (2009) The in vivo neuron-to-astrocyte lactate shuttle in human brain: evidence from modeling of measured lactate levels during visual stimulation. J Neurochem 109(Suppl 1):55–62.

Mano I, Teichberg VI. A tetrameric subunit stoichiometry for a glutamate receptor-channel complex. Neuroreport. 1998;9:327–331

Massey P.V. et al., Differential roles of NR2A and NR2B-containing NMDARs in cortical long-term potentiation and long-term depression, J. Neurosci., 24, 7821, 2004.

McIlwain H (1953) Substances which support respiration and metabolic response to electrical impulses in human cerebral tissues. J Neurol Neurosurg Psychiatr 16:257–66.

Min Li, (1999). NMDA receptor protocols. Methods in Molecular Biology. Volume 128. ISBN 978-1-59259-683-6

Monyer H, Sprengel R, Schoepfer R, Herb A, Higuchi M, Lomeli H, Burnashev N, Sakmann B, Seeburg PH. Heteromeric NMDA receptors: molecular and functional distinction of subtypes. Science 1992; 256:1217 - 21; http://dx.doi.org/; PMID: 1350383 10.1126/science.256.5060.1217

Morgello S, Uson RR, Schwartz EJ, Haber RS (1995) The human blood-brain barrier glucose transporter (GLUT1) is a glucose transporter of gray matter astrocytes. Glia 14:43–54.

Paoletti P., Ascher P., Neyton J. (1997). High-affinity zinc inhibition of NMDA NR1-NR2A receptors. J. Neurosci. 17, 5711–5725.

Partin KM, Bowie D, Mayer ML (1995) Structural determinants of allosteric regulation in alternatively spliced AMPA receptors. Neuron 14:833–843.

Partin KM, Patneau DK, Winters CA, Mayer ML, Buonanno A. Selective modulation of desensitization at AMPA versus kainate receptors by cyclothiazide and concanavalin A. Neuron. 1993;11:1069–1082.

Pellerin, L., & Magistretti, P. J. (1994). Glutamate uptake into astrocytes stimulates aerobic glycolysis: a mechanism coupling neuronal activity to glucose utilization. Proceedings of the National Academy of Sciences of the United States of America,

91(22), 10625–9.

Pellerin L, Magistretti PJ (2003) How to balance the brain energy budget while spending glucose differently. J Physiol 546:325.

Pellerin L, Magistretti PJ. Sweet sixteen for ANLS. J Cereb Blood Flow Metab. 2012;32:1152–66.

Petralia R. S., Wenthold R. J. (2008). “NMDA receptors,” in The Glutamate Receptors, eds Gereau R. W., Swanson G. T., editors. (Totowa, NJ: Humana Press;), 45–98.

Pierre K, Pellerin L (2005) Monocarboxylate transporters in the central nervous system: distribution, regulation and function. J Neurochem 94:1–14.

Pihlaja, R. et al. (2008) Transplanted astrocytes internalize deposited beta-amyloid peptides in a transgenic mouse model of Alzheimer’s disease. Glia 56, 154 –163

Ramos M, del Arco A, Pardo B, Martínez-Serrano A, Martínez-Morales JR, Kobayashi K, Yasuda T, Bogónez E, Bovolenta P, Saheki T, Satrústegui J (2003) Developmental changes in the Ca2+-regulated mitochondrial aspartate-glutamate carrier aralar1 in brain and prominent expression in the spinal cord. Brain Res Dev Brain Res 143:33–46.

Raoul, C. et al. (2006) Viral-based modelling and correction of neurodegenerative diseases by RNA interference.

Gene Ther. 13, 487 – 495

Rinholm JE, Hamilton NB, Kessaris N, Richardson WD, Bergersen LH, Attwell D (2011) Regulation of oligodendrocyte development and myelination by glucose and lactate. J Neurosci 31:538–4

Rouach N, Koulakoff A, Abudara V, Willecke K, Giaume C(2008) Astroglial metabolic networks sustain hippocampal synaptic transmission. Science 322:1551–5

Santucci DM, Raghavachari S (2008) The Effects of NR2 Subunit-Dependent NMDA Receptor Kinetics on Synaptic Transmission and CaMKII

Activation. PLoS Comput Biol 4(10): e1000208. doi:10.1371/journal.pcbi.1000208

Serres S, Bezancon E, Franconi JM, Merle M. Ex vivo analysis of lactate and glucose metabolism in the rat brain under different states of depressed activity. J Biol Chem. 2004;279:47881–47889

Siegwart P, Côté J, Male K. Adaptive control at low glucose concentration of HEK-293 cell serum-free cultures. Biotechnol Prog. 1999;15:608–616. doi: 10.1021/bp990077v.

Smith D, Pernet A, Hallett WA, Bingham E, Marsden PK, Amiel SA. Lactate: a preferred fuel for human brain metabolism in vivo. J Cereb Blood Flow Metab. 2003;23:658–664

Sofroniew, M.V. and Vinters, H.V. (2010) Astrocytes: biology and pathology. Acta Neuropathol.119, 7 –35

Sullivan, J. M., Traynelis, S. F., Chen, H. S., Escobar, W., Heinemann, S. F., and Lipton, S. A. (1994). Identification of two cysteine residues that are required for redox modulation of the NMDA subtype of glutamate receptor. Neuron 13, 929–936. doi: 10.1016/0896-6273(94)90258-5

Suzuki, A., Stern, S.A., Bozdagi, O., Huntley, G.W., Walker, R.H., Magistretti, P.J., and Alberini, C.M. (2011). Astrocyte-neuron lactate transport is required for long-term memory formation. Cell 144, 810-823.

Takahashi S, Driscoll BF, Law MJ, Sokoloff L (1995) Role of sodium and potassium ions in regulation of glucose metabolism in cultured astroglia. Proc Natl Acad Sci USA 92:4616–20.

Tang LH, Aizenman E. Long-lasting modification of the N-methyl-D-aspartate receptor channel by a voltage-dependent sulfhydryl redox process. Mol Pharmacol. 1993a;44:473–478

Thomas C.G., Miller A.J., and Westbrook G.L., Synaptic and extrasynaptic NMDAR NR2 subunits in cultured hippocampal neurons, J. Neurophysiol., 95, 1727, 2006.

Urrila AS, Hakkarainen A, Heikkinen S, Vuori K, Stenberg D, Häkkinen AM, Lundbom N, Porkka-Heiskanen Tzens. Stimulus-induced brain lactate: effects of aging and prolonged wakefulness. J Sleep Res. 2004;13:111–119. doi: 10.1111/j.1365-2869.2004.00401.x.

Vanhoutte P. and Bading H., Opposing roles of synaptic and extrasynaptic NMDARs in neuronal calcium signalling and BDNF gene regulation, Curr. Opin. Neurobiol., 13, 366, 2003.

Whitlock J. R., Heynen A. J., Shuler M. G., Bear M. F. (2006). Learning induces long-term potentiation in the hippocampus. Science 313 1093–1097. 10.1126/science.1128134

Xu Y, Ola MS, Berkich DA, Gardner TW, Barber AJ, Palmieri F, Hutson SM, LaNoue KF (2007) Energy sources for glutamate neurotransmission in the retina: absence of the aspartate/glutamate carrier produces reliance on glycolysis in glia. J Neurochem 101:120–31.

Yang, J., Ruchti, E., Petit, J.M., Jourdain, P., Grenningloh, G., Allaman, I., and Magistretti, P.J. (2014). Lactate promotes plasticity gene expression by potentiating NMDA signaling in neurons. Proceedings of the National Academy of Sciences of the United States of America 111, 12228-12233.

Yu S, Ding WG (1998) The 45 kDa form of glucose transporter 1 (GLUT1) is localized in oligodendrocyte and astrocyte but not in microglia in the rat brain. Brain Res 797:65–72.